Hydrodynamics through redistribution rings for a rotating packed bed reactor

Vercoelen, Thomas P.M.

Award date:
2018

Technische Universiteit Eindhoven University of Technology

Department of Chemical Engineering and Chemistry

Laboratory of Chemical Reactor Engineering

Hydrodynamics Through Redistribution Rings for a Rotating Packed Bed Reactor

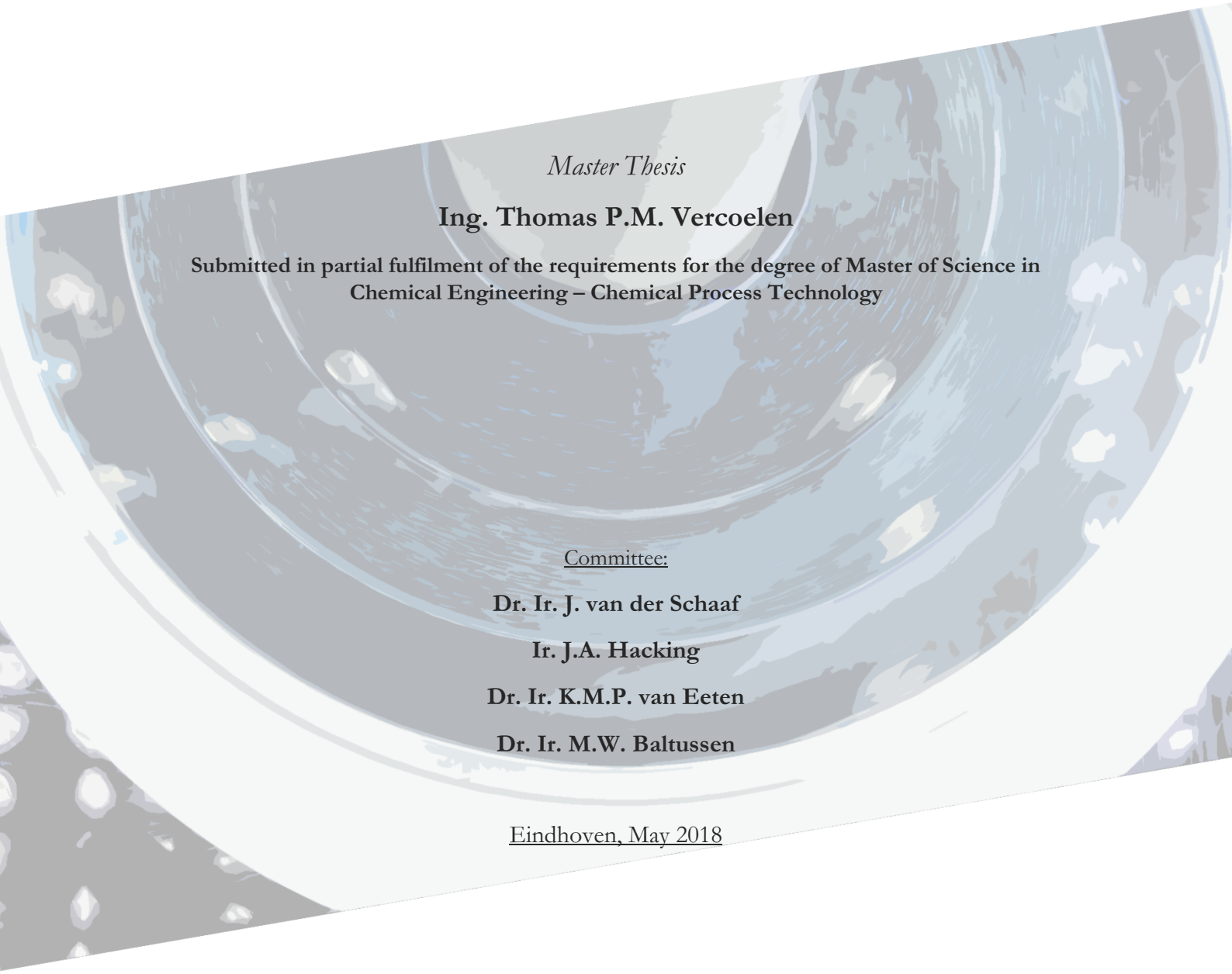

Master Thesis

Ing. Thomas P.M. Vercoelen

Submitted in partial fulfilment of the requirements for the degree of Master of Science in Chemical Engineering – Chemical Process Technology

Committee:

Dr. Ir. J. van der Schaaf

Ir. J.A. Hacking

Dr. Ir. K.M.P. van Eeten

Dr. Ir. M.W. Baltussen

Eindhoven, May 2018

Graduating student:

Ing. Thomas P.M. Vercoelen

Student ID:

0974714

May 2018

"Look up at the stars and not down at your feet. Try to make sense of what you see, and wonder about what makes the universe exist. Be curious."

- Stephen Hawking

Acknowledgments

This project would not have been possible without the support and teamwork with my direct supervisor, Jasper Hacking. Through the insightful meetings held during the duration of this project, we have always managed to come up with smart solutions for the problems we were facing on the topics of this research.

I would also like to thank John van der Schaaf and Kevin van Eeten as they have been inexhaustible sources of new and smart ideas on the project.

Lastly, I would like to thank the rest of the Chemical Reactor Engineering group for giving me the opportunity and for the help I have received from various people during my graduation period.

Summary

Rotating packed beds (RPB) as high gravity gas-liquid contactors/reactors come in many varieties. Examples are the single-block rotating packed bed, split-packing rotating bed, rotating zigzag bed and two-stage counter-current rotating packed bed. Each of these reactors has its own benefits and drawbacks but neither of these has integrated heat exchange possibilities which can be problematic while executing endothermic or exothermic processes. A new type of rotating packed bed, the cooled rotating packed bed (CRPB) was designed, which consists of a rotor with three concentric fine mesh redistribution rings and integrated heat exchange channels. The redistribution rings help to overcome another difficulty in RPBs which is the proper distribution of the liquid. The packing is placed in the cavity between the redistribution rings and heat exchange channels. As this is a new type of RPB, research is still in an early phase with future potential. The characterization consists of three topics which include the physical gas-liquid behaviour, mass transfer properties and heat transfer properties. This report is focused on the characterization of the hydrodynamics through the redistribution rings of the CRPB. To characterize this behaviour, a dedicated setup was built that allows for visual analysis of the liquid through the redistribution rings. Liquid flow behaviour was experimentally studied over a broad range of operating variables with different patterns of holes in the mesh rings. The liquid behaviour was quantified on several aspects including liquid flight paths, jet formation and breakup, liquid layer build up and jet coalescence. The data from the experiments was accompanied by computational fluid dynamics simulations performed in ANSYS Fluent and combined with knowledge from literature to model the liquid behaviour through the redistribution rings.

During the experiments, several important findings were done. The liquid flow through the rings can be divided in two main regimes. The main regime of interest is the jet flow regime. Here, each hole in the mesh produces a jet that is stable over the required flight distance which is the optimal case for the gas-liquid interfacial area. The jet flow regime is on the one extremum limited by the maximum flow capacity of each ring called the flooding line which is the maximum flow capacity of each ring. On the other extremum, the jet flow regime transitions to a regime with jet breakup within the flight path. This reduces the interfacial area but is also accompanied, in many cases, by maldistribution of the liquid through the reactor. These two regimes and the flooding line are positioned at different liquid flow rates for the different rings. One reason for this is the centrifugal force on the liquid that depends on the ring diameter and determines the flow velocity. Another reason is the open area available for flow which increases with an increasing ring diameter as all rings use the same mesh. Jet coalescence behaviour was found to increasingly happen as the inter-hole spacing is decreased where, with the smallest inter-hole spacing, at some rotational velocities and flow rates, no individual jets were observed. At rotational velocities above 800 RPM and in the upper limit of the flow rate, the jet fusing was reduced to a minimum. However, the liquid flow capacities of the three rings does not allow for each ring to be in the optimal operating range at the same time.

The simulations which were used to gain knowledge on the local flow velocities inside the liquid, showed a symmetrical and almost spherical flow approach towards the hole from within the water layer. Turbulence in the jets showed to be about 5%. This data was used to explain and substantiate some of the behaviour seen during the experiments. The liquid flight path during the simulations showed a small consistent deviation from the experimental and calculated flight paths as all jets in the simulations were slightly more curved than the experimental and calculated paths.

The Matlab model written to calculate the liquid behaviour through the redistribution rings showed a high level of similarity with the experiments. A parity plot on water layer thickness and comparison of the jet shape were used to determine the comparability. The model is however still in its nascent stage and could be elaborated to improve accuracy by including more of the phenomena observed during the experiments.

Concluding this part of the research it would be of great interest in future research to investigate some of the following. As the current redistribution rings have an equal mesh, their optimum operation range does not overlap over a broad range of operating parameters. Therefore, it might be beneficial for the reactor to slightly decrease the hole density in the larger rings. This would shift the operating range of the three rings to have more overlap and reduce the amount of jet fusing in the larger rings which could consequently lead to an increase of interfacial area. Additionally, to determine the effective gas-liquid interfacial area in the reactor while in operation, experiments could be done using a simple and well known gas-liquid adsorption followed by an irreversible reaction.

Table of Contents

Chapter 1. Introduction

1.1 Research background

In the chemical industry, many types of reactors are available, each with its own purpose and benefits suiting the specific needs for the intended reaction. The selection of the reactor type, to a great extent, depends on the different phases involved in the reaction. Those can include liquids, gasses and solids, or any combination of those. Gas-liquid reactions more specifically, which include many types of reactions like oxidations, hydrogenations, sulfonations, polymerizations and gas absorptions (e.g. CO_2, H_2S, SO_2, Cl_2 and NO_x) that generally need a high gas-liquid mass transfer to achieve optimal reaction rates because they are usually not kinetically limited (Guo et al., 2013; Harmsen, 2007; Jähnisch et al., 2000; Joelianingsih et al., 2008; Lucas et al., 2010; Puxty et al., 2010). To achieve this, there are many types of reactors that can be exploited, one of which being high gravity reactors (HiGee reactors). HiGee reactors generate a high gravity field by fast rotation of the reactor. The first patent on rotating packed beds, a type of HiGee reactor, dates back over three decades by Ramshaw et al. (Ramshaw, 1981). Since then, many kinds of RPB have been developed, such as the single-block rotating packed bed, split-packing rotating bed, rotating zigzag bed and two-stage counter-current rotating packed bed. These and several more are well reviewed in literature on their capabilities, advantages and disadvantages (Cortes Garcia et al., 2017; Rao et al., 2004a). The high mass transfer rates and throughput achieved through increased gravity fields (100-1000 times earth's gravity) in HiGee reactors can get 1-2 orders of magnitude higher than in conventional packed columns which allows for a size reduction of up to 10 times (Rao et al., 2004b; Wang et al., 2011; Zhao et al., 2010). The high gravity field is not the primary cause of the improved mass transfer rates, but rather an aid to generate thin liquid films and smaller droplets that result in large interfacial areas and high levels of micro-mixing.

Rotating packed beds consist of only a few key parts but come in many different configurations. The important parts include the annular, cylindrical packed bed(s) that can hold the catalyst and concentric baffles to guide or redistribute the liquid. These can be configured in different combinations to serve different purposes with the option to have one rotor or a combination of rotors and stators (Chandra et al., 2005; Y Luo et al., 2012; Wang et al., 2008).

The most commonly mentioned rotating packed bed in literature is the single-block rotating packed bed reactor (Cortes Garcia et al., 2017). This reactor has a single rotor containing the packing, a liquid distributor in the centre and gas inlets and outlets that can be configured as demanded either co-current, counter-current or cross-current. A schematic view of a counter-current single block rotating packed bed is shown in Figure 1.

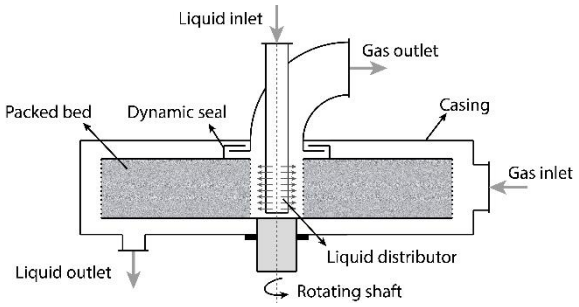

Figure 1. Schematic drawing of a single-block counter-current rotating packed bed.

The rotating zig-zag bed as illustrated in Figure 2 is composed of a rotor and stator with concentric baffles or packing that are alternately attached to the rotor and stator. The gas and liquid flow in a zig-zag pattern through the reactor, hence the name. Fast rotation of the reactor causes the liquid to be broken up in very fine droplets as it flows over the baffles attached to the rotor. A rotating zig-zag bed has a comparable mass transfer performance to that of a single block rotating packed bed but its configuration allows higher turndown ratios due to the very low limit of the minimum operation load (Wang et al., 2008).

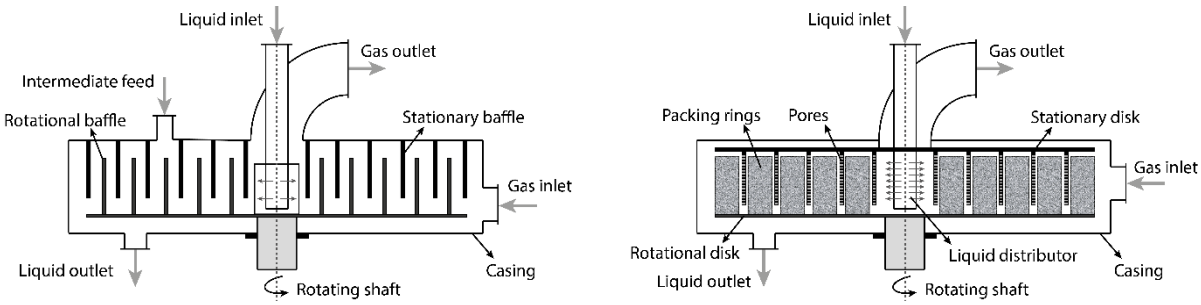

Figure 2. Schematic drawings of two rotor-stator versions of RPBs. Left: Rotating zig-zag bed. Right: One stage of a two stage counter-current rotating packed bed

The two stage counter-current rotating packed bed (Figure 2) is a variation of the zig-zag bed. The flow pattern through the reactor is very similar but the baffles on the rotor are replaced by annular packed bed rings to increase the contact area and possibly support a catalyst. This reactor has not one, but two stages of which both rotors are mounted through the shaft to one motor (Chu et al., 2013). While the presence of a stator makes it possible to supply intermediate feeds into the reactor, thus allowing for continuous distillation in one stage, the complex structure of this reactor is its main drawback and inhibits the industrial application (Chu et al., 2015).

The performance characterization, important to determine the best operating parameters, of RPBs can be done using various methods. The most relevant research topics being the fluid dynamics, mass transfer and heat transfer. Fluid dynamics can be characterized in a number of ways e.g. via visual experiments or computational fluid dynamics (CFD). Both methods have previously and extensively been used in literature to characterize the performance and observe critical phenomena that determine the operation a RPB. During visual analysis, relations were found on the droplet size distribution as a function of the rotational velocity and ligament or droplet flow regimes as a function of rotational velocity and outer packing radius (Burns and Ramshaw, 1996; Guo et al., 2000; Li et al., 2015; Sang et al., 2017). For fluid dynamics analysis, CFD has been used to determine liquid holdup, flow patterns and velocities (Sang et al., 2017) but also gas flow maldistribution and pressure drop (Llerena-Chavez and Larachi, 2009). Through reading these papers, useful insight was generated.

1.2 Research objectives

A problem that can reduce the optimal operation of a RPB is the distribution of the liquid. As the liquid advances through a RPB, the diameter of the reactor increases thus decreasing the liquid density. Further, gravity tends to slightly concentrate the fluid in the lower part of the reactor. To counteract this problem and achieve a better distribution of the liquid, a new kind of RPB was designed with three concentric fine mesh redistribution rings. The space between the rings holds heat exchange channels to overcome the heat exchange problems in RPBs (Pohorecki et al., 2010) and has the possibility to be loaded with a packing. This new type of RPB, the so called

Cooled Rotating Packed Bed (CRPB) (Figure 3 and Figure 4) however, still needs extensive research on its capabilities and performance. The research to be done includes exploration of the fluid dynamics, mass transfer coefficients and heat transfer coefficients.

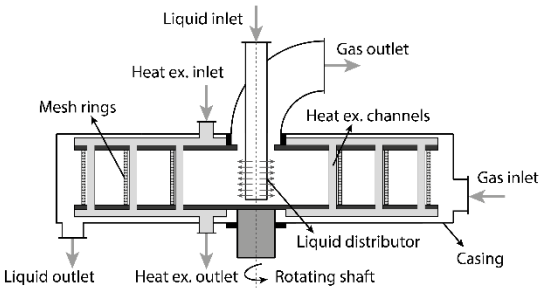

Figure 3. Schematic drawing of the CRPB.

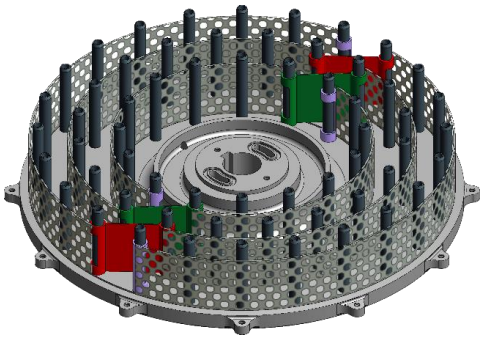

Figure 4. CAD drawing of the rotor of the CRPB with its integrated cooling channels.

This report, as it is part of the initial research, focuses on the physical properties of the liquid that interacts with the redistribution rings. The goal was to quantify the behaviour of the liquid in regimes that determine the performance of the reactor and more specifically the redistribution rings. To achieve this, a special setup was designed and built, the Visual Reactor For CRPB (VIREFOC) setup (Figure 5 and Figure 6). The VIREFOC setup, that holds redistribution rings of the same mesh and diameter as the CRPB but without the diagonal pieces that connect the different rings, is a tool that was designed to aid the research on and gain understanding of the hydrodynamics that can then, later, be applied in the CRPB. Subtopics of interest on the hydrodynamics include the water layer build-up on the redistribution rings, jet or droplet flow through the holes in the mesh, the influence of rotational velocity and liquid flow rate, flight paths of jets and droplets, interactions between adjacent holes and distribution of the liquid through the reactor. The scope of this research is limited to the investigation of the hydrodynamics in the VIREFOC setup. The experimental part of this research, executed in the VIREFOC setup that has a transparent top plate, was done using high speed camera analysis. The analysis with high speed camera equipment allows for direct analysis of the hydrodynamics through the rings. A picture of the VIREFOC setup reactor is shown in Figure 5. The three concentric redistribution rings, mounted between a white bottom plate and transparent top plate can be clearly noticed here.

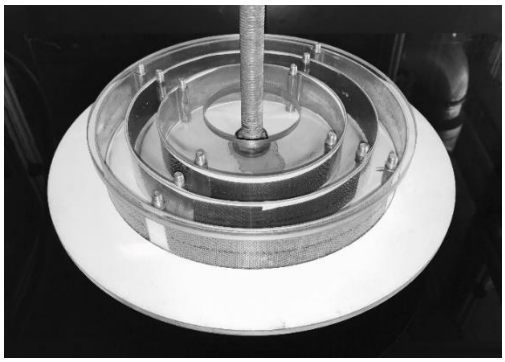

Figure 5. Close-up of the reactor inside the VIREFOC setup used for visual analysis of the liquid flow behaviour through the redistribution rings.

1.3 Thesis outline

This research can be divided in three subtopics. First, the experiments done in the VIREFOC setup (Figure 6 and Appendix A). These gave an excellent insight into fluid behaviour through the redistribution rings. Second, simulations using CFD to generate more detail on the local flow velocities otherwise very difficult to determine in experimental setups (Xie et al., 2017). The third part is the combination of the results into a model that mimics and predicts the liquid behaviour and operating window of the VIREFOC setup which can be used for the CRPB. Below, these three topics are briefly discussed and what can be expected for each of them in the rest of the report.

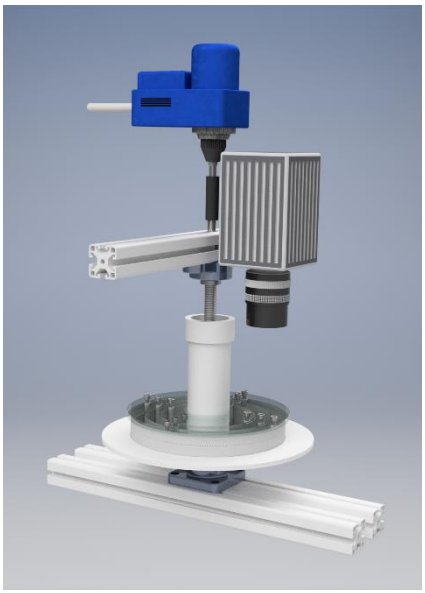

Figure 6. CAD drawing of some of the key parts in the VIREFOC setup.

The experiments in the VIREFOC setup, a setup that is similar to the CRPB but with special modifications to aid the visual analysis, was used to do experiments with a high speed camera. This setup made it possible to empirically determine the different flow regimes, operating ranges and gas liquid interfacial areas.

As from this type of visual analysis it is not possible to directly quantify the local flow velocities through the water layer, jets and droplets, simulations were done using ANSYS Fluent. Some interesting flow patterns were discovered that can justify the results from the experiments.

The results from the experiments and simulations were then used, in combination with equations and knowledge from other literature sources to develop a model in Matlab that simulates the VIREFOC setup. The model requires input about the different operating parameters of the reactor and then uses these to, in a transient way, calculate the operation performance. The knowledge from this model, with slight modifications could be used for the CRPB.

Chapter 2. Methods

As mentioned in the introduction, this research can be divided in three main parts: experiments, simulations and modelling. Each of these parts is introduced below regarding the methods used to execute the particular parts of the research.

2.1 Experiments for visual analysis of the hydrodynamics

For the experimental study on the hydrodynamics through the redistribution rings a special setup was designed. This setup, the VIREFOC setup, has the same redistribution rings as the CRPB but is also, in many ways different as this setup was solely designed for the visual experiments. The main differences between the VIREFOC and the CRPB include:

- The VIREFOC rotor is placed within a transparent and much larger splash cover compared to the tight metal casing around the CRPB.
- The mesh rings in the VIREFOC setup are continuous and not interconnected with baffles like the CRPB.
- There is no option to have a cross current gas flow through the reactor.
- The VIREFOC setup has only one stage of multiple rings while the CRPB has 3 stages of multiple rings.
- The cooling channels are not present inside the VIREFOC setup, instead there are four connecting screws holding the rings in place that are very similar in shape.

The key parts of the VIREFOC setup are schematically shown in Figure 7.

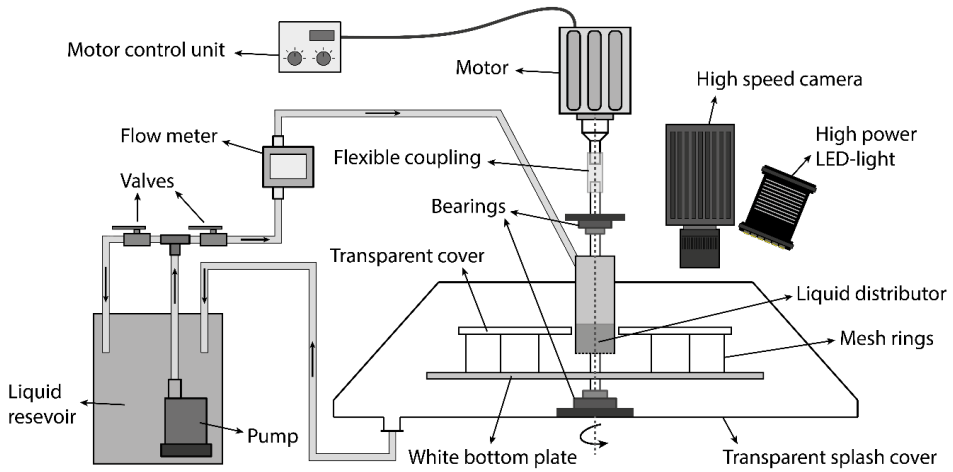

Figure 7. Schematic drawing of the experimental setup for visual analysis in the reactor.

Despite the differences mentioned above, the rings inside the VIREFOC setup have the same diameter and are made of the same mesh as in the CRPB. The liquid is therefore assumed to have a similar flow behaviour through the mesh and water layer build-up in the VIREFOC as in the CRPB.

When the setup is in operation, water is pumped from the reservoir through two valves that are used to control the liquid flow to the reactor. The actual liquid flow is measured using a 100-1000 LPH (Brooks MT3809) flowmeter. The water flows into the liquid distributor, shown in Figure 8, which is fitted inside the feeding tube of the reactor. The shaft runs between two ball bearings that are fixed within the frame and through the top bearing where it is connected via a flexible coupling to the motor (IKA-Werk RE162 10-1600 RPM) that drives the reactor. Using the control unit of the motor it can be rotated at velocities of 50-1500 RPM. The reactor itself

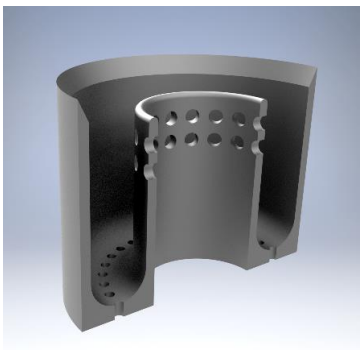

Figure 8. Cut-out of the CAD drawing of the liquid distributor.

has a transparent polycarbonate top cover and a white aluminium bottom plate. Operation can be done using any combination of the three rings and different patterns of open holes were used to investigate the flow behaviour. The analysis is done using the MotionPro X3 plus high speed camera that can record at up to 1000 fps with shutter speeds as low as 1 μs. The camera is used in combination with the constellation 120E15 LED-light which can be synced with the camera for optimal light efficiency. The effective minimal shutter speed, the shutter speed at which the images are clear enough for analysis, is around 11 μs. This is sufficient to eliminate major motion blur in the images, see appendix C.

The experiments were run over a wide variety of flow rates and rotational velocities. The different ranges of settings that were used are shown in Table 1.

Table 1. Operation limits and values for the VIREFOC setup during experiments.

	Lower limit		**Higher limit**	
Liquid flow	0.63	$L\ hole^{-1}\ h^{-1}$	3.86	$L\ hole^{-1}\ h^{-1}$
Rotational velocity	400	RPM	1200	RPM
Shutter speed	11	μs	25	μs
Frames per second	1000		fps	
Frames per experiment	200		-	

The mesh used for the rings has holes of 0.57 mm with an average spacing between the holes of 1.09 mm as illustrated in Figure 9. The diameters of the three rings are 13.6, 18.0 and 22.0 cm with a height of 3.0 cm. This adds up to a total number of holes per ring of $\pm$ 12400, 16400 and 20100 holes respectively. More measurments of the mesh dimensions can be found in appendix B.

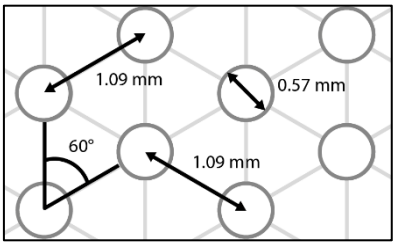

Figure 9. Schematic drawing of the mesh used in the CRPB and VIREFOC.

Since the mesh rings are filled with many holes, for the visual analysis experiments, special patterns were used to investigate the flow behaviour. The large number of jets and droplets would otherwise make it impossible to distinguish them individually. Three different patterns were used that are shown in Figure 10 hereafter referred to as pattern 1, 2 and 3. The main differences between the three patterns are the decreasing distance between the holes and the total number of open holes. For all three patterns the open holes were positioned at half the height of the total mesh ring. These patterns were chosen to investigate how individual holes behave, but also the interaction that adjecent holes could possibly have with a decreasing inter-hole spacing.

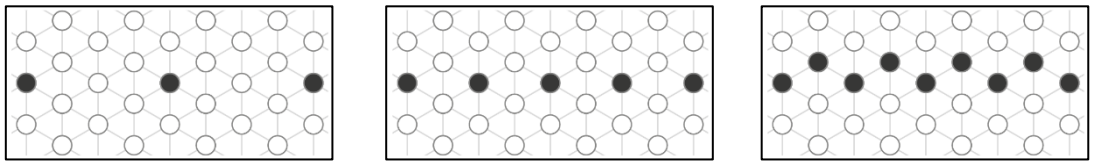

Figure 10. The three patterns used during the experiments. From left to right: Pattern 1; One hole spacing between every open hole on one row. Pattern 2; One complete row of open holes. Pattern 3; Two adjacent rows of open holes.

A thing to note is the way the patterns are made. A special kind of aluminium tape is used to first cover all the holes and then the tape is punctured in the desired pattern. The tape and the manual method of puncturing it could potentially have an influence on the jets and this was thus investigated. To do this, of the four quarters of ring 2, two quarters have the tape on the inside while the other two have the tape on the outside. Although this resulted in visually different configurations between the two methods, it was found not to have any significant effect on the liquid behaviour.

For all three rings, experiments were done with the individual rings to eliminate the influence of the previous rings on the water flow and to remove the obstruction of the next ring in the flight path. This however, is not how the CRPB will be operated so experiments with all three rings or two rings present in the VIREFOC were also executed. The analysis of the experimental results can be found in the next chapter: results and discussion.

2.2 Simulations of a single hole in Fluent

As mentioned before, computational fluid dynamics (CFD) simulations were done using ANSYS Fluent to obtain a greater understanding of the local flow velocities and estimations on the turbulence in the fluid. Since the reactor is approximately symmetrical, only a fraction of a ring has to be simulated to understand the flow behaviour through the holes. Simulating a fraction of the reactor also greatly reduces the simulation cost with the same level of accuracy. Additionally, the academic Fluent license only allows up to 500.000 grid cells which also eliminates the possibility to simulate a larger part of the reactor with a high accuracy. Figure 11 shows the domain for ring 1 that was used during simulations. The domain is a small volume before and after mesh ring 1 with the same cylindrical edges. To mimic the rotation of the CRPB, the domain is subject to a frame motion equal to the demanded rotational velocity with periodic boundaries to allow flow as if the domain was fully cylindrical. To simulate both water and air, a volume of fluid (VOF) method was used that is readily available in Fluent. Furthermore, many other settings have to be chosen to obtain a working simulation and accurate solution. A table with the relevant settings can be found in appendix D. Several cases were simulated with different flow

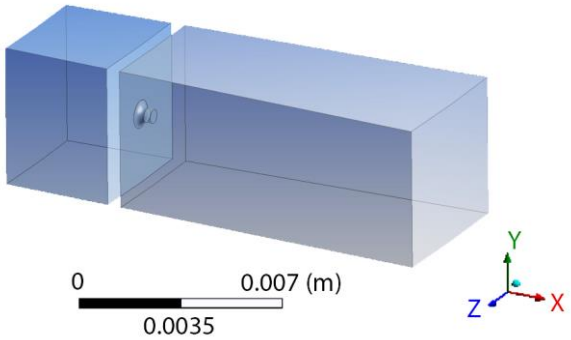

Figure 11. The fluid domain as it was used for the simulations.

rates and rotational velocities to observe the flow at a series of operational parameters. These cases include rotational velocities of 600, 900 and 1200 RPM with flow rates of 1.04 and 2.08 $kg\ hole^{-1}h^{-1}$. These settings for the simulations overlap with the experimental operation values.

The discretization method used by ANSYS Fluent is the finite volume method which was combined with the k-ε turbulence model. The k-ε turbulence model solves two additional partial differential equations (PDE's). One for the turbulent kinetic energy (k) and one for the turbulent kinetic energy dissipation (ε).

2.3 Redistribution ring hydrodynamics model

Using the data from the experiments and knowledge from literature, a mathematical model was written in Matlab to be used as a model for the operation of the CRPB. To accurately calculate the behaviour of the fluid in the RPB, there are several important phenomena to be considered. These include the fluid layers that build up inside the mesh rings, the fluid flight path once it passes through the mesh and the breakup or fusing behaviour of the jets. Provided that all these can be accurately calculated or empirically derived, a well-defined model of the rotating packed bed can be constructed.

To understand the general approach in the model, the different steps taken during the calculation are shown in the block diagram (Figure 12) and shortly discussed. The full code can be found in appendix I.

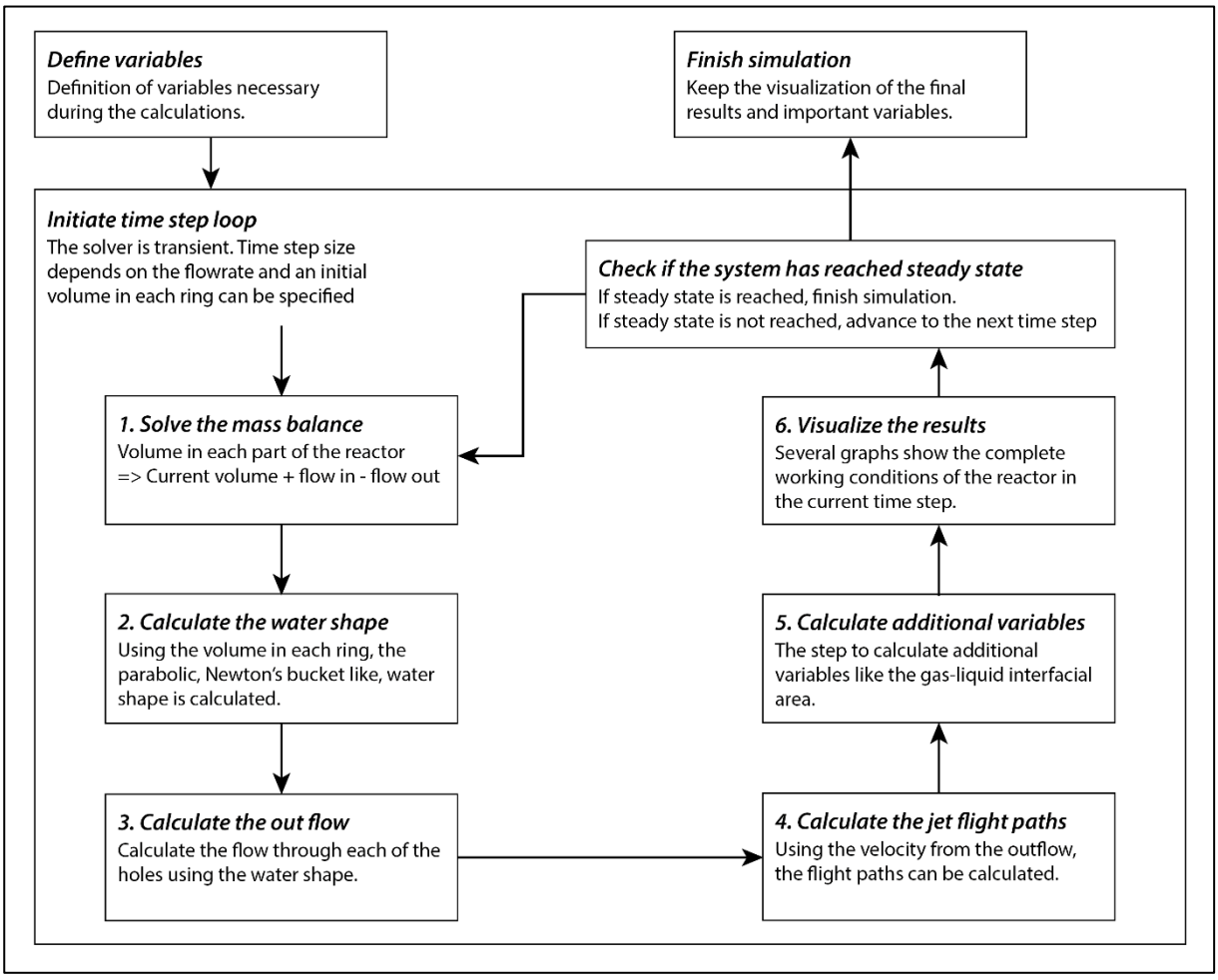

Figure 12. Scheme of the different steps taken during the model created to simulate the hydrodynamics through the redistribution rings.

Step 1: solving the mass balance for the liquid on the inner side of each ring is fairly straightforward. The volume in the film layer inside one ring is equal to the flow into the ring minus the flow out of the ring since there is no reactive term. Equation 1, 2 and 3 show the mass balances for the three rings respectively:

$$\frac{dV_{r,1}}{dt} = \varphi_{in} - \varphi_{holes,r,1} \quad (eq.1)$$

$$\frac{dV_{r,2}}{dt} = \varphi_{holes,r,1} - \varphi_{holes,r,2} \quad (eq.2)$$

$$\frac{dV_{r,3}}{dt} = \varphi_{holes,r,2} - \varphi_{holes,r,3} \quad (eq.3)$$

These equations ultimately reach a steady state, but as can be seen in the code description, the system is solved in a transient way. This was implemented to observe the behaviour as the system is reaching its steady state.

Step 2: the fluid layer shape, is important to calculate since it determines the outflow through every hole in the reactor. To calculate this shape, there are two important factors, namely the volume of water in every ring and the rotational velocity. The rotational velocity determines the parabolic shape of the water layer and the volume in the ring determines the thickness. When the surface tension of the fluid is not taken into account the parabolic shape of a fluid inside a rotating cylinder is well known and follows the following equation (Lubarda, 2013):

$$z(r) = h + \frac{R^2\omega^2}{4g}\left(2\frac{r^2}{R^2} - 1\right) \quad (eq.4)$$

This equation however, cannot be directly implemented to calculate the shape because the water will usually not cover the complete bottom of the cylinder. Further, it actually will touch the top cover of the cylinder resulting in the shape of a ring rather than a cylindrical one except for the inner most compartment. This deviation is illustrated in Figure 13 where the dashed line is the situation from equation 4 and the solid line illustrates a

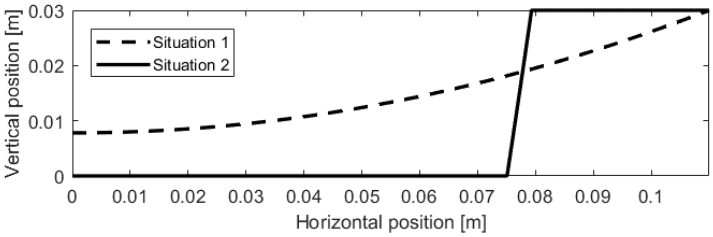

Figure 13. Two examples of water layer shapes in the RPB. Situation 1: 57 RPM. Situation 2: 285 RPM.

situation that will most commonly be observed in the rotating packed bed. At a constant rotational velocity and distance from the rotation axis, the theoretical angle of the water will remain constant but the water is (in the limits) forced to take the shape of the reactor. The angle of the fluid at a certain distance r from the axis can be calculated using a force balance as it depends on the ratio of centrifugal force versus gravitational force:

$$\alpha = \arctan\left(\frac{F_c}{F_g}\right) \quad (eq.5)$$

Where F_g and F_c are the force exerted on the fluid by gravitation and rotation respectively.

$$F_g = mg \quad (eq.6)$$

$$F_c = m\omega^2 r \quad (eq.7)$$

Inserting these into equation 5 gives:

$$\alpha = \arctan\left(\frac{m\omega^2 r}{mg}\right) = \arctan\left(\frac{\omega^2 r}{g}\right) \quad (eq.8)$$

The angles, that give the same water shape as equation 4, were used while coding to determine the final shape of the water layer iteratively. In short, this is done by starting with the water layer shape to touch the top of the ring only at the maximum radius in the ring and either lowering or increasing the level of the water until the volume calculated actually meets the volume present in the ring. Figure 14 shows the initial guess as the solid line and the dashed lines represent the up and down movement of the water shape to find the actual shape with the present volume.

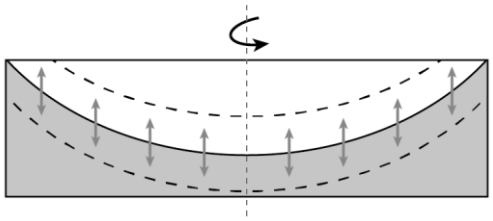

Figure 14. Schematic view of the approach used to find the water shapes.

Once the shape of the water layer is known, the thickness of the water layer exerting force on the holes can be used to calculate the flow through every hole in step 3. To calculate the flow through each hole, a derivation from Bernoulli's equation can be used. It should be noted that to use Bernoulli's equation some assumptions need to be done that should be reasonable for the applied situation. These include a steady flow, which means the velocity is constant in time at any point in the fluid and incompressibility of the fluids (Landau and Lifshitz, 1987; Lautrup, 2005). Bernoulli's equation for fluid along a streamline in a rotating frame like Newton's bucket takes the form of (Mcdonald, 2012):

$$P(r,\phi,z) - \frac{\rho(\omega r)^2}{2} + \rho g z = constant \qquad (eq.9)$$

Where P is the pressure at a certain point inside the fluid that rotates about the z-axis. Neglecting the minimal pressure generated from the height which is 1-2 order of magnitude lower than the pressure from rotation (Figure 15) and with the assumption that the system is symmetrical along its rotating axis ϕ, this leads to (Lautrup, 2005):

$$P_2 - \frac{\rho(\omega r)^2}{2} = P_1 \;=\; P(r) - \frac{\rho(\omega r)^2}{2} = P_{atm} \qquad (eq.10)$$

$$P(r) = P_{atm} + \frac{\rho(\omega r)^2}{2} \qquad (eq.11)$$

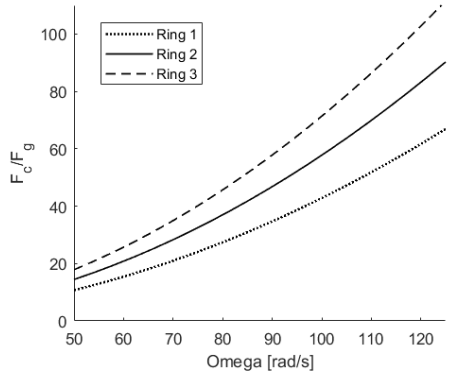

Figure 15. Centrifugal force over gravitational force versus different rotational velocities for all three rings.

In most cases the liquid does not fill up the complete cylinder and only a layer of liquid is present. For this case, as shown in Figure 16, the pressure at a position r_2 in the ring can be calculated by accounting for the reduced pressure due to the change of the liquid surface position:

$$P(r_2) - \frac{\rho\omega^2 r_2^2}{2} = P(r_1) - \frac{\rho\omega^2 r_1^2}{2} \qquad (eq.12)$$

$$P(r_2) = P(r_1) + \frac{\rho\omega^2 r_2^2}{2} - \frac{\rho\omega^2 r_1^2}{2} \qquad (eq.13)$$

$$P(r) = P_{atm} + \frac{\rho\omega^2(r_2^2 - r_1^2)}{2} \qquad (eq.14)$$

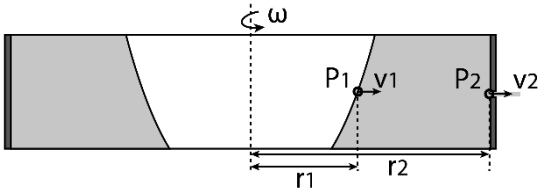

Figure 16. Schematic representation of the variables used in equation 10.

As the flow through the hole depends on the pressure exerted by the liquid on the hole, rewriting Bernoulli's equation as shown below, gives equation 14 that can be used to determine the velocity through one hole:

$$P_1 + \rho g h_1 + \frac{1}{2}\rho v_1 = P_2 + \rho g h_2 + \frac{1}{2}\rho v_2 \qquad (eq.15)$$

Since both points are at the same height and the velocity of the liquid layer is assumed to be negligible, several terms cancel from equation 13 leading to:

$$\frac{1}{2}\rho v_2 = P_1 - P_2 \qquad (eq.16)$$

Inserting equation 12 into equation 14:

$$\frac{1}{2}\rho v_2 = \frac{\rho\omega^2(r_2^2 - r_1^2)}{2} \qquad (eq.17)$$

$$v_2 = \sqrt{\omega^2(r_2^2 - r_1^2)} \qquad (eq.18)$$

Where r_1 is equal to the ring radius minus the water layer thickness and a velocity coefficient C_v should be added to account loss of actual velocity compared to theoretical velocity through the hole (Ghassemieh et al., 2006). This ultimately leads to:

$$v_{out} = C_v\sqrt{\omega^2(r^2 - (r - \delta_{water})^2)} \qquad (eq.19)$$

The volumetric flow rate, which is equal to the total flow, can now be calculated by multiplying with the surface area of the holes:

$$\varphi = A_{holes} \cdot v_{out} = n_{holes}\pi r_{hole}^2 \cdot C_v\sqrt{\omega^2(r^2 - (r - \delta_{water})^2)} \qquad (eq.20)$$

Step 4: the calculation of the fluid flight path can now be done. The liquid flight path, if it exits the ring perpendicular to the ring, has a velocity vector depending on two velocities. These are the radial velocity of the liquid through the ring and the tangential velocity of the ring. As there are no forces working on the droplet once it leaves the ring, this results in a straight flight path, which is in accordance with the two parts of the velocity vector. Rotation of the bed however, causes the shape of a jet to appear different due to the motion of the bed as the jets are flying. The tangential velocity and radial velocity can be calculated using equation 19 and 20:

$$v_\phi = \omega r \qquad and \qquad v_r = C_v\sqrt{\omega^2(r^2 - (r - \delta_{water})^2)} \qquad (eq.21\ and\ 22)$$

When the droplets exit the rings, it holds both velocities which are approximately preserved over the studied length. These velocities have a certain equivalent Cartesian velocity in (x,y)-coordinates. The droplets will each follow the straight path according to this velocity after they leave the orifice. Nonetheless, the liquid streams appear curved in the laboratory frame of reference due to a Coriolis Effect induced by the rotation of the reactor.

The compensation for the rotation of the reactor as the liquid is flying can be done using the following equation:

$$\phi^t_{\text{comp.}} = \phi^t_{uncomp.} + \omega \cdot t_{flight} \qquad (eq.23)$$

Where t_{flight} is the time since the fluid has left the hole. Figure 17 shows the uncompensated and compensated liquid paths. The uncompensated path is the trajectory one droplet follows once it has left the ring, in accordance with equation 19 and 20. The compensated flight path is the actual shape of one jet or droplet stream as they are produced by each hole and visible in the reactor.

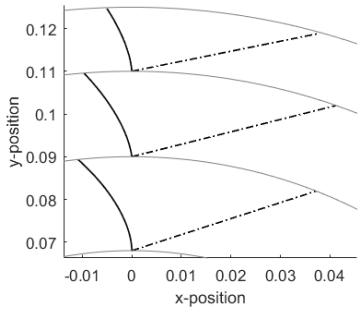

Figure 17. Illustration of the uncompensated flight path (dashed line) and compensated flight path (solid line).

Once the flight paths are calculated, all necessary information about the liquid is known for the reactor and the gas-liquid interfacial area in the reactor can be calculated. The current state of the reactor is then visualised and the model advances to the next time step.

Chapter 3. Results and discussion

In line with the description given on the different parts of this research, the results and discussion are divided in three topics. Starting with the experimental results, followed by the Fluent simulations and the final part is focused on the Matlab model.

3.1 Experimental results of the visual analysis

Many experiments were done with different flow rates, rotational velocities, hole patterns and rings present in the VIREFOC setup. A total of 467 experiments were performed in the setup. The results are therefore subcategorized in several parts where the different phenomena are discussed that were observed in the reactor. Figure 18 and Figure 19 show the flow rates versus rotational velocities for all the experiments that were done. In Figure 18 the flow is expressed in the mass flow per hole per hour, whereas in Figure 19 the flow rates are

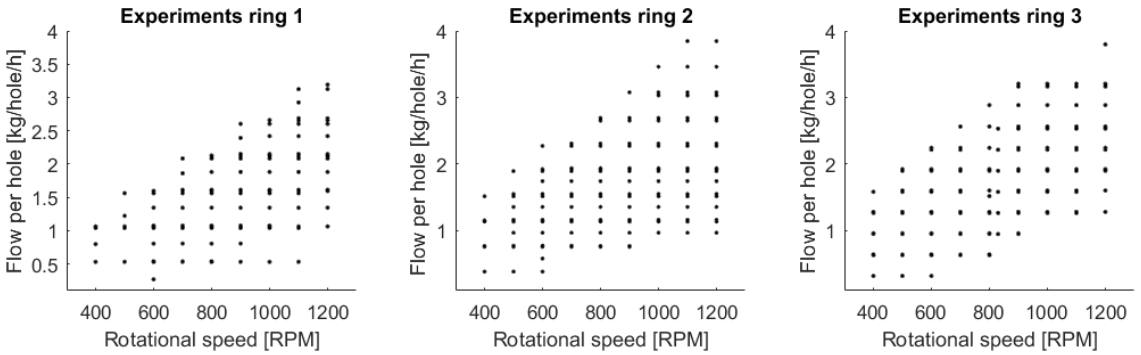

Figure 18. Overview of all the experiments done plotted in three graphs for the different rings. The experiments are plotted for flow rate per hole versus rotational velocity.

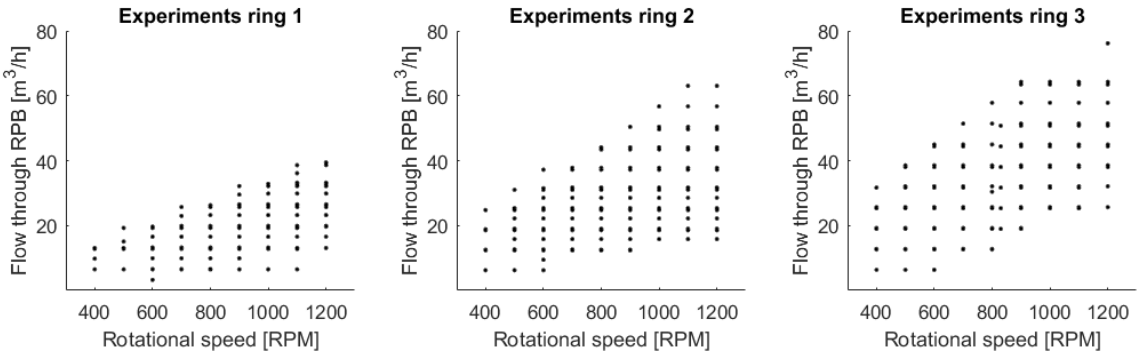

Figure 19. Overview of all the experiments done plotted in three graphs for the different rings. The flow values used during the experiments are converted to total flow values through the CRPB.

converted to total flow rate through the VIREFOC in cubic meters per hour. The holes of each ring can handle similar flow rates but the rings have an increasing number of holes as the radius increases. The operational limit is therefore constrained to the flow rates where all three rings get a sufficient water flow while e.g. ring 3 would be capable of processing much more water than ring 1 due to its greater number of holes.

Figure 20 clearly shows what the reactor part of the experimental setup looks like while in operation with evident visibility of the liquid jets, droplets and redistribution ring 1 (with pattern 1). The visual analysis however, happens from a different angle with a specialized high speed camera, contrary to Figure 20 which is an image taken with a normal photo camera not intended to be used for analysis. Two sample images from the experiments with the high speed camera are shown in Figure 21.

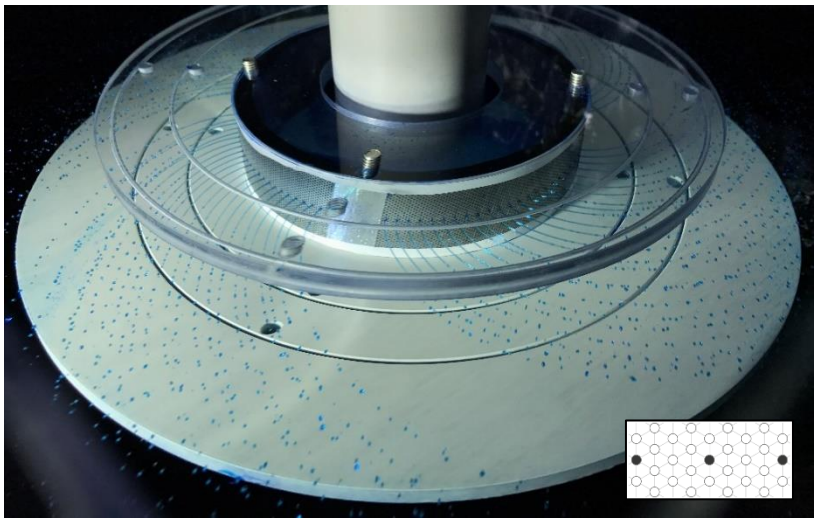

Figure 20. Picture of the reactor in the VIREFOC setup during one of the experiments with ring 1 and pattern one present.

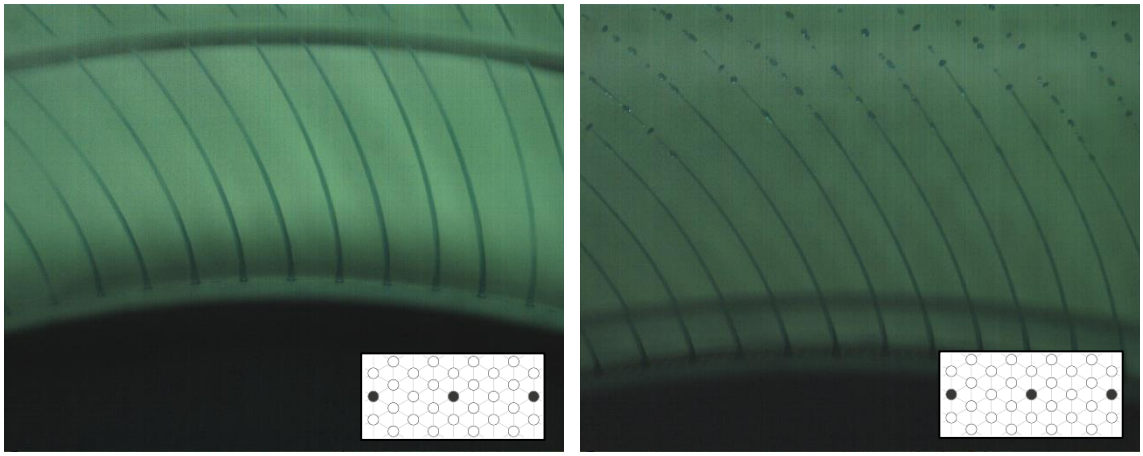

Figure 21. Two sample images from the high speed camera. The image on the left was taken during an experiment with ring 2. The image on the right was taken during an experiment with ring 3.

3.1.1 Jet and droplet flow regimes

The first phenomena considered is the flow behaviour through the holes. The fluid can either leave the holes as stable jets, unstable jets that break up quickly or only droplets. These regimes are important performance parameters as they greatly influence the gas-liquid surface area.

To categorize the flow, jet or droplet, for the experiments, three regimes are defined of which some examples can be found in appendix F. The regimes considered are:

1. Full jet
2. Partial jet
3. Full droplet

The method of creating the patterns in the mesh caused imperfect opening of some holes. This resulted in an abnormal water flow from those particular holes. The number of holes facing this problem however is only very small (up to $\pm$ 2%). Holes experiencing this problem can be easily recognized as their flow clearly differs from the surrounding holes as can be seen in Figure 22. Thus, these holes are excluded from the analysis on the jet and droplet flow regime because they would give a false measurement.

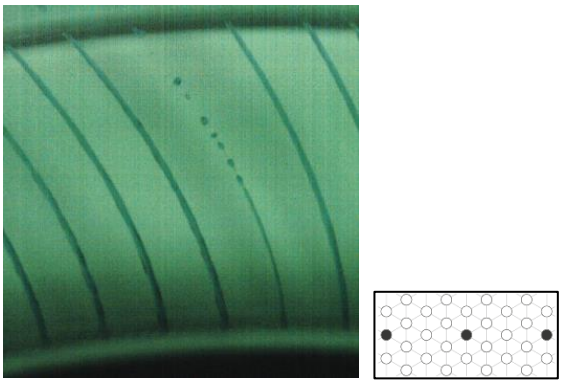

Figure 22. Example of a hole that is not properly opened in the pattern.

Furthermore, the experiments for pattern 3 show a very high level of jet fusing that make it impossible to determine whether there would be jet or droplet flow from the individual jets. Therefore, in the presented results on the flow regimes, only the experiments from pattern 1 and 2 are considered.

Figure 23 shows the regimes found after analysing the data. The regimes to be distinguished in the graphs are the flooding lines, jet flow regime, transition zone and droplet flow and maldistribution regime. For the area above the experimental flooding line, the ratio between the flow and the rotational velocity is too high and the rings fill up with water completely. The flooding values seem to be directly proportional to the rotational velocity but with a different slope for the different rings. This behaviour is explained by the dependency of the fluid velocity through the holes in the mesh as shown in equation 17 in the Methods section. The part on the right hand side shows that the velocity is directly proportional to the rotational velocity (ω) as the quadratic value is inside the root. The theoretical flooding line is also plotted in Figure 23 which shows a high comparability with the flooding line measured during the experiments. The different slopes in these lines arise from the difference in ring radius and maximum water layer thickness for each ring.

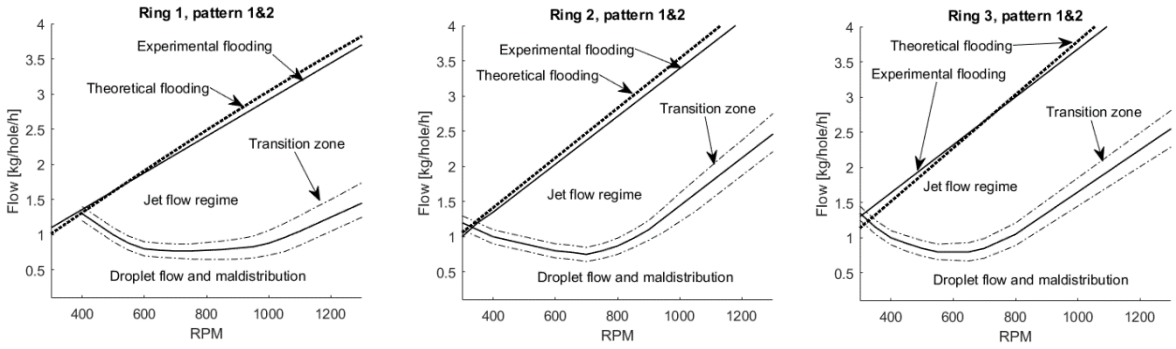

Figure 23. Different flow regimes observed during the experiments for pattern 1 and 2. The main regimes are separated by the solid lines whereas the dotted line shows the theoretical flooding limit and the dashed line the transition zone.

The jet flow regime, droplet flow regime and transition zone in Figure 23 arise from the instability behaviour of a jet and the dependency of the stable length on the velocity and diameter of the jet (Mccarthy, 1974). As the liquid flow increases, the jet velocity increases which results in longer stable jets. A decrease in diameter however, decreases the stable length of a jet as can be derived from equation 22 (Mccarthy, 1974):

$$\frac{Z}{d} = \ln\left(\frac{a}{\delta_{j,0}}\right)\left\{(We)^{0.5} + \frac{3\,We}{Re}\right\} \qquad (eq.24)$$

Where We is the Weber number, equal to $\rho v^2 d/\sigma$, Re is the Reynolds number, equal to $\rho v d/\mu$, Z is the stable length of a jet and d, σ and μ are the diameter of the jet, surface tension and viscosity of the liquid respectively. The term $\ln(a/\delta_{j,0})$ represents the initial instabilities in the jet as it leaves the nozzle and was found to be represented by equation 23 (Mccarthy, 1974):

$$\ln\left(\frac{a}{\delta_{j,0}}\right) = -2.66\ln(Oh) + 7.68 \qquad (eq.25)$$

Where Oh represents the Ohnesorge or stability number equal to $\mu/(\rho d\sigma)^{0.5}$. Using equation 22 to calculate the stable jet length for different jet diameters and velocities, Figure 24 was found. Several different lines are plotted that show the stable length for different hole/jet diameters. It can be observed that thinner jets break up faster, which can accordingly be observed in Figure 22. The one hole that is not properly opened produces a thinner jet that breaks up earlier.

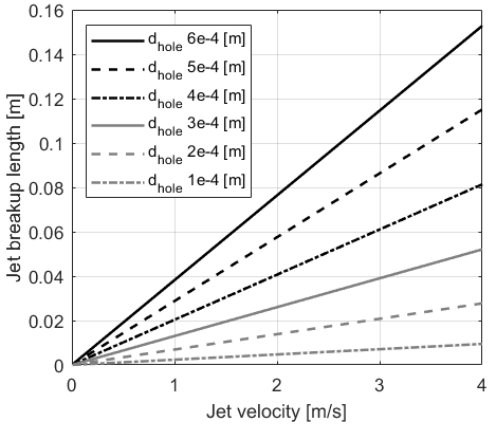

Figure 24. Stable jet length plotted versus the jet velocity for several jet diameters.

To explain the curves in the transition zone in Figure 23, the straight part is explained first. At a constant rotational velocity but with a decreasing flow rate, the jets will at a certain point start to decrease in diameter. The flow rate and thus the velocity through the holes decreases but the velocity of the ring stays equal. This will cause elongation of the jets resulting in thinner jets. As can be seen in Figure 24, a decrease in jet diameter will result in a decrease of the stable jet length. For the straight part of the transition zone, the breakup within the measured range only occurs once the jets become thinner as the jets with the diameter of the hole will always be stable over the measured length in the reactor. However, once the rotational velocity is decreased below 600-700 RPM, even jets with the diameter of the hole start to break up within the measured distance. To compensate this, at lower rotational velocities, a higher flow rate is needed to generate stable jets over the required length.

The exact relation of the jet diameter, velocity and breakup length is an aspect that could be investigated in future research. Investigation of the fit of equation 22 with the jets generated from the redistribution rings, could help to improve the model to describe the hydrodynamics through the redistribution rings.

The flowrates through each of the rings at different water layer thicknesses and rotational velocities can also be plotted in a dimensionless flow map. An elaborate explanation of how the different terms were determined using the Buckingham-π theorem can be found in Appendix E (Szirtes and Rózsa, 2007). The three terms found to plot the dimensionless flow map include two Reynolds like numbers Re' and Re", where Re' is derived for the flow through the holes and Re" represents the flow through the rotating cylinder respectively. The third term which defines the filling of each ring is represented by the water layer thickness over radius of the ring (δ/r) .

Whereas the complete flow map is three-dimensional, there are several lines of interest. These include the lines where the complete rings would be filled and the lines at the maximum water layer thickness in each of the rings (Figure 25). The graph can be used to compare the Re' number of the rotating liquid in the cylinder to the Re" number of the flow through the open area of the redistribution rings. A similar linear dependency can be observed as in Figure 23 for the maximum flow rates through each of the rings.

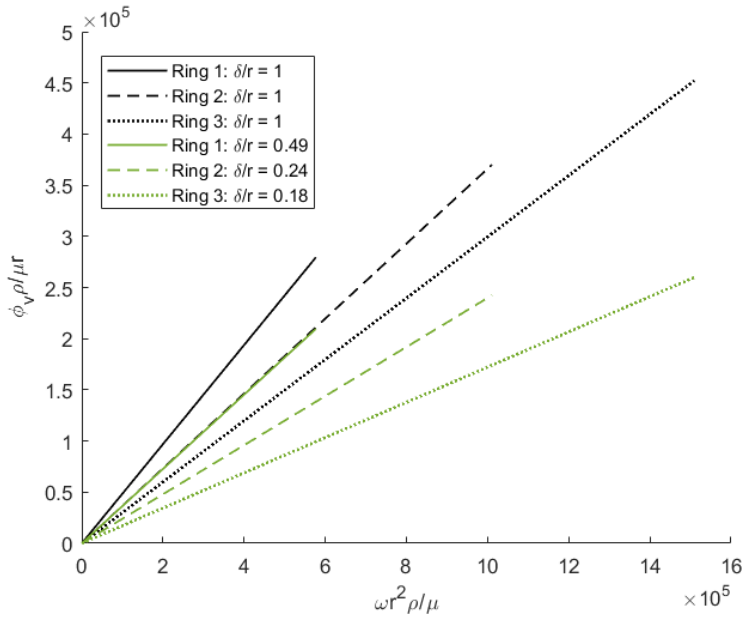

Figure 25. Lines of interest from the dimensionless flow map shown in Appendix E. Two lines are plotted for each ring, one for completely filled cylinders and one for the rings with their respective maximum water layer thickness.

The dimensionless flow map that was generated is not independent of the ring radius and different rings thus needs to be represented by different surfaces as shown in Appendix E. Although a generic representation was not found here, it might be possible to design a flow map where all rings can directly be compared.

3.1.2 Liquid layer build-up

The build-up of a liquid layer on the inside of each of the mesh rings is an important phenomenon in the determination whether the redistribution rings are working properly and the reactor is within its operating range. On the one hand, the liquid layers should be thick enough to have a continuous layer on the mesh to prevent gas flow through the mesh. On the other hand, they should be thin enough not to limit the surface area in the cavity between the rings to a large extent by filling it almost completely or completely. The main parameters influencing the liquid layer are the rotational velocity, liquid in-flow, ring diameter and the flow through the mesh. The rotational velocity and ring diameter can be seen as the variables influencing the surface shape of the liquid while all variables together determine the thickness of the water layer.

The experimental determination of the shape and thickness of the water layer was done in a set of experiments with the light source in a different position. Using this approach, there is enough light to observe the water layers in the rings. The camera lens however, has a very shallow depth of field and obtaining a sharp image of the water layer was therefore very difficult. Some examples of the average images from the water layer thickness experiments can be found in appendix G. After all thicknesses were measured, they were compared with the theoretical thickness of the water layer which can be calculated by rewriting equation 18 to:

$$\delta_{water} = R - \sqrt{R^2 - \frac{\left(\frac{\varphi}{AC_v}\right)^2}{\omega^2}} \qquad (eq.26)$$

This gives the parity plot shown in Figure 26. The experimental and theoretical values are generally in good agreement. The greatest percentage difference is apparent at the smaller water layer thicknesses. The cause for this is the larger relative measurement errors in the experimental values. Additionally, the measured values are slightly higher than the theoretical values which is probably caused by the difference in measurement position. The calculated values are at the height of the holes, while the measured values are taken from the bottom of each ring.

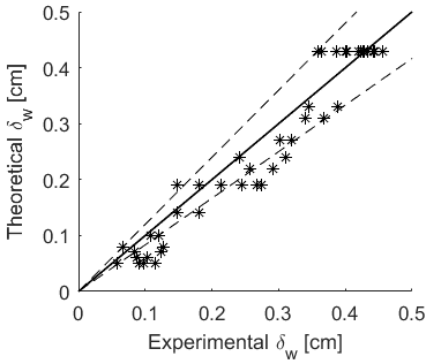

Figure 26. Parity plot with a 20% interval for the experimental water layer thicknesses versus theoretical water layer thicknesses from equation 24.

3.1.3 Jet coalescence

Jets that fly near each other have, due to slight instabilities, a chance to touch each other and coalesce. As this decreases the surface area to volume ratio, it reduces the surface energy. If the force to coalesce is stronger than the force applied to separate (mainly kinetic energy), the jet will remain coalesced of which an example is shown in Figure 27. The jet coalescence is an intriguing phenomena and something that will increasingly occur as the distance between the holes is decreased. The chance of jets touching each other increases and the energy needed to reshape the flight path is reduced. The jet coalescence behaviour observed during experiments mainly occurred

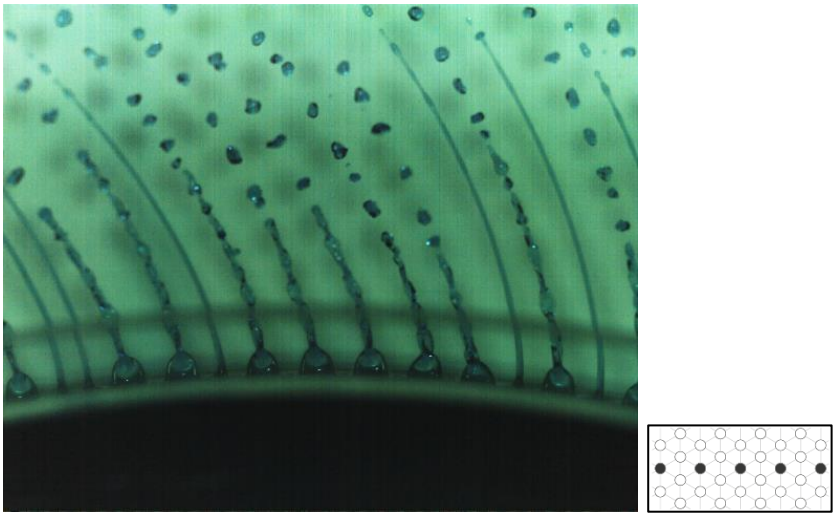

Figure 27. Example of jet coalescence observed in ring 2 with pattern 2 at 400 RPM and a flow of 1.15 $kg\ hole^{-1}\ h^{-1}$.

using pattern 3. Pattern 1 did not experience any jet coalescence, pattern 2 only experienced jet coalescence at low rotational velocities and flow rates but pattern 3 did experience extensive jet coalescence even at moderate rotational velocities and flow rates. Five categories were arbitrarily defined to quantify jet coalescence:

0. No coalescence: 0 - 10% of the jets
1. Little coalescence: 10 - 30 % of the jets
2. Medium coalescence: 30 - 60 % of the jets
3. Lots of coalescence: 60 - 90 % of the jets
4. Complete coalescence: 90 - 100 % of the jets

All experiments were analysed for jet coalescence and the results are plotted in Figure 28. As mentioned before and can be seen in the graphs, jet coalescence mainly occurs in pattern 3 and only in pattern 2 at low rotational velocities and flows. This difference is easily explained by the different separation distances for each pattern. The hole core to core separation distances are 3.74, 1.87 and 0.94 mm for pattern 1, 2 and 3 respectively with the effective average distance between the holes being 3.17, 1.30 and 0.37 mm.

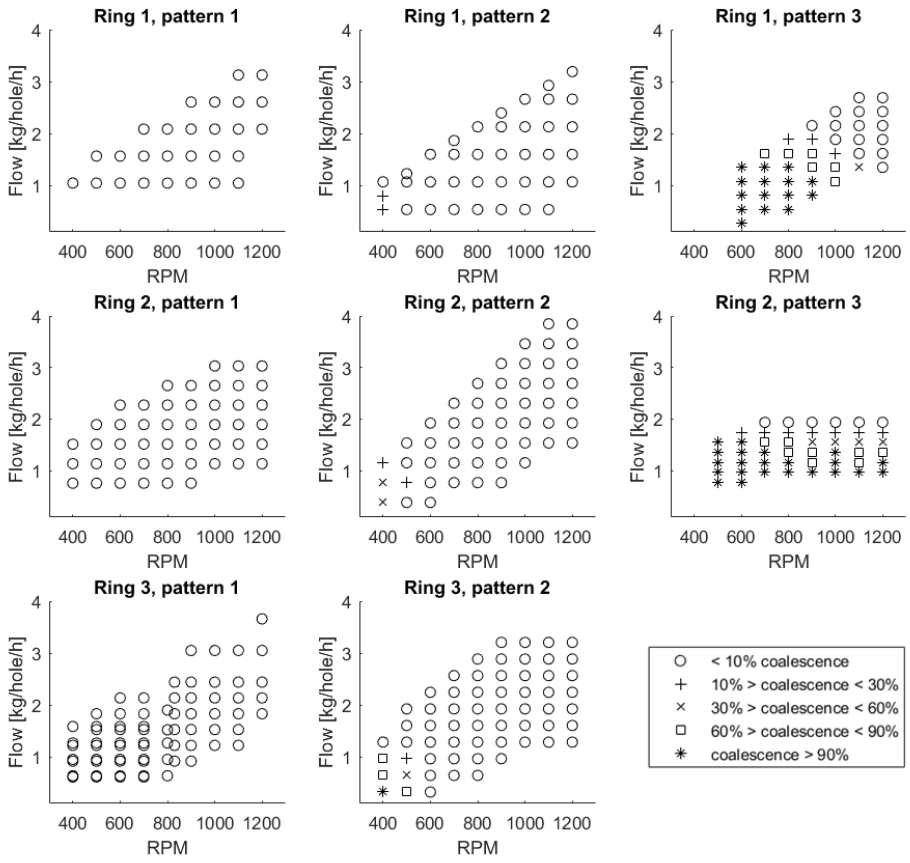

Figure 28. Amount of jet coalescence for every experiment plotted versus flow per hole and rotational velocity.

Jet coalescence of two or even multiple jets has a big influence on the gas-liquid interfacial area. To calculate the decrease of surface area compared to all individual jets, the following approximation equation can be used, assuming that all jets are round:

$$\frac{A_{coal.}}{A_{singles}} = \frac{\pi D_{coal.} L}{n_{coal.} \pi D_{single} L} = \frac{\pi\left(2\sqrt{n_{coal.}} \cdot a_{single}\right) L}{n_{coal.} \pi D_{single} L} = \frac{2\sqrt{n_{coal.}} \cdot a_{single}}{n_{coal.} D_{single}} = \frac{1}{\sqrt{n_{coal.}}} \qquad (eq. 27)$$

Where r_{single} and D_{single} are the radius and diameter of single jets, $D_{coal.}$ is the diameter of the coalesced jets and $n_{coal.}$ is the number of jets that coalesce into one jet. Figure 29 shows the effect on the surface area where it can be observed that if every two jets coalesce together, the surface area is already decreased to 70.7 % of the original surface area.

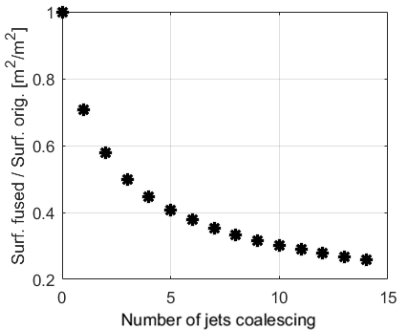

Figure 29. Decrease of surface area as more jets coalesce together. The number of jets coalescing stand for the average number of jets that coalesce into one inside the reactor.

The jet coalescence is problematic for an even distribution of the liquid by the rings and also when the interfacial area is important for the operating performance of the reactor. Besides the increase of the inter-hole spacing, a

surface treatment of the rings might help to decrease the coalescence. The surface treatment should decrease the liquid adhesion to the rings which would decrease the likelihood of liquid film formation between jets which is an important factor in the coalescence. The tiny liquid films can be clearly observed in Figure 27. Investigation of the optimal inter-hole spacing or surface treatment for individual jet formation could be done in future research.

To get an idea of the severity of the jet coalescence in pattern 3, Figure 30 shows some examples of heavy coalescence. It can be observed that once a large number of jets coalesce together, a film of water is formed that takes more time to fully coalesce to a single jet. Additionally, the flow in coalesced jets is disturbed and jets tend to break up earlier. Jet coalescence might also become even more severe when more rows of open holes are present.

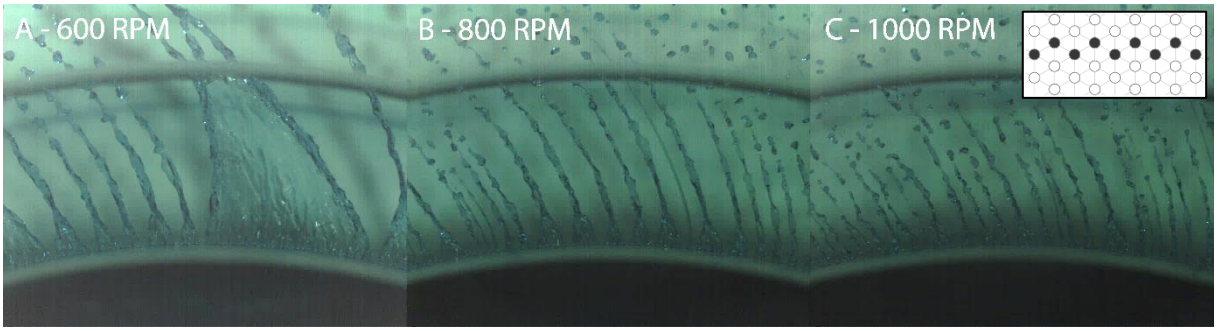

Figure 30. Three images from experiments done in ring 2 using pattern 3. The images have different rotational velocities of 600, 800 and 1000 RPM but an equal water flow rate of 1.16 $kg\ hole^{-1}\ h^{-1}$.

3.1.4 Liquid flight path

The jets that are formed by the redistribution rings flow through the tiny holes in the mesh. Due to the rotation, the jets take a certain shape depending on rotational velocity and water flow. Although the liquid flight path of an individual liquid element is a straight line, due to the Coriolis Effect, the visual jets in the reactor have a different shape. Where the flight path is a straight line away from the hole and the visual jet is a curved path as shown in Figure 17 in Methods. Figure 31 shows the jets from three different experiments fused into one image at 800 RPM with liquid flows of 2.65, 1.89 and 1.14 $kg\ hole^{-1}\ h^{-1}$ for the dotted, dashed and solid line respectively. It is clearly visible that at higher flow rates of liquid, the jets are less curved. This is a simple cause of the increase in radial velocity with a constant displacement by rotation.

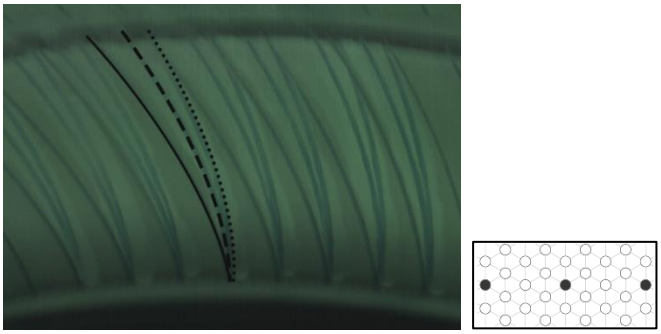

Figure 31. Jets from three experiments at 800 RPM. Dotted line: 2.65 $kg\ hole^{-1}\ h^{-1}$; Dashed line: 1.89 $kg\ hole^{-1}\ h^{-1}$; Solid line: 1.14 $kg\ hole^{-1}\ h^{-1}$.

The flight path of the liquid follows the paths that can be calculated using equation 19 - 20 with high accuracy. However, when the flow rate to rotational velocity ratio is low, the jets start to deviate from the calculated paths. The flight path is more curved than predicted by the equations. This deviation from the normal liquid flight paths at low liquid flow rates could be influenced by the way the liquid flows through the holes. Figure 32 shows an example where the water layer on the ring is thin but jets are still formed. Contrary to experiments where the water layer is thicker, an indent in the water layer can be observed here at the position of the holes. This indent will cause a different flow of the water towards the hole as it cannot hold the nice spherical shape that was found and is discussed further on in the results part for the simulations. The difference in flow towards the hole might prefer the flow from one side of the hole which causes a slight angle in the flow through the hole. To support

this thought, the diameter of the holes is the same as the thickness of the rings. The liquid therefore does not have time to be forced into the direction of the hole but could flow at the slight angles which are observed. If this hypothesis is true the effect should occur less when there are longer flow channels which could be tested with thicker mesh rings. This is something that could be investigated in future research although it does not have a big impact on the performance of the rings.

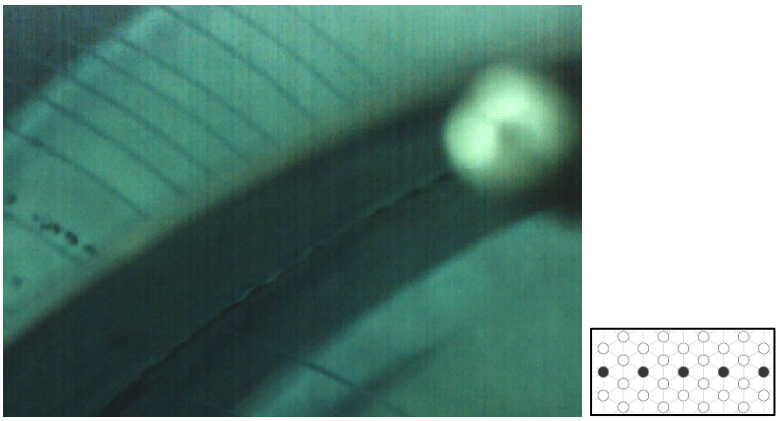

Figure 32. Close up view of the indent in the water layer around the holes that occurs when the water layer on the redistribution ring is very thin.

3.1.5 Fluid maldistribution

As the rings are meant to redistribute the liquid for a better performance of the reactor, it is important to analyse the distribution of the liquid. One effect that was apparent during the experiments is maldistribution of the liquid at relatively low liquid flows. The main causes for this effect are the anchor points for the redistribution rings that prevent free flow of the liquid on the rings. Figure 33 schematically shows this effect. The liquid inside ring 1 is well distributed as the layer thickness is greater than the thickness of the anchor points and the water can thus freely flow between the different quadrants of the reactor. In ring 2 however, the liquid flow rate is too low to establish a liquid layer similar to the one in ring 1. The jets coming from ring 1 that feed ring 2 have a constant tangential velocity that is lower than the tangential velocity of ring 2. The liquid therefore will accelerate as it comes in contact with ring 2. The time it takes for the acceleration determines the final position of the water in the ring. As the liquid is accelerating, the net movement of the liquid through the ring is in the direction opposite of the rotation and accumulation will therefore occur behind the anchor points as shown in Figure 33. This effect, which was only apparent in the visual analysis during very few experiments, should be avoided whenever possible as it greatly reduces the performance and limits the operating range of the reactor.

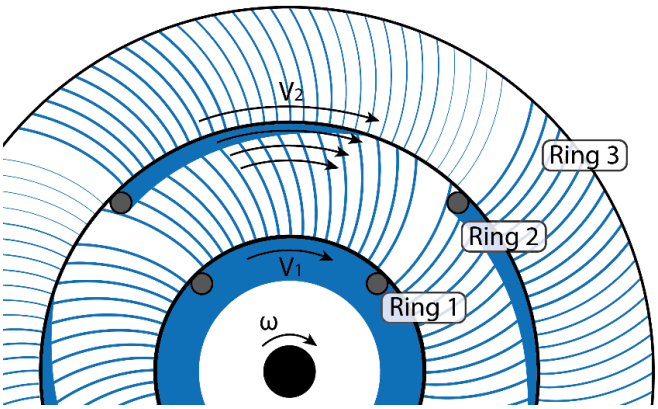

Figure 33. Schematic view of the maldistribution effect that can occur due to the presence of anchor points and cooling channels present in the reactor.

Two cases, one without and one with maldistribution are shown in Figure 35 and Figure 34. The effect, if present in ring n will also amplify itself in ring n+1. The individual cases where maldistribution was apparent only occurred in the droplet regime where the liquid flow is very low compared to the rotational velocity.

Figure 35. Example of an experiment with proper distribution of the water.

Figure 34. Example of an experiment with maldistribution of the fluid. It is clearly visible that the holes on right lack the water to produce similar jets as seen on the left.

3.1.6 Fluid distortion by previous jets/droplets

Smooth, identical jet generation only occurs if the liquid flow through the holes is equally smooth. During the experiments with only one ring present in the reactor, liquid layer build-up and the flow inside the liquid layer seemed to be smooth enough to generate these jets under the right conditions. The experiments with two or more rings present in the reactor however, seemed to have problems generating proper jets. Figure 36 compares two experiments at the same rotational velocity and flow rate but different rings present in the setup. The image on the right, with two rings present, clearly shows more distortion in the jets while all other conditions were the same during both experiments. The effect that is observed can easily be explained by distortions in the liquid layer due to the impact of the jets and is less apparent with thicker layers of water on the rings. The radial velocity of the jets is an order of magnitude higher than the radial velocity of the liquid layer (with the patterns used during the experiments) and an impact will therefore distort the fluid layer to a large extent. The ratio between the radial velocities will be smaller during real operation with all holes open as the velocity through the holes will not change but the radial velocity of the liquid layer will be several times higher. Equation 26 calculates the ratio between radial jet velocity and liquid layer velocity which depends on the surface area available for flow.

$$v_{ratio} = \frac{v_{rad,jets}}{v_{rad,layer}} = \frac{\varphi_{in}/A_{holes}}{\varphi_{in}/A_{ring}} = \frac{A_{holes}}{A_{ring}} \qquad (eq.28)$$

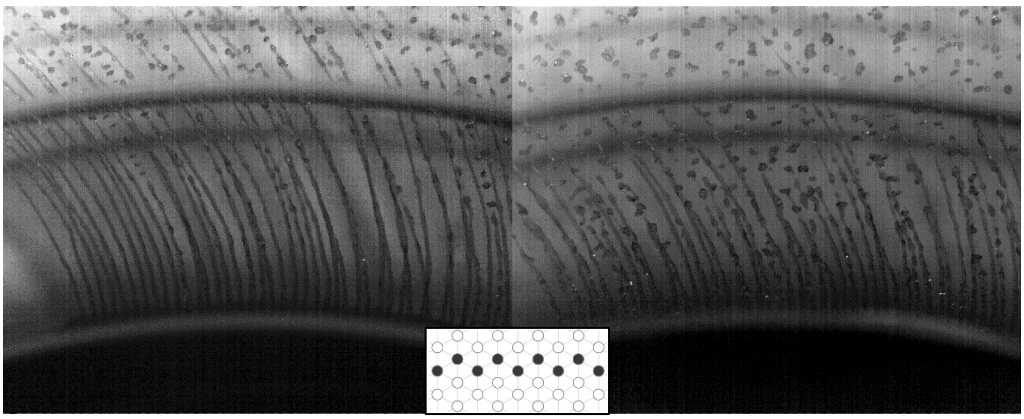

Figure 36. Comparison of two experiments focussed on the jets of ring 2. Image on the left: 1100 RPM, 1.94 $kg\ hole^{-1}\ h^{-1}$, pattern 3 and ring 2 present. Image on the right: 1100 RPM, 1.94 $kg\ hole^{-1}\ h^{-1}$, pattern 3 and both ring 1 and 2 present.

The decrease in the ratio of radial jet velocity versus radial liquid layer velocity might decrease the distortion effect. This possible decrease and the exact influence of the distortion on the reactor performance is difficult to quantify and will also have to be investigated in future research. Figure 37 shows the effect of the distortions in the fluid layer in one picture together with undisturbed jets. The left side (left of the red line) of the image suffers from jet impact as can be seen on both rings. The right part is not affected by the jets as the part of the previous ring is covered and thus does not produce jets.

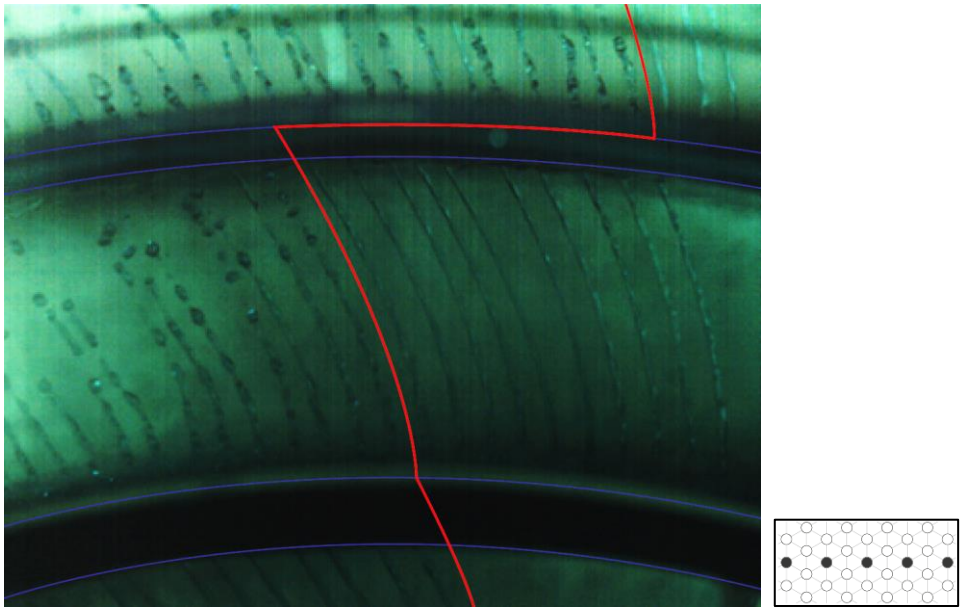

Figure 37. Image from the experiment at 1000 RPM with pattern 2 and a water flow rate of 1.92 $kg\ hole^{-1}\ h^{-1}$ for ring 2.

Additionally, the thickness of the water layer on a ring influences the amount of distortion by jets from previous rings. When a thicker water layer is present, there is more liquid to absorb and damp out the disturbances created by incoming jets.

3.1.7 Overall result experiments

The experiments show an overall good performance of fluid distribution by the rings. There is however only a limited range of liquid flows and rotational velocities where all three rings are in a well performing window in terms of the water layer thickness. Ring one, as it has less holes and a smaller radius than ring two and three, is not able to process as much liquid since the centrifugal force and flow area are smaller. The requirement for proper jet formation to create a high gas-liquid interfacial area limits the range even more. When all holes are open, jet velocity needs to be in the upper limit to prevent extensive jet fusing. Operation in the upper limit of the jet velocity requires operation with high liquid flow rates. This increases the water layer thickness on the rings and reduces the length of the jets resulting in a decrease of the interfacial area. It therefore might be beneficial for the operation of the reactor to investigate the operation with different types of meshes. A slight increase in the inter-hole spacing could greatly reduce the jet fusing behaviour. Also, due to the different sizes and curvatures in the three rings, the first ring is not able to process as much water as the third ring but will experience less jet fusing. Use of three different meshes for the three rings might be an option to overcome the limitations due to different capacities of the rings. The rings would then need to be produced from a mesh with an increasing inter-hole spacing as the ring size increases. This equalizes the liquid flow capacity of the different rings and decreases the jet fusing for rings with the smaller curvature.

3.2 Single hole Fluent simulations

The simulations in ANSYS Fluent were used to better understand the local flow inside the water layer and its turbulent properties. The three cases used during the simulations are discussed below and were analysed to create a greater insight on the flow through the hole, flight path and turbulent intensity.

The nature of the flow through the holes seems to be laminar as the jets are very smooth for the experiments with one ring present in the reactor. A quick estimation of Reynolds number gives us (for flow velocities between 5.5 and 0.8 m/s used in experiments) a Reynolds number between 2740 and 400 which is mostly within the laminar regime and partially in the transition regime (Laminar Re < 2000, Turbulent Re > 3000) (Janssen and Warmoeskerken, 2006). When analysing the flow through the hole in the simulations, this laminar flow is also observed. Figure 38 shows the radial velocity within the domain plotted as a contour plot (grey) and velocity vectors scaled by the radial velocity. The same results for half the flow rate can be found in appendix H. To be observed is the almost round shape of the contour plot around the hole that indicates that the fluid is pushed through the holes evenly from all directions. Notably is that the radial flow velocity through the hole is almost identical for the three cases as the inflow into the domain is the same. The main difference between the three rotational velocities is the direction of the velocity vectors.

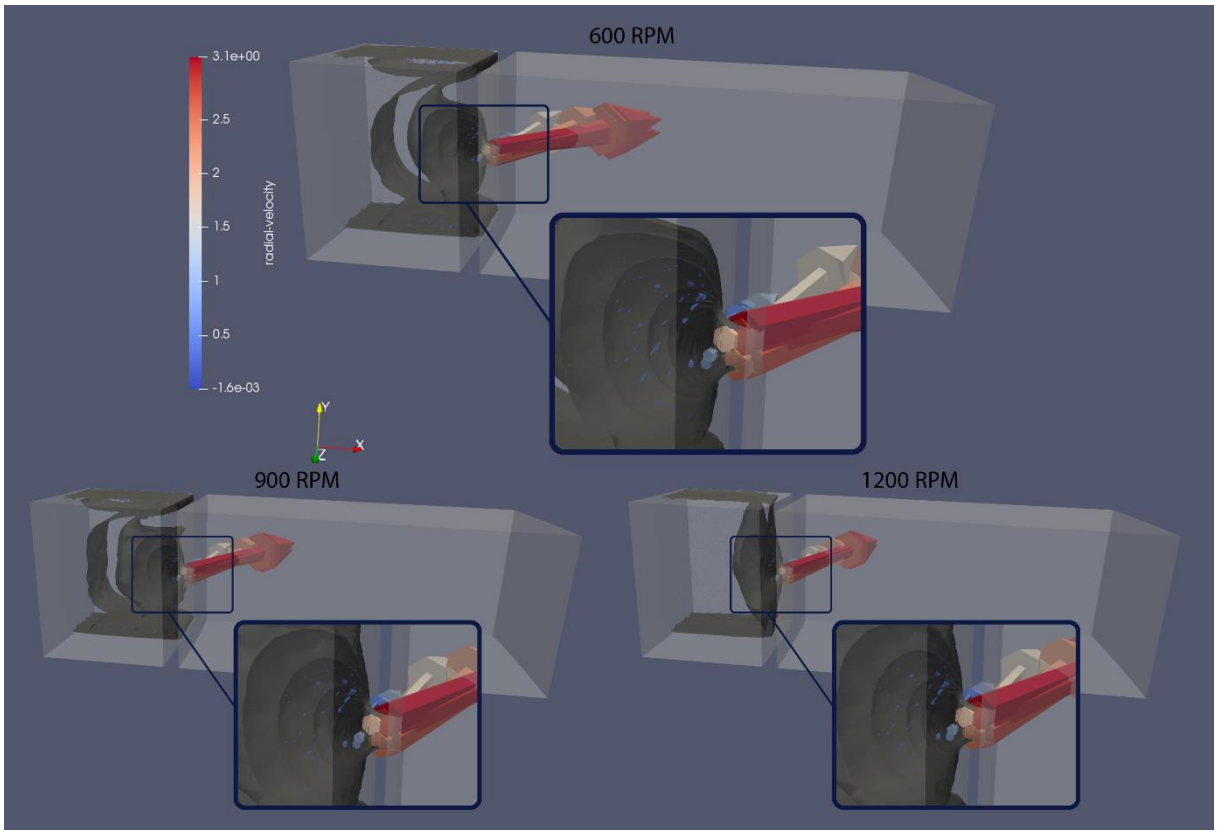

Figure 38. Contour and vector plot of the radial velocity inside the simulated domain at a rotational velocity of 63 rad/s (600 RPM), 94 rad/s (900 RPM) and 125 rad/s (1200 RPM) at a flow rate of 2.08 $kg\ hole^{-1}\ h^{-1}$.

The flight path of the jets, which depends on the rotational velocity and radial jet velocity, as described in equation 19 and 20 can also be observed and compared to the theoretical paths. The flight paths, shown in Figure 39 qualitatively show a level of similarity with the predicted flight paths from theory. However, the paths during the simulations are all more curved than the paths as predicted from theory. Both for the cases with a flow rate of 2.08 and 1.04 $kg\ hole^{-1}\ h^{-1}$ (the latter can be found in appendix H). The simulations follow the behaviour of more curved jets at higher rotational velocities.

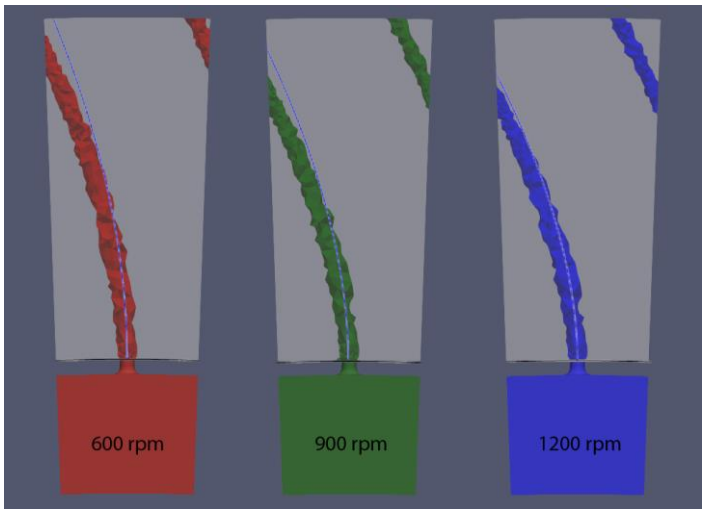

Figure 39. Liquid flight paths of the simulations with a flow rate of 2.08 $kg\ hole^{-1}\ h^{-1}$. The theoretical flight path are shown as a thin line on top of the simulation results.

The turbulence in the jets determines the amount of gas-liquid mass transfer. Ideally, the turbulence would be high and the surface area large to increase mass transfer. Figure 40 shows the turbulent intensity of the jets according to the simulations. Because there is a transition zone from liquid to gas in the CFD simulations, there appears to be an increased turbulent intensity in the jets. This increased turbulent intensity however, is in practice probably in the gas layer around the jet as the inside of the jets shows a value approximately similar to the inlet turbulent intensity of 5%. A turbulent intensity value of 5% is on the transition of medium to high turbulence cases and indicates that there will be some surface renewal as the turbulent intensity defines the smoothness of the flow and velocity fluctuations (ANSYS Inc., 2018). The mixing in the liquid layer on the rings however, will probably have a much larger influence as the residence time in the jets is very short and the impact on the liquid layer fairly large, hence the disturbance of the liquid jets from the next ring. Jet flight times are within the range of 0.0275 and 0.004 seconds for radial velocities of 0.8 to 5.5 m/s and a travel distance of 2.2 cm.

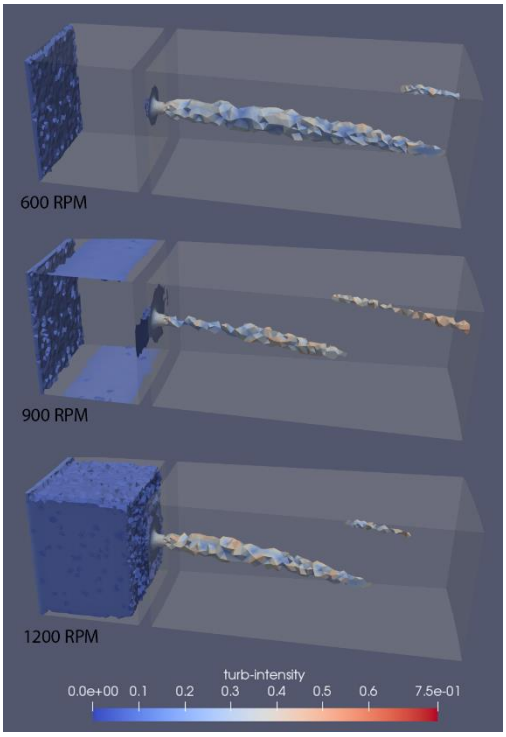

Figure 40. Turbulence intensity levels of the three simulations run with the flow of 2.08 $kg\ hole^{-1}\ h^{-1}$.

3.3 Redistribution ring hydrodynamics model

The results gathered from the experiments and simulations as well as knowledge from literature were combined to create a model of the VIREFOC reactor that could be used to predict the operating conditions in the CRPB. The components incorporated into the model as mentioned and described in the methods are:

- Mass balance over the different rings
- Water layer shape calculations
- Water flow through the holes at different heights
- Jet flight path calculation
- Interfacial gas-liquid area calculation

Most of the parts were initially modelled seperately and later combined to create one model that calculates the operation in a transient way. Figure 41 is an example of what the results look like. In this example the reactor is operated at 900 RPM with a flow rate of 2 $m^3\ h^{-1}$ through five rows of holes in every ring with 188, 260 and 312 holes for ring 1, 2 and 3 respectively. The shape of the water layers is shown in the wide graph at the top.

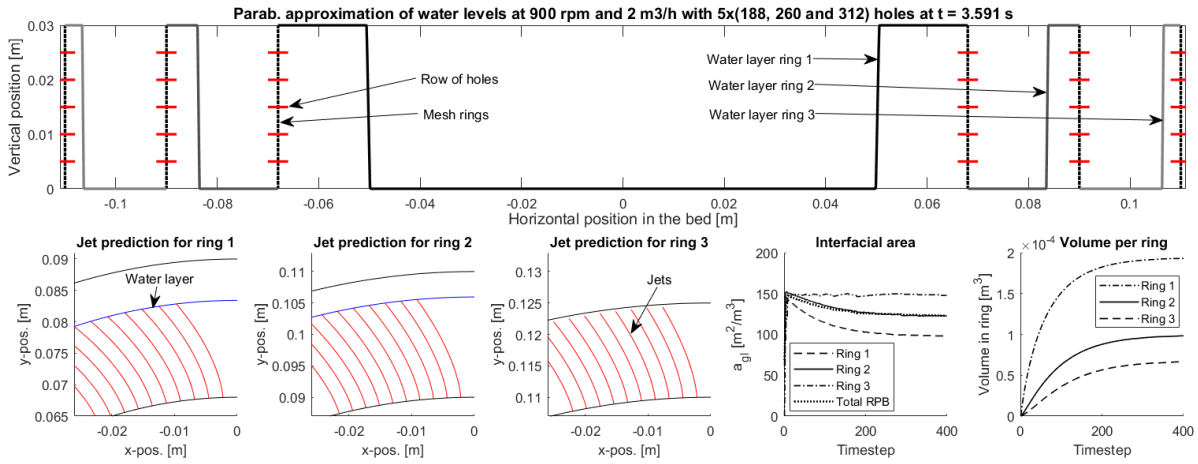

Figure 41. Visualization from the Matlab model to calculate the operation of the VIREFOC setup.

The first three figures at the bottom show a prediction of the jet shape for the bottom most holes in each ring and the remaining two graphs at the bottom show the interfacial gas-liquid area and volume in each ring over time. Note that the interfacial area experiences a decrease over time as the amount of liquid in each ring increases and the length of the jets is reduced. The jets also experience a slight decrease in length because of the increase in velocity as the water layers grow. This effect (to be observed in the line for ring 3 in Figure 42) however, is neglegible compared to the decrease in length due to water layer growth. The volume and interfacial area clearly show the systems approach to the steady state situation. The time to reach steady state depends on the number of open holes and the rotational velocity as these determine the residence time of the liquid.

3.3.1 Model verification

Some of the individual parts of the model have already been compared to experimental results and justified in the experimental results and discussion section. The complete model should however, also be verified to determine its reliability. For this verification, it can only be compared to the experimental results in the VIREFOC setup, the water layer thickness and jet flight paths are compared. These variables are the best indication of the model accuracy in this stage of the research. Additionally, the limits of the model e.g. flooding and insufficient filling can be tested.

The model is designed in a way that the reactor parameters e.g. number of open holes, hole diameter, inter-hole distance, ring diameter and ring height can all be modified without breaking the model. Virtually the only requirement is that the reactor holds three rings. Also, some safety measures are build into the model that increase it's operability. Two examples are the limits of the water layer and the jet formation. If the water flow is either too high or too low for proper operation of the reactor, the rings will flood or only partially cover the

redistribution rings. If the water flow is too high, and one or more rings fill up, the outflow through the holes automatically switches to the inflow. If there is insufficient water flow for proper operation, the holes not covered by the water layer produce no jets. Both of these measures would also occur in the VIREFOC and CRPB setup. To check if these systems work, two graphs where these effects can be observed are shown in Figure 42. The jumps in the increase of interfacial area indicate the points where new holes are covered by the water layer and start producing jets. The sudden angle changes in the volume lines best indicate the flooding of certain rings. The changes can also be observed in the interfacial area graph but are less apparent. Also worth noting is the point where ring 2 floods and the jets from ring 1 naturally have no interfacial area anymore.

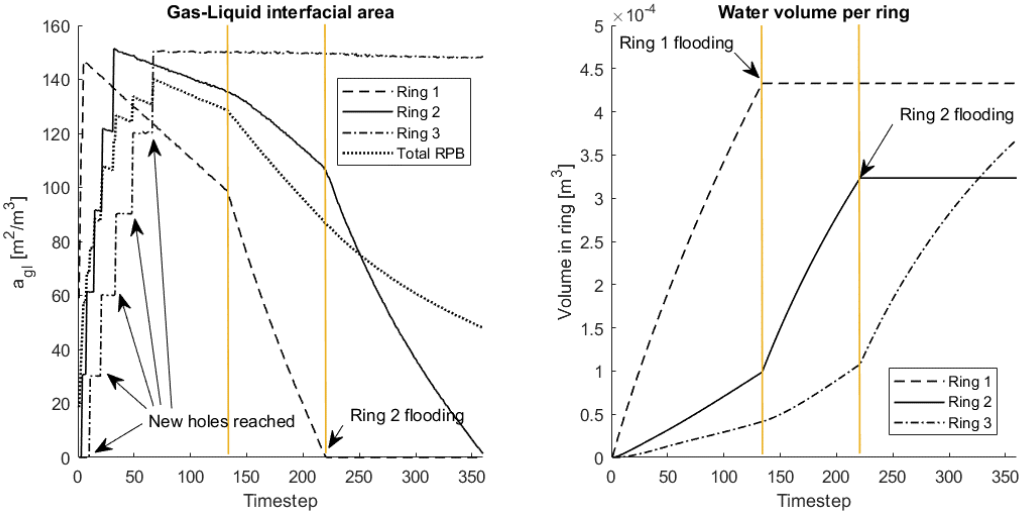

Figure 42. Enlarged version of the interfacial area and volume per ring graphs from the model visualization. The vertical lines depict the flooding time of ring 1 and ring 2.

To validate the models accuracy in calculating the water flow and water layer thickness, several experimental and theoretical cases were compared. Individual data from the different rings is compared to the model results because no experiments were run with all rings present in the system where a complete view of the reactor was possible. The water layer thickness was compared for several cases between the experimental and model data. The thicknesses were measured for both and a parity plot is shown in Figure 43 with 20 % deviation. There was no data available from the experiments on the water layer thickness in ring 1 but the results from ring 2 and 3 show a good correlation between the experimental and modelled water layer thickness. An extra set of experiments can be done in future research but since the thickness depends on a right calculation of the flow through the holes and water layer shape, it can be concluded that these calculations are done accurately. This implies that for ring 1, the values should have a similar high correlation between experimental and modelled data. Together with the water layer shape, the liquid flight paths were compared to the experimental data. The experimental and modelled jets were compared visually of which some examples are shown in Figure 44. The examples show the jets from the three rings at 1100 RPM for two different flow rates for each ring. The jets at

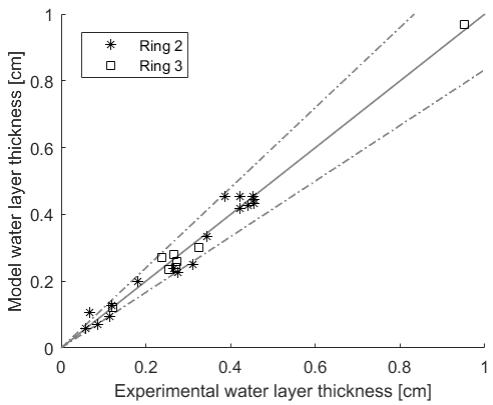

Figure 43. Parity plot with a 20% interval for the experimental and model water layer thickness.

the highest flow rates (the left images) show excellent correlation with an outflow angle of 0 degrees. This means that the flight velocities are equal to the tangential velocity of the ring and radial velocity through the ring. The images on the right however, at lower flow rates need compensation in radial and tangential velocity to achieve the best fit with experimental data. The applied velocity compensations using an outflow angle are 5, 8 and 15 degrees for ring 1, 2 and 3 respectively. The exact cause of this effect is yet unclear as mentioned in the experimental results on the liquid flight path. The hypothesis proposed is that the deviation is cause by a slightly angled flow through the holes, however, this needs to be investigated in future research.

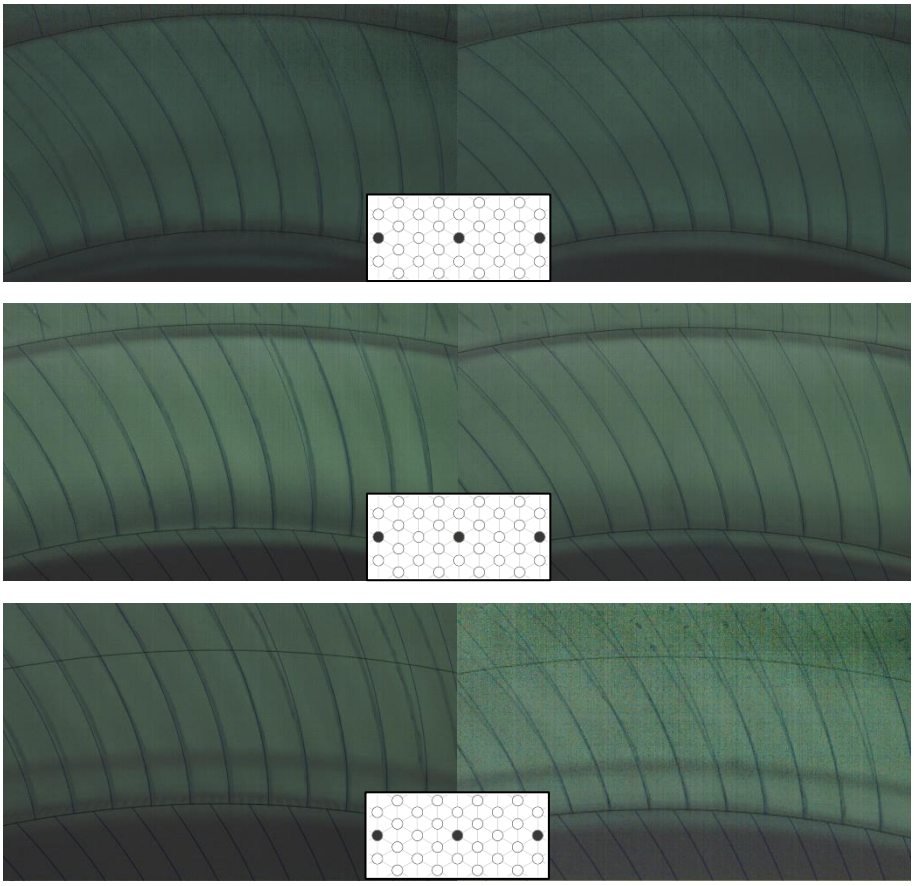

Figure 44. Images from experiments at 1100 RPM with pattern 1 with an overlay of the calculated jet paths. The upper two images are taken from ring 1 at a flow rate of 2.6 (left) and 1.0 $kg\ hole^{-1}\ h^{-1}$ (right). The middle two images are taken from ring 2 at a flow rate of 3.0 (left) and 1.5 $kg\ hole^{-1}\ h^{-1}$ (right). The bottom two images are taken from ring 3 at a flow rate of 3.0 (left) and 1.8 $kg\ hole^{-1}\ h^{-1}$ (right). The images on the right needed a flight path compensation of 5, 8 and 15 degrees for ring 1, 2 and 3 respectively.

3.3.2 Optimum operating conditions

Combining the knowledge gained from the experiments, simulations and Matlab model, an optimum operating range can be found. For the optimal operating range it is important that all three redistribution rings are fully covered with a layer of water while leaving maximum space for the jets. This prevents unwanted gas flow through the rings. Also, the majority of the holes should produce steady individual jets with the least amount of fusing or breakup. To find the best operating condition, the graphs on jet fusing (Figure 28) are very informative. It can be observed that for ring 1 and 2, there is the least jet fusing above ±800 RPM and a flow rate of about 2 $\mathrm{kg\,hole^{-1}\,h^{-1}}$. Assuming that this is similar for ring 3, the graphs in Figure 45 can be combined as shown. The grey areas in the individual graphs show the jet flow regime where in the darkest part there is extensive jet fusing and in the light grey part, jet fusing is minimal. In the white area, the flow is either too low or too high for proper operation. The last graph combines the three individual graphs. In the white parts of this graph, one of the rings does not have a sufficient flow. In the grey part, all rings have sufficient flow. The jet fusing limit for the different rings is also shown and divided with the grey lines. As can be seen, there is no operation condition within the grey area where no rings experience fusing. To be as close to this point as possible however, the best operating condition is at 1100 RPM with a flow rate of 40 $\mathrm{m^3\,h^{-1}}$. The visualization from the Matlab model at these

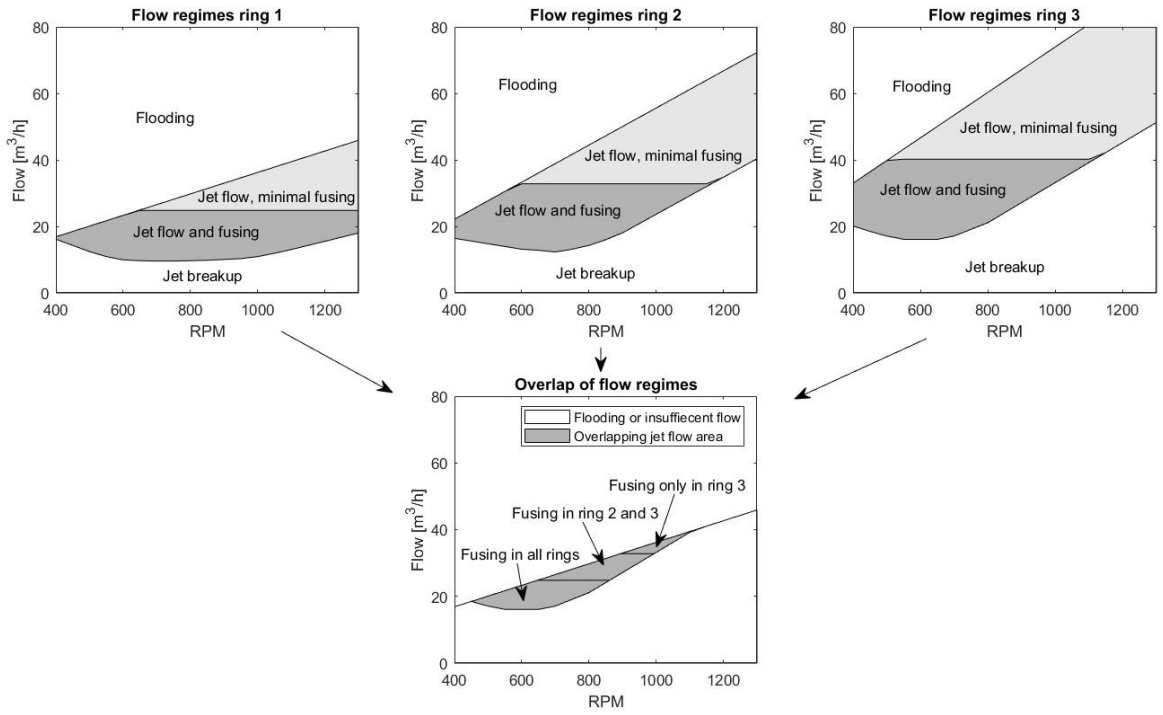

Figure 45. Flow regimes of the three separate rings without the transition zone combined to one graph with the operating flow regime for all three rings. In the grey part of the bottom graph, all three rings produce jets. The horizontal lines show the approximate flow rates above which certain rings have minimal jet fusing behaviour.

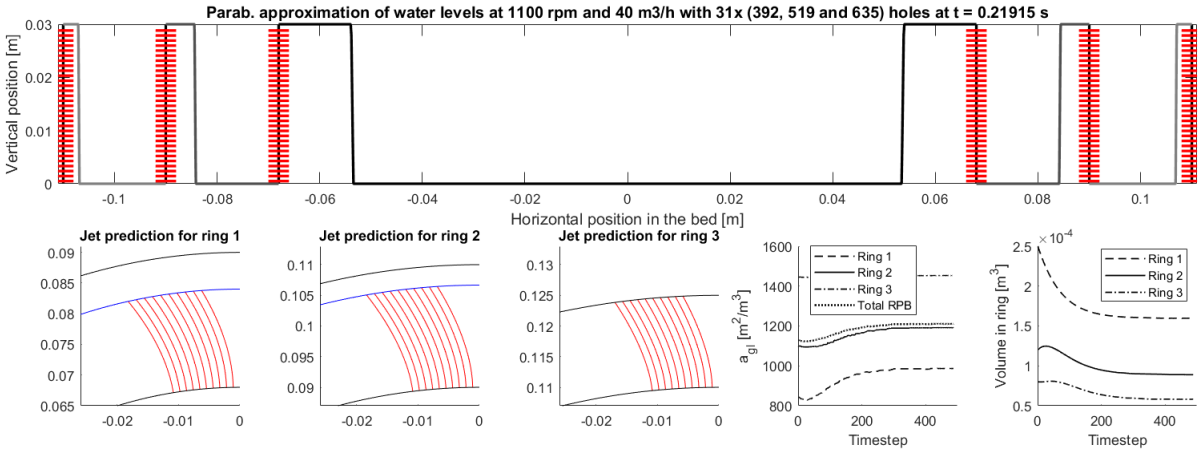

Figure 46. Visualization of the optimum operating conditions at a rotational velocity of 1100 RPM with a flow rate of 40 $m^3\ h^{-1}$.

operating conditions is shown in Figure 46 and indicates that the steady state interfacial gas-liquid area will be 1210 $\mathrm{m^2\ m^{-3}}$. As the calculation of the interfacial area in the model assumes there is no jet fusing, this should be compensated for to get a better estimation of the real interfacial area. Using the jet fusing information, it can be extracted that at these operational condition the total jet fusing will be in the range of 4 - 18 %. If all fused jets consist are fused from two separate jets, this brings the interfacial area down to 1195 – 1145 $\mathrm{m^2\ m^{-3}}$. It should be noted that for this calculation, the reactor volume is calculated from the outside of ring 1 (0.136 m diameter) and the inside of the size of the casing (0.25 m diameter). Also, the jet fusing behaviour in full operation is assumed to be similar to the jet fusing behaviour of pattern 3.

If the mesh in the three rings would be changed to have overlapping flow regimes by increasing the inter-hole spacing in the larger rings, the grey area in Figure 45 would be larger and the reactor would have a larger usable operating window.

Chapter 4. Conclusions

As shown in the results of the experiments, the redistribution rings for the liquid perform best in a small operation range. The optimal operation range however, is different for every ring as the rings have a different radius and curvature. This results in a different liquid flow capacity and behaviour of the liquid. The smaller rings can process less liquid but experience slightly less jet fusing as the curvature is larger. The jet fusing, especially apparent with operation of pattern 3, greatly reduces the gas-liquid interfacial area and reactor performance. The optimum performance range of the redistribution rings currently lies at 900 RPM with a liquid flow rate of 40 $m^3\ h^{-1}$. At these operating conditions, all three rings have proper water layers to ensure a good distribution of the liquid. These flow rates however, are in the upper limit of ring one and the lower limit of ring three. In this range, if there is no jet fusing, the interfacial gas-liquid area is about 1210 $m_{gl}^2\ m_R^{-3}$. Due to the jet fusing the interfacial area is reduced. Assuming that a fully open ring will experience the same level of jet fusing as pattern three with data from the graphs in the experimental results section. It can be concluded that the reduction of the interfacial area is between 4 and 18 % which leads to a realistic interfacial gas-liquid area of 1145 – 1195 $m_{gl}^2\ m_R^{-3}$. This interfacial area only takes into account the reactor space beyond ring one (diameter of 0.136 m) up to a diameter of 0.25 m where the reactor casing will be. These values are higher but in the same order as more conventional gas-liquid contactors.

From the CFD simulations it can be concluded that the liquid flow towards the holes, in case of an undisturbed water layer is very smooth and about equal from all directions. A very small inter-hole distance and impact of the liquid jet from previous rings disturbs the flow pattern that creates the smoothest and most stable jets. During real operation with the current mesh, the jets will therefore not be as smooth as the jets observed with pattern one and two but will be much more like the jets observed with pattern three as shown in the fluid distortion part of the experimental results. This positively influences the turbulence intensity in the jets but will decrease the interfacial area as more jets will fuse under the same conditions. The influence of this effect on mass – and heat transfer rates is something to be tested in future research.

The Matlab model, created to calculate the operation of the VIREFOC setup, shows a high correlation with the experimental results in terms of water layer thicknesses, water layer shapes and jet flight paths. The data from the model can be used to accurately determine the operation, with some modifications, of the CRPB in the future. For more accurate calculations of the gas-liquid interfacial area, the fusing and breakup behaviour of the liquid jets should also be included in the model.

Chapter 5. Recommendations

As this report only treats the initial research of the hydrodynamics through the redistribution rings in the VIREFOC setup, also used in the CRPB, an extensive amount of research can still be done to optimize the reactor performance. In terms of possible modifications to the reactor to increase the performance, the influence of a slight increase in inter-hole spacing for the larger rings can be investigated. As mentioned, this might reduce the amount of jet fusing in the larger rings and shift the operation window of the three rings to overlap in a greater range of operation conditions. Since the jets from a previous ring disturb the smooth fluid layer on impact, it might be beneficial for the jet formation to include a packing to absorb the impact and improve the jet formation on the next rings. The packing could be made of concentric rings that fit inside the distribution rings or from small packing blocks that are randomly packed in the reactor. The last recommended modification to the reactor would be to leave a small gap between cooling channels and the redistribution rings as this would reduce the chances of liquid maldistribution.

To investigate the effective gas liquid surface area generated by the redistribution rings with all holes open, a gas absorption followed by an irreversible reaction could be used. For example the reaction of carbon dioxide with hydroxide to carbonate which has previously been used to effectively determine gas-liquid interfacial areas in gas-liquid contactor reactors (Yong Luo et al., 2012; Song and Rochelle, 2017). Introduction of a packing inside the reactor might also positively alter the effective gas-liquid interfacial area which could be tested with a similar reaction.

Up and until now, the model includes the general equations and calculations that are needed for a good approximation of the liquid behaviour in the reactor. To achieve an even more accurate model, some things could be improved or added for a better functionality. Some examples of useful additions to the model include:

- For operating cases where there is a large cavity area in the reactor, accurate gas-liquid surface area calculations of the jets and droplets are necessary for an accurate prediction of the performance. To improve the current calculation, jet breakup and jet coalescence behaviour could be included. Jet breakup could be implemented using equation 24. While for the jet coalescence it is probably most practical to empirically derive the coalescing behaviour for the final mesh and liquids.
- The model could be used to estimate conversions for reactions. To get a good estimation however, information on residence times in the reactor is an important variable. The overall residence time can already be easily calculated as the flow rates and volume in the reactor are known but a calculation of the residence time distribution in the jets and water layers at the different heights would make it more accurate.
- Adding the option for cross current gas flow through the reactor would open up possibilities to model reactions and the ability to calculate the concentration profiles throughout the reactor. As gas flow is introduced, pressure drop should be included as well. How large is the pressure drop and what is the required water layer thickness to prevent shortcuts of the gas through the redistribution rings.

- Investigate the level of mixing in the water layers. Determine if water that initially flows through the bottom holes, stays in the bottom of the reactor or if there is extensive mixing in the water layers. Possible to investigate in the experimental setup and useful for the model as it influences the residence time and thus reaction over the height of the reactor.
- Changing the assumption of rotational symmetry which is not 100% accurate, especially with the presence of cooling channels in the CRPB. The tubes/anchor points cause maldistribution of the liquid.
- As the model could be used to find the best operating range for the reactor, it would be useful to modify the model in a way that it automatically finds the best operating conditions. Possibly by looping over different flow rates and rotational velocities and narrating to the optimal conditions.
- The jets are found not to have the diameter of the holes at low flow rate to rotational velocity ratios. This behaviour could be investigated more and incorporated into the model as it determines the interfacial area and thus mass transfer and reaction rates.

List of Symbols

a	Jet radius	(m)
A	Area	(m^2)
C_v	Velocity coefficient	
d	Diameter of the nozzle	(m)
D	Jet diameter	(m)
F_c	Centrifugal force	$(kg\ m\ s^{-2})$
F_g	Gravitational force	$(kg\ m\ s^{-2})$
g	Gravitational acceleration	$(m\ s^{-2})$
h	Liquid height	(m)
k	Turbulent kinetic energy	$(J\ kg^{-1})$
m	Mass	(kg)
n_{fuse}	Average number of original jets per fused jet	
Oh	Ohnesorge number	$(\mu/\rho d\sigma)^{1/2}$
P	Pressure	$(kg\ m^{-1}\ s^{-2})$
r	Radial position	(m)
R	Radius of cylinder	(m)
Re	Reynolds number	$(\rho v d/\mu)$
t	Time	(s)
v	Velocity	$(m\ s^{-1})$
$V_{r,n}$	Liquid volume in ring n	(m^3)
We	Weber number	$(\rho v^2 d/\sigma)$
z	Vertical position	(m)
Z	Stable jet length	(m)
φ	Liquid flow rate	$(m^3\ s^{-1})$
ω	Rotational velocity	$(rad\ s^{-1})$
α	Angle due to centrifugal and gravitational force	(rad)
ε	Turbulent kinetic energy dissipation	$(J\ kg^{-1}\ s^{-1})$
ρ	Density	$(kg\ m^{-3})$
ϕ	Rotational position	(rad)
δ	Layer thickness	(m)
δ_j	Amplitude of disturbance	(m)
CFD	Computational fluid dynamics	
CRPB	Cooled rotating packed bed	
HiGee	High gravity	
RPB	Rotating packed bed	
RPM	Rotations per minute	
VIREFOC	Visual reactor for cooled rotating packed bed	
VOF	Volume of fluid	

References

ANSYS Inc., 2018. ANSYS Fluent User's Guide, Release 19.0.

Burns, J.R., Ramshaw, C.R., 1996. Process Intensification: Visual Study of Liquid Maldistribution in Packed Beds. Chem. Eng. Sci. 51, 1347–1352. https://doi.org/10.1016/0009-2509(95)00367-3

Chandra, A., Goswami, P.S., Rao, D.P., 2005. Characteristics of flow in a rotating packed bed (HIGEE) with split packing. Ind. Eng. Chem. Res. 44, 4051–4060. https://doi.org/10.1021/ie048815u

Chu, G.W., Gao, X., Luo, Y., Zou, H.K., Shao, L., Chen, J.F., 2013. Distillation studies in a two-stage counter-current rotating packed bed. Sep. Purif. Technol. 102, 62–66. https://doi.org/10.1016/j.seppur.2012.09.029

Chu, G.W., Sang, L., Du, X.K., Luo, Y., Zou, H.K., Chen, J.F., 2015. Studies of CO2absorption and effective interfacial area in a two-stage rotating packed bed with nickel foam packing. Chem. Eng. Process. Process Intensif. 90, 34–40. https://doi.org/10.1016/j.cep.2015.02.007

Cortes Garcia, G.E., van der Schaaf, J., Kiss, A.A., 2017. A review on process intensification in HiGee distillation. J. Chem. Technol. Biotechnol. 92, 1136–1156. https://doi.org/10.1002/jctb.5206

Ghassemieh, E., Versteeg, H.K., Acar, M., 2006. The effect of nozzle geometry on the flow of small water jets . https://doi.org/10.1243/0954406JMES430

Guo, D., Thee, H., Tan, C.Y., Chen, J., Fei, W., Kentish, S., Stevens, G.W., da Silva, G., 2013. Amino Acids as Carbon Capture Solvents: Chemical Kinetics and Mechanism of the Glycine + CO_2 Reaction. Energy & Fuels 27, 3898–3904. https://doi.org/10.1021/ef400413r

Guo, K., Guo, F., Feng, Y., Chen, J., Zheng, C., Gardner, N.C., 2000. Synchronous visual and RTD study on liquid flow in rotating packed-bed contractor. Chem. Eng. Sci. 55, 1699–1706. https://doi.org/10.1016/S0009-2509(99)00369-3

Harmsen, G.J., 2007. Reactive distillation: The front-runner of industrial process intensification. A full review of commercial applications, research, scale-up, design and operation. Chem. Eng. Process. Process Intensif. 46, 774–780. https://doi.org/10.1016/j.cep.2007.06.005

Jähnisch, K., Baerns, M., Hessel, V., Ehrfeld, W., Haverkamp, V., Löwe, H., Wille, C., Guber, A., 2000. Direct fluorination of toluene using elemental fluorine in gas/liquid microreactors. J. Fluor. Chem. 105, 117–128. https://doi.org/10.1016/S0022-1139(00)00300-6

Janssen, L.P.B.M., Warmoeskerken, M.M.C.G., 2006. Transport Phenomena Data Companion. VVSD.

Joelianingsih, Maeda, H., Hagiwara, S., Nabetani, H., Sagara, Y., Soerawidjaya, T.H., Tambunan, A.H., Abdullah, K., 2008. Biodiesel fuels from palm oil via the non-catalytic transesterification in a bubble column reactor at atmospheric pressure: A kinetic study. Renew. Energy 33, 1629–1636. https://doi.org/10.1016/j.renene.2007.08.011

Landau, L.D., Lifshitz, E.M., 1987. Fluid mechanics: Landau and Lifshitz: course of theoretical physics. Image Rochester NY. https://doi.org/10.1007/b138775

Lautrup, B., 2005. Physics of Continuous Matter Exotic and Everyday Phenomena. Institure of Physics Publishing.

Li, Y., Wang, S., Sun, B., Arowo, M., Zou, H., Chen, J., Shao, L., 2015. Visual study of liquid fl ow in a rotor-stator reactor 134, 521–530.

Llerena-Chavez, H., Larachi, F., 2009. Analysis of flow in rotating packed beds via CFD simulations-Dry pressure drop and gas flow maldistribution. Chem. Eng. Sci. 64, 2113–2126. https://doi.org/10.1016/j.ces.2009.01.019

Lubarda, V.A., 2013. The shape of a liquid surface in a uniformly rotating cylinder in the presence of surface tension. Acta Mech. 224, 1365–1382. https://doi.org/10.1007/s00707-013-0813-6

Lucas, M.S., Peres, J.A., Li Puma, G., 2010. Treatment of winery wastewater by ozone-based advanced oxidation processes (O3, O3/UV and O3/UV/H2O2) in a pilot-scale bubble column reactor and process economics. Sep. Purif. Technol. 72, 235–241. https://doi.org/10.1016/j.seppur.2010.01.016

Luo, Y., Chu, G., Zou, H., Xiang, Y., Shao, L., Chen, J., 2012. Characteristics of a two-stage counter-current rotating packed bed for continuous distillation. Chem Eng Procedd Process Intensif 52, 55–62.

Luo, Y., Chu, G.W., Zou, H.K., Zhao, Z.Q., Dudukovic, M.P., Chen, J.F., 2012. Gas-liquid effective interfacial area in a rotating packed bed. Ind. Eng. Chem. Res. 51, 16320–16325. https://doi.org/10.1021/ie302531j

Mccarthy, M.J., 1974. Review of Stability of Liquid Jets and the Influence of Nozzle Design 7, 1–20.

Mcdonald, K.T., 2012. Bernoulli 's Equation for a Rotating Fluid Solution Bernoulli 's Equation in the Lab Frame 08544, 2–5.

Pohorecki, R., Bridgwater, J., Molzahn, M., Gani, R., Gallegos, C., 2010. Chemical Engineering and Chemical Process Technology. Eolss Publishers Co. Ltd.

Puxty, G., Rowland, R., Attalla, M., 2010. Comparison of the rate of CO2 absorption into aqueous ammonia and monoethanolamine. Chem. Eng. Sci. 65, 915–922. https://doi.org/10.1016/j.ces.2009.09.042

Ramshaw, 1981. Mass Transfer Process. U.S. Patent 4,283,255.

Rao, D.P., Bhowal, A., Goswami, P.S., 2004a. Process Intensification in Rotating Packed Beds (HIGEE): An Appraisal. Ind. Eng. Chem. Res. 43, 1150–1162. https://doi.org/10.1021/ie030630k

Rao, D.P., Bhowal, A., Goswami, P.S., 2004b. Process Intensification in Rotating Packed Beds (HIGEE): An Appraisal. Ind. Eng. Chem. Res. 43, 1150–1162. https://doi.org/10.1021/ie030630k

Sang, L., Luo, Y., Chu, G.W., Zhang, J.P., Xiang, Y., Chen, J.F., 2017. Liquid flow pattern transition, droplet diameter and size distribution in the cavity zone of a rotating packed bed: A visual study. Chem. Eng. Sci. 158, 429–438. https://doi.org/10.1016/j.ces.2016.10.044

Song, D., Rochelle, G.T., 2017. Reaction kinetics of carbon dioxide and hydroxide in aqueous glycerol. Chem. Eng. Sci. 161, 151–158. https://doi.org/10.1016/j.ces.2016.11.048

Szirtes, T., Rózsa, P., 2007. Applied Dimensional Analysis And Modeling. https://doi.org/http://dx.doi.org/10.1016/B978-012370620-1.50000-9

Wang, G., Xu, Z., Ji, J., 2011. Progress on HiGee distillation - Introduction to a new device and its industrial applications. Chem Eng Res Des 89, 1434–1442.

Wang, G.Q., Xu, O.G., Xu, Z.C., Ji, J.B., 2008. New HIGEE-rotating zigzag bed and its mass transfer performance. Ind. Eng. Chem. Res. 47, 8840–8846. https://doi.org/10.1021/ie801020u

Xie, P., Lu, X., Yang, X., Ingham, D., Ma, L., Pourkashanian, M., 2017. Characteristics of liquid flow in a rotating packed bed for CO2 capture: A CFD analysis. Chem. Eng. Sci. 172, 216–229. https://doi.org/10.1016/j.ces.2017.06.040

Zhao, H., Shao, L., Chen, J., 2010. High-gravity process intensification technology and application. Chem. Eng. J. 156, 588–593.

Appendix

Appendix A: Experimental setup

This appendix gives some extra view angles on the experimental setup.

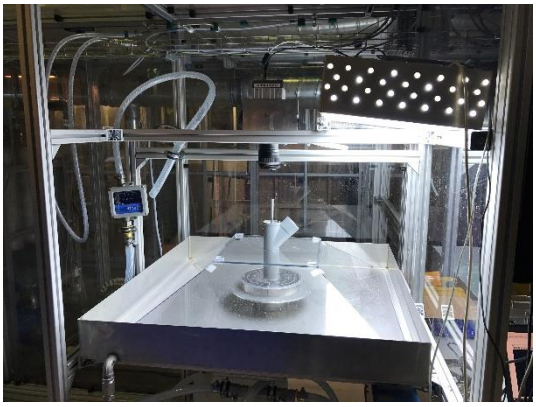

Figure 47. Picture of the rig that holds the VIREFOC setup.

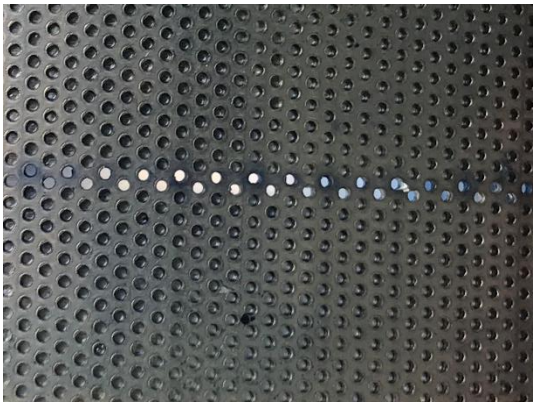

Figure 48. Close-up picture of pattern three in the ring.

Figure 49. Picture of the white painted bottom plate of the visual reactor.

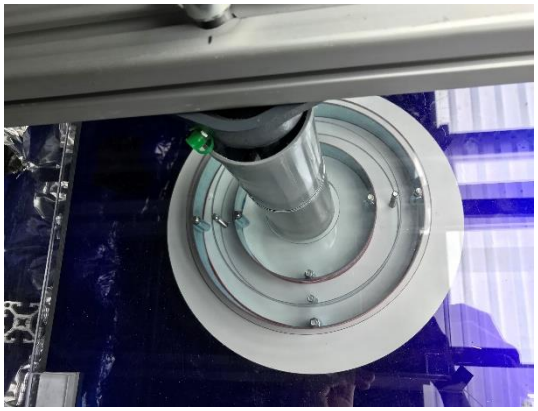

Figure 50. Top view of the reactor through the transparent top plate and splash cover.

Appendix B: Mesh dimensions

The dimensions of the mesh in the rings were accurately measured using a light projector. The important dimensions are shown in Figure 51. Most dimensions are in line with the specifications. The holes however, have a diameter of 0.57 mm rather than the specified 0.50 mm. Also, there is a slight shift in the pattern every two rows as can be observed in Figure 52. The red lines should for every hole be in the middle, but this is only the case for every other hole. This misalignment will cause a slight deviation in inter hole spacing between part of the holes.

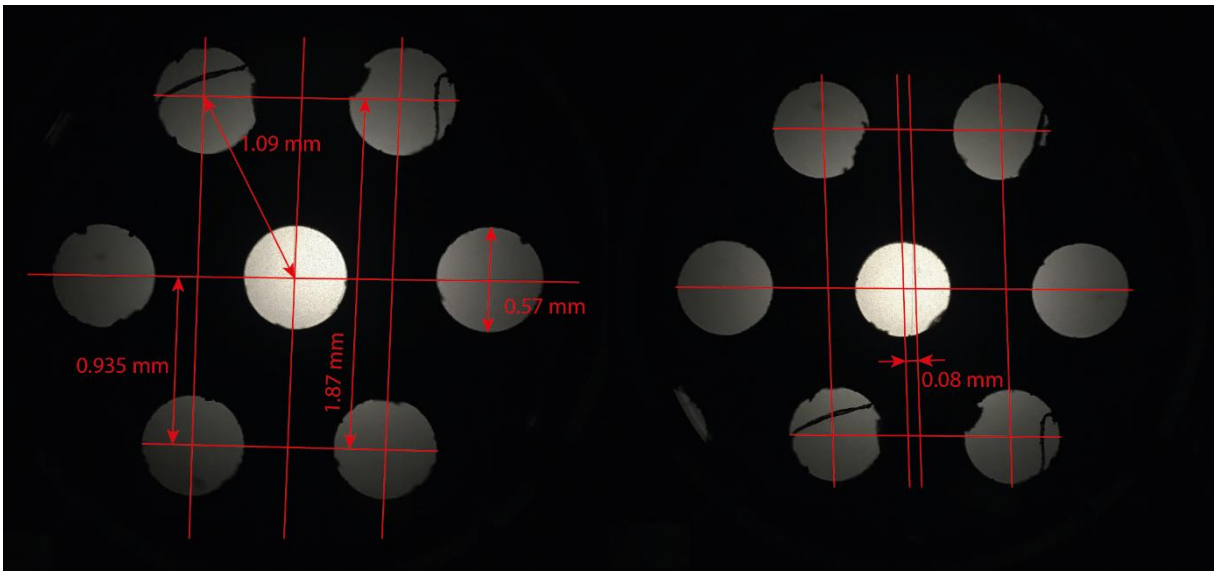

Figure 51. Dimensions of the mesh measured using a light projector. The right part shows the slight shift present in the pattern.

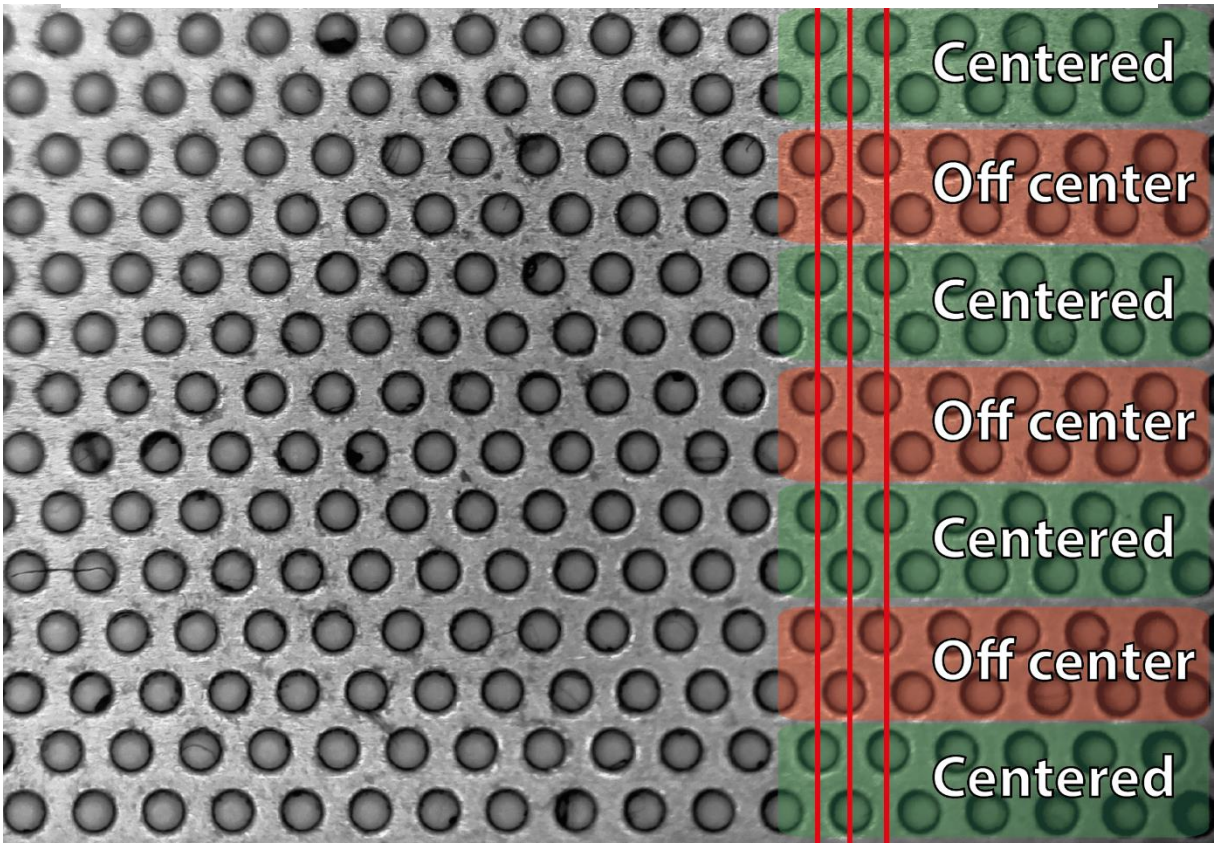

Figure 52. Microscope photograph of the mesh where the slight shift in the pattern is highlighted using the vertical red lines.

Appendix C: Motion blur calculation

Motion blur, the effect that occurs when an object that is photographed moves significantly during the exposure time of the image, should be minimized during the experiments. Large amounts of motion blur make the visual analysis inaccurate and difficult. Small amounts of motion blur, unavoidable when photographing object with high velocities, can be compensated for when known. The amount of motion blur, or distance moved while the picture is being taken can be calculated using the shutter speed and droplet velocity.

$$M_{blur} = v_{droplet} \cdot t_{shutter} \qquad (eq.C1)$$

The velocity of the droplets depends on the ring diameter, flow rate and rotational velocity and falls within the range of 3 – 15 m/s. Figure 53 shows the amount of motion blur for different velocities at different shutter speeds. The highest velocity experiments used an 11 μs shutter speed which with the liquid velocity of 15 m/s equals a motion blur of 0.15 mm. The experiments at the lowest rotational velocities at a shutter speed of 25 μs have, with the liquid velocity of 2.5 m/s a motion blur of 0.06 mm. As a comparison, the jet diameters are in the order or 0.5 mm and droplet sizes are in the order of 1 - 2 mm. For jets, the motion blur is in the range of 12 - 30 %.

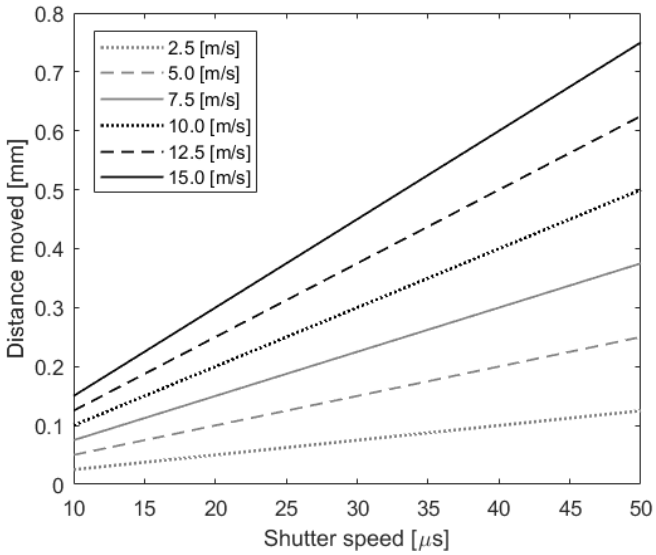

Figure 53. Graph of the moved distance during the shutter opening of the camera for different movement speeds.

Appendix D: Simulation parameters

The table below shows the important settings used in ANSYS Fluent for the simulations of the VIREFOC.

Table 2. Overview of the different settings used for the simulations in ANSYS Fluent.

Solver	Type		Pressure based
	Velocity formulation		Absolute
	Time		Transient
	Gravity		$-9.81\ m/s^2$
Models	Multiphase	VOF	
		Volume fraction parameters	Implicit
		Interface modelling	Sharp
		Surface tension	0.072
	Viscous	k-epsilon realizable	
		$C_{2\epsilon}$	1.9
		TKE Prandtl number	1
		TDR Prandtl number	1.2
		Near-wall treatment	Standard wall functions
Cell zone conditions	Frame motions	Rotational velocity	$[rad/s]$
Materials	Air	Density	1.225 kg/m^3
		Viscosity	1.7894e-5 $kg/m/s$
	Water	Density	998.2 kg/m^3
		Viscosity	1.003e-3 $kg/m/s$
Boundary conditions	Velocity inlet	Angular velocity	63 – 125 $[rad/s]$
		Radial velocity	$[m/s]$
		Water volume fraction	1.0
	Pressure outlet	Backflow pressure speccif.	Total pressure
	Periodic boundaries	Periodic type	Rotational
Solution method	Pressure velocity coupling	Scheme	SIMPLE
	Spatial discretization	Gradient	Least squares cell-based
		Pressure	PRESTO!
		Momentum	Second order upwind
		Volume fraction	Compressive
		Turbulent kinetic energy	First order upwind
		Turbulent dissipation rate	First order upwind
	Transient formulation		First order implicit
Calculations	Time stepping method	Fixed	
		Time step size	0.0002 $[s]$
		Max iterations/time step	100

Appendix E: Conversion to a dimensionless flow map

To create a more general insight in the hydrodynamics, a dimensionless flow-map is generated. The variables that determine the liquid layer build-up and flow through the holes include:

φ_v, ω, ρ, μ and r

To use the above mentioned variables to generate a dimensionless flow map, the Buckingham-π theorem is exploited from which the dimensionless groups can be found. The theorem states that a physically meaningful equation including a set of n physical variables can be rewritten in a number of dimensionless parameters equal to $\pi = n - x$ with x being the number of physical dimensions (Szirtes and Rózsa, 2007). The first step is definition of the dependent and independent variables.

The defined dependent variables are:

φ_v and ω

The defined independent variables are:

ρ, μ and r

The dependent and independent variables can now be used for find the two π-terms:

Solving for the different π-terms

First π-term:

$$\pi_1 = \varphi_v \rho^a \mu^b r^c = \frac{m^3}{s}\left(\frac{kg}{m^3}\right)^a \left(\frac{kg}{ms}\right)^b (m)^c \qquad (eq.E1)$$

$$\begin{array}{l} m: 0 = 3 - 3a - b + c \rightarrow c = 3a + b - 3 \\ s: \ 0 = -1 - b \quad\ \rightarrow b = -1 \\ kg: 0 = a + b \quad\ \rightarrow a = -b \end{array} \qquad \begin{cases} a = \ \ 1 \\ b = -1 \\ c = -1 \end{cases} \qquad (eq.E2)$$

This gives, for the first π-term:

$$\pi_1 = \frac{\varphi_v \rho}{\mu r} \qquad (eq.E3)$$

As the volumetric flowrate through each ring can be calculated with equation 20, this equation can be inserted into equation E3:

$$\pi_1 = \frac{\rho(v_{holes} A)}{\mu r} = \frac{\rho(C_v \omega \sqrt{r_2^2 - (r_2 - \delta_w)^2} A)}{\mu r} = \frac{\rho(C_v \omega \sqrt{r_2^2 - (r_2 - \delta_w)^2} A}{\mu r} \qquad (eq.E4)$$

Where A is equal to $2\pi r h C_{mesh}$ with C_{mesh} being a constant for the type of mesh indicating the open area versus closed area. Inserting this gives equation E5 which can be used to plot the theoretical dimensionless flow through the rings.

$$\pi_1 = Re' = \frac{\rho(C_v \omega \sqrt{r_2^2 - (r_2 - \delta_w)^2} 2\pi r h C_{mesh})}{\mu r} = \frac{\rho(C_v \omega \sqrt{r_2^2 - (r_2 - \delta_w)^2} h 2\pi C_{mesh}}{\mu} \qquad (eq.E5)$$

This first π-term can be seen as a Reynolds number for flow through the open area of the rings.

Second π-term:

$$\pi_2 = \omega \rho^a \mu^b r^c = \frac{1}{s}\left(\frac{kg}{m^3}\right)^a \left(\frac{kg}{ms}\right)^b (m)^c \qquad (eq.E6)$$

$$\begin{array}{lll} m: 0 = -3a - b + c \rightarrow c = 3a + b & \left\{ \begin{array}{l} a = \ \ 1 \\ b = -1 \\ c = \ \ 2 \end{array} \right. \\ s: \ \ 0 = -1 - b \ \ \ \ \ \ \rightarrow b = -1 & \\ kg: 0 = a + b \ \ \ \ \ \ \ \rightarrow a = -b & \end{array} \qquad (eq.E7)$$

This gives, for the second π-term:

$$\pi_2 = \frac{\omega \rho r^2}{\mu} \qquad (eq.E8)$$

Where ωr is equal to the tangential velocity of the ring (v_{tang}) which can be replaced to acquire equation E9:

$$\pi_2 = Re'' = \frac{v_{tang} \rho r}{\mu} \qquad (eq.E9)$$

The second π-term can be seen as a type of Reynolds number for flow in a rotating cylinder.

As the velocity through the holes depends on the layer thickness of the liquid on the mesh rings, this could be inserted as a fixed variable but an additional term was added which determines how full a certain ring is. This variable is defined as δ/r where δ is the thickness of the water layer. When δ/r is equal to 1, the ring is completely filled whereas when δ/r is equal to 0, the ring is empty.

With the different dimensionless term that were found, a three-dimensional dimensionless flow map can be plotted. This is shown in Figure 54. The height of each surface is determined by the ring diameter.

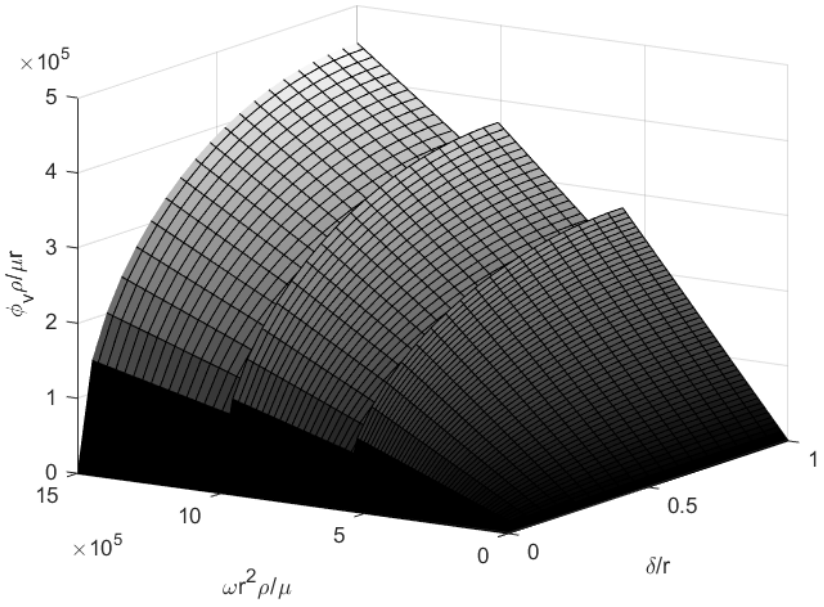

Figure 54. Dimensionless flow map of the flow through the three rings of the VIREFOC. Each surface represent one ring radius.

Appendix F: Sample images for the flow regimes

The pictures below are sample pictures from the experiments giving an idea of experiments falling into the jet regime, partial jet regime and full droplet regime.

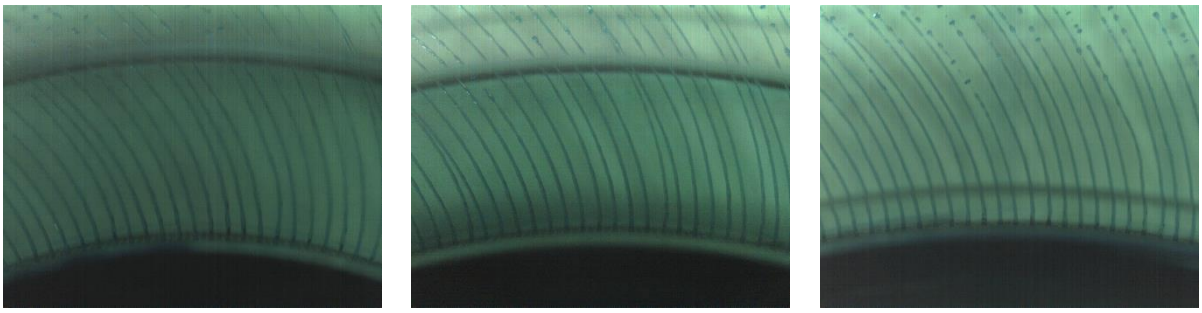

Figure 55. Three examples of experiments classified as full jet regime.

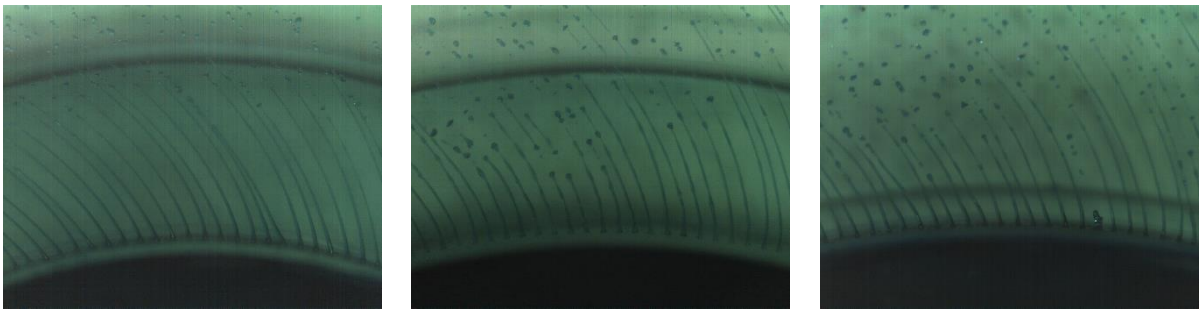

Figure 56. Three examples of experiments classified as partial jet regime.

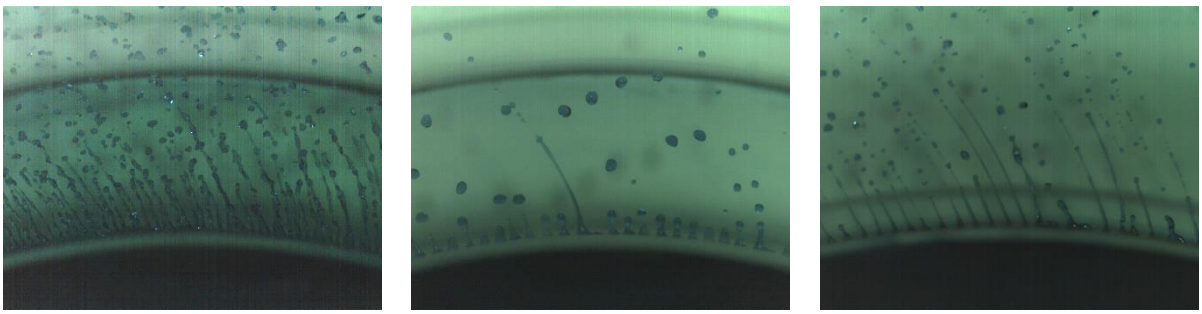

Figure 57. Three examples of experiments classified as full droplet regime.

Appendix G: Averaged images from experiments

To measure the water layer thickness on the rings, all 200 images from the special set of experiments were combined and averaged. Some examples of these images are shown below.

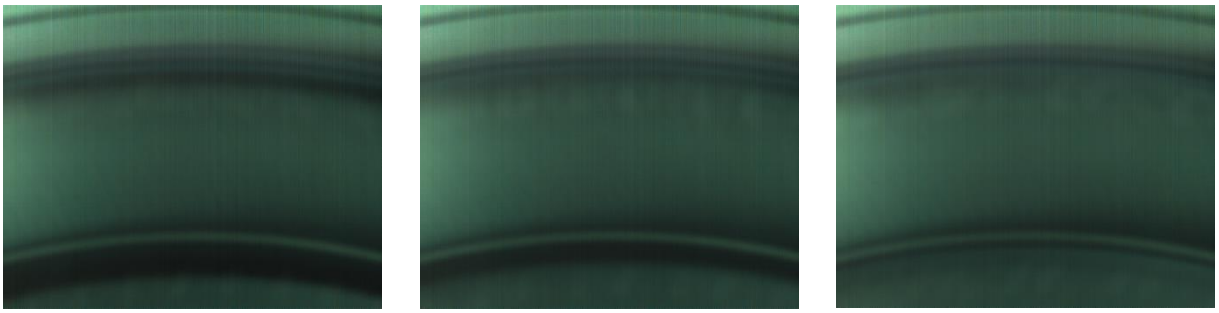

Figure 58. Pictures from an experiment at 1200 RPM with pattern 2 focussed on ring 2 with a flow-rate of 600, 400 and 200 L/h.

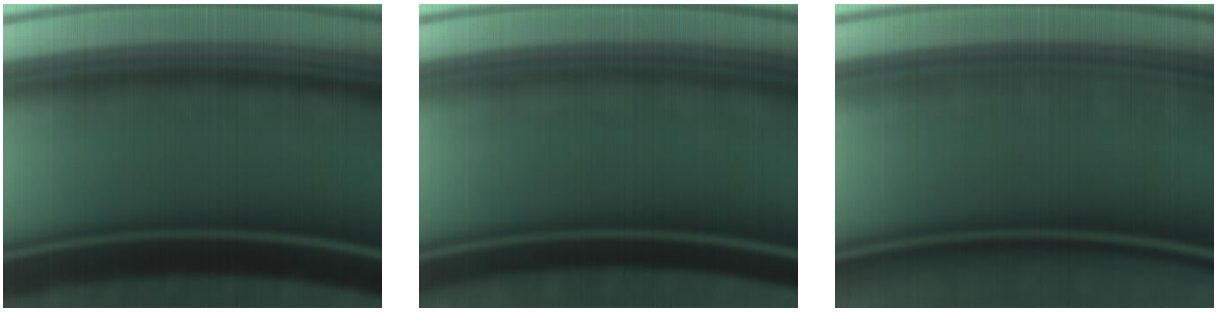

Figure 59. Pictures from an experiment at 700 RPM with pattern 2 focussed on ring 2 with a flow-rate of 350, 300 and 200 L/h.

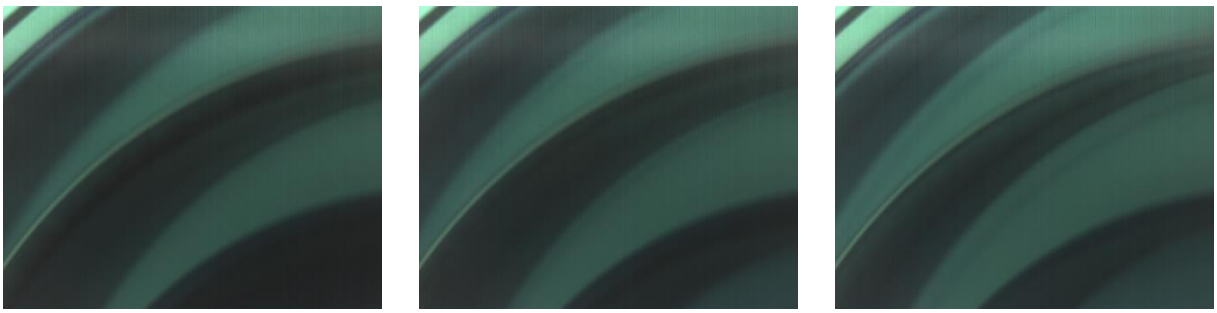

Figure 60. Pictures from an experiment at 1200 RPM with pattern 2 focussed on ring 2 with a flow-rate of 600, 400 and 200 L/h.

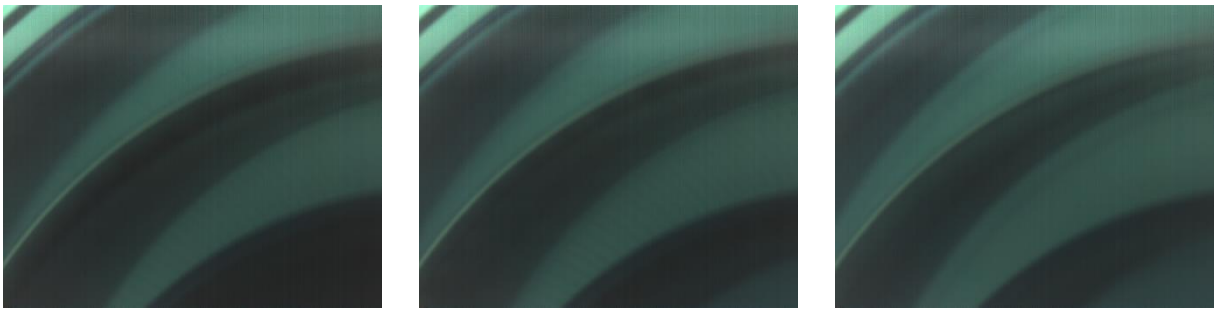

Figure 61. Pictures from an experiment at 800 RPM with pattern 2 focussed on ring 2 with a flow-rate of 400, 300 and 200 L/h.

Appendix H: Additional results simulations

The simulation results for the simulations with a flow rate of 1.08 $kg\ hole^{-1}\ h^{-1}$.

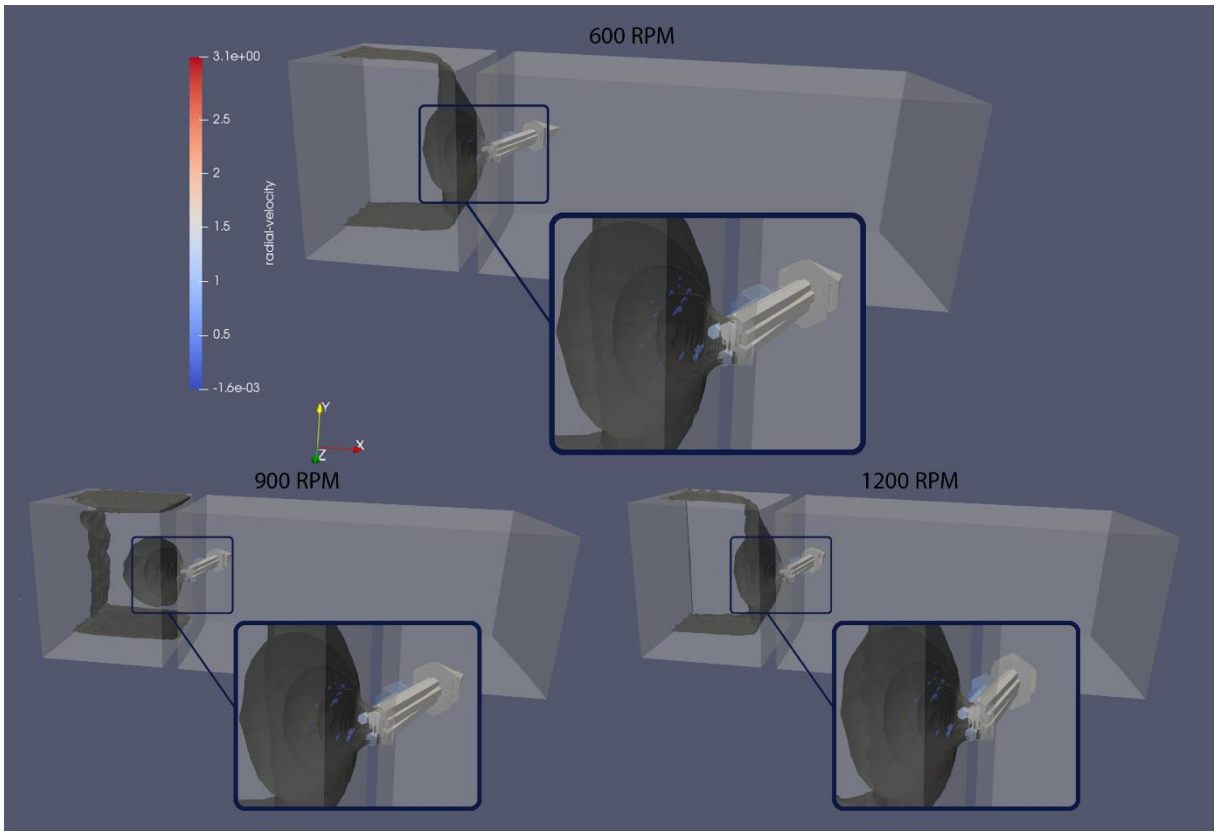

Figure 62. Contour and vector plot of the radial velocity inside the simulated domain at a rotational velocity of 63 rad/s (600 RPM), 94 rad/s (900 RPM) and 125 rad/s (1200 RPM) at a flow rate of 1.04 $kg\ hole^{-1}\ h^{-1}$.

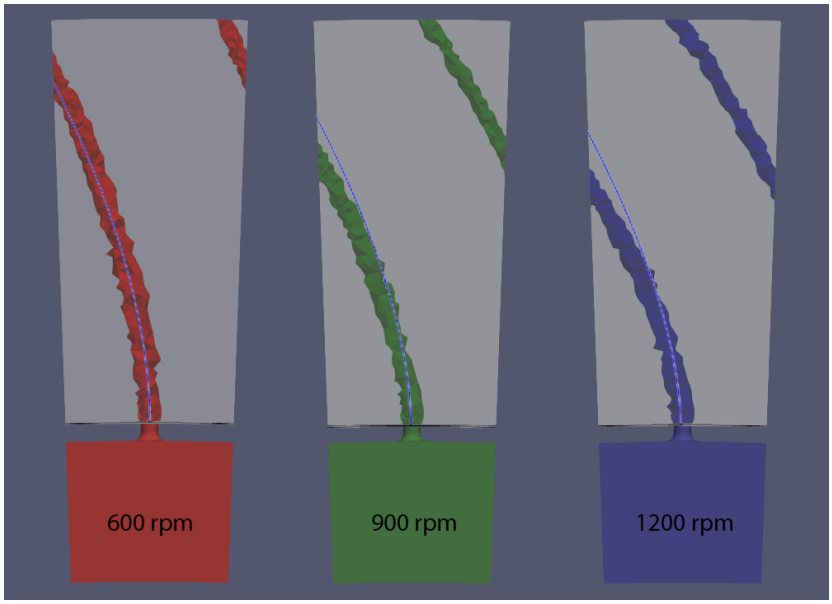

Figure 63. Liquid flight paths of the simulations with a flow rate of 1.04 $kg\ hole^{-1}\ h^{-1}$. The theoretical flight path are shown as a thin line on top of the simulation results.

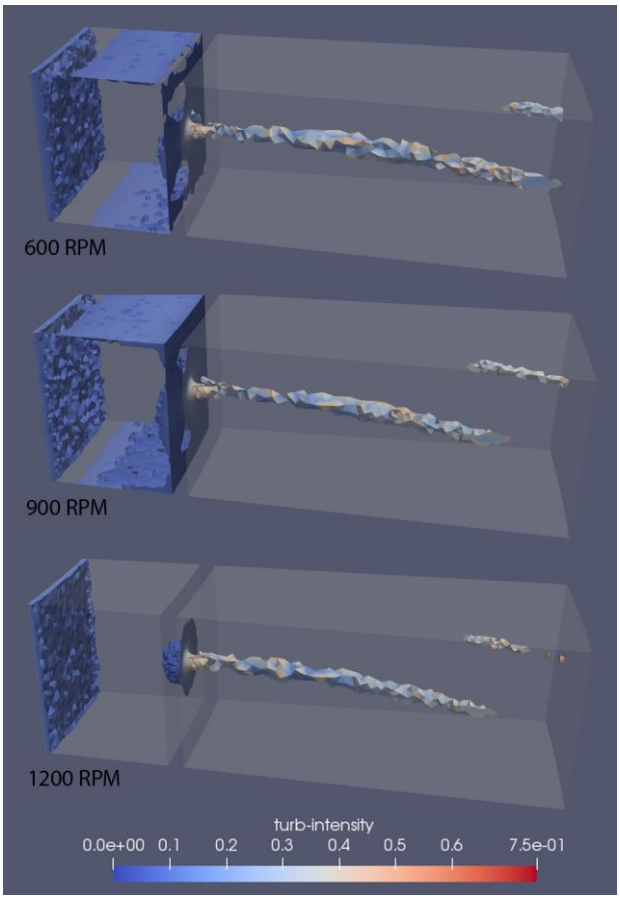

Figure 64. Turbulence intensity levels of the three simulations run with the flow of 1.04 $kg\ hole^{-1}\ h^{-1}$.

Appendix I: Matlab model code

- The main code should be run.
- The code for the mass balance is called from within the main code.
- The code to calculate the shape of the water layer is called within the mass balance code.
- The code to calculate the jet flight paths is called from within the main code.

Main code that runs the time loop and visualizes the data

```
% Main code to predict the operation of the VIREFOC-RPB
% Author:           Tom Vercoelen
% Date created:     21-3-2018
% Date last edited: 24-4-2018
%
% This program takes several inputs that are listed below and should be
% specified correctly to make a prediction about the operational conditions
% of the VIREFOC setup based on experiments and literature knowledge. The
% information includes water layers that will build up, shape of the
% jets/droplet flight paths and gas-liquid surface area.
clear

%% PARAMETER DEFINITION:
% Operational conditions:
RPM             =   300;                    %           Rotations per minute
phiIn           =   5;                      % [m3/h]    Flow into the reactor
volumeOld       =   [0.00025 0.00012 0.00008];% [m3]    % Set the initial volume in the rings

% RPB defenitions:
hBed            =   0.03;                   % [m]       Height of the bed
ringRadius      =   [0.068 0.09 0.11];      % [m]       Radius of the rings in the RPB
ringDistance    =   [0.068 0.022 0.02];     % [m]       Distance to the next ring/centre
casingRadius    =   0.125;                  % [m]       Radius of the casing around the reactor
openHoles       =   1;                      % [-]       If 1: all holes open, otherwise specify the ...
                                            %           ... height of the rows that are open
nHoles          =   1;                      % [-]       If 1: all holes open per row, otherwise ...
                                            %           ... specify how many holes per row are open
diamHoles       =   0.0005;                 % [m]       Diameter of the holes
exitAngle       =   [0 0 0];                % [deg]     Angle at which the jets exit the rings, to ...
                                            %           ... be later taken from dedicated file
compNextLayer   =   1;                      % [-]       Compensate the length of the jets for the ...
                                            %           ... thickness of the water layer on the next ring

% Other parameters:
ps.Cv           =   0.97;                   % [-]       Velocity coefficient
ps.g            =   9.81;                   % [m/s^2]   Gravitational acceleration
ps.Gval         =   1.118e-3;               % [m/s^2]   Constant used for calculation of the ...
                                            %           ... additional G-force
ps.dt           =   0.5e-5/(phiIn/3600);    % [s]       Time step size for the filling of the RPB
ps.tEnd         =   10;                     % [s]       Time to stop the simulation if steady state ...
                                            %           ... is not reached
ps.nRad         =   500;                    % [-]       Number of steps in the radial direction used ...
                                            %           ... to calculate the water shape


% Do some preliminary calculations
if openHoles == 1
    hHoles  = 0.0005:0.00094397:(hBed-0.00025);   % Height of the holes in the bed            [m]
else
    hHoles  = openHoles;                          % Copy the values supplied in the variables [m]
end

if nHoles == 1
    nHoles  = ceil(ringRadius*2*pi/0.00109);      % Number of open holes in 1 row (at 1 height)
else
    nHoles  = nHoles;                             % Copy the number of holes per row from the variables
end


% Check if initial volumes can be true
maxVolRings = pi * (ringRadius.^2 - (ringRadius - ringDistance).^2) * hBed;
if volumeOld(1) > maxVolRings(1)
    msgbox(['Initial volume ring 1 too high, max volume = ' num2str(maxVolRings(1)) ' m^3'])
    return
elseif volumeOld(2) > maxVolRings(2)
    msgbox(['Initial volume ring 2 too high, max volume = ' num2str(maxVolRings(2)) ' m^3'])
    return
elseif volumeOld(3) > maxVolRings(3)
    msgbox(['Initial volume ring 3 too high, max volume = ' num2str(maxVolRings(3)) ' m^3'])
    return
end
```

```
%% PREDICTION OF WATER LAYERS AND JETS/DROPLET PATHS
figure % Open a new figure for the visualization
% Call the funtions iteratively as the RPB is filling
for i = 1:3000

    % WATER PROFILE CALCULATION %%%%%%%%%%%%%%%%%%%%%%%%%%%%%%%%%%%%%%%%%%%%%%%%
    if i == 1 % Use the initial volumes present to calculate the first time step
        [waterShape,volume,phiOutSep] = CalcWaterLayerParabolic(RPM,phiIn,hBed,ringRadius,hHoles,...
            nHoles,diamHoles,volumeOld,i,ps);
    else % Use the volume from the previous timestep for every other timestep
        [waterShape,volume,phiOutSep] = CalcWaterLayerParabolic(RPM,phiIn,hBed,ringRadius,hHoles,...
            nHoles,diamHoles,volumeOld(i,:),i,ps);
    end
    volumeOld(i+1,:) = volume; % Save the current volume of the water to track it over time


    tic % Time how long the jet calculation takes

    % JET FLIGHT PATH CALCULATION %%%%%%%%%%%%%%%%%%%%%%%%%%%%%%%%%%%%%%%%%%%%%%
    clear posJetX1Data posJetX2Data posJetX3Data posJetY1Data posJetY2Data posJetY3Data
    [X,Y] = size(phiOutSep); % Determine
    phiOutSepSave(:,:,i) = phiOutSep; % Save the outflow of the different rings
    for n = 1:Y % Check for each ring if there are jets and store the data accordingly
        if phiOutSep(1,n) == 0
            [posJetX1,posJetX2,posJetX3,posJetY1,posJetY2,posJetY3,posRingX,posRingY] = ...
                JetCalculator(RPM,phiOutSep(:,n),diamHoles,ringRadius,exitAngle,nHoles,...
                compNextLayer,waterShape,hHoles(n),ringDistance,ps);
            [x,y] = size(posJetX1); posJetX1Data(1:x,1:y,n) = 0;
            [x,y] = size(posJetX2); posJetX2Data(1:x,1:y,n) = 0;
            [x,y] = size(posJetX3); posJetX3Data(1:x,1:y,n) = 0;
            [x,y] = size(posJetY1); posJetY1Data(1:x,1:y,n) = 0;
            [x,y] = size(posJetY2); posJetY2Data(1:x,1:y,n) = 0;
            [x,y] = size(posJetY3); posJetY3Data(1:x,1:y,n) = 0;
            clear posJetX1 posJetX2 posJetX3 posJetY1 posJetY2 posJetY3
        elseif phiOutSep(2,n) == 0
            [posJetX1,posJetX2,posJetX3,posJetY1,posJetY2,posJetY3,posRingX,posRingY] = ...
                JetCalculator(RPM,phiOutSep(:,n),diamHoles,ringRadius,exitAngle,nHoles,...
                compNextLayer,waterShape,hHoles(n),ringDistance,ps);
            [x,y] = size(posJetX1); posJetX1Data(1:x,1:y,n) = posJetX1;
            [x,y] = size(posJetX2); posJetX2Data(1:x,1:y,n) = 0;
            [x,y] = size(posJetX3); posJetX3Data(1:x,1:y,n) = 0;
            [x,y] = size(posJetY1); posJetY1Data(1:x,1:y,n) = posJetY1;
            [x,y] = size(posJetY2); posJetY2Data(1:x,1:y,n) = 0;
            [x,y] = size(posJetY3); posJetY3Data(1:x,1:y,n) = 0;
            clear posJetX1 posJetX2 posJetX3 posJetY1 posJetY2 posJetY3
        elseif  phiOutSep(3,n) == 0
            [posJetX1,posJetX2,posJetX3,posJetY1,posJetY2,posJetY3,posRingX,posRingY] = ...
                JetCalculator(RPM,phiOutSep(:,n),diamHoles,ringRadius,exitAngle,nHoles,...
                compNextLayer,waterShape,hHoles(n),ringDistance,ps);
            [x,y] = size(posJetX1); posJetX1Data(1:x,1:y,n) = posJetX1;
            [x,y] = size(posJetX2); posJetX2Data(1:x,1:y,n) = posJetX2;
            [x,y] = size(posJetX3); posJetX3Data(1:x,1:y,n) = 0;
            [x,y] = size(posJetY1); posJetY1Data(1:x,1:y,n) = posJetY1;
            [x,y] = size(posJetY2); posJetY2Data(1:x,1:y,n) = posJetY2;
            [x,y] = size(posJetY3); posJetY3Data(1:x,1:y,n) = 0;
            clear posJetX1 posJetX2 posJetX3 posJetY1 posJetY2 posJetY3
        else
            [posJetX1,posJetX2,posJetX3,posJetY1,posJetY2,posJetY3,posRingX,posRingY] = ...
                JetCalculator(RPM,phiOutSep(:,n),diamHoles,ringRadius,exitAngle,nHoles,...
                compNextLayer,waterShape,hHoles(n),ringDistance,ps);
            [x,y] = size(posJetX1); posJetX1Data(1:x,1:y,n) = posJetX1;
            [x,y] = size(posJetX2); posJetX2Data(1:x,1:y,n) = posJetX2;
            [x,y] = size(posJetX3); posJetX3Data(1:x,1:y,n) = posJetX3;
            [x,y] = size(posJetY1); posJetY1Data(1:x,1:y,n) = posJetY1;
            [x,y] = size(posJetY2); posJetY2Data(1:x,1:y,n) = posJetY2;
            [x,y] = size(posJetY3); posJetY3Data(1:x,1:y,n) = posJetY3;
            clear posJetX1 posJetX2 posJetX3 posJetY1 posJetY2 posJetY3
        end
    end

    time1 = toc; % End timer and display
    disp(['Time for jet calculation ' num2str(time1)]);


    % PLOT THE DATA EVERY TIMESTEP HAS FINISHED %%%%%%%%%%%%%%%%%%%%%%%%%%%%%%%%
    clf % Clear the figure
    % Plot the jets for ring 1
    subplot(2,5,6); hold on
    for m = 1:10
        posJetX1Plot = posJetX1Data(:,m,1); posJetX1Plot(posJetX1Plot == 0) = [];
        posJetY1Plot = posJetY1Data(:,m,1); posJetY1Plot(posJetY1Plot == 0) = [];
        plot(posJetX1Plot,posJetY1Plot,'Color','r');
    end
    plot(posRingX(:,1),posRingY(:,1),'k');
    plot(posRingX(:,2),posRingY(:,2),'k');
    axis([-0.026 0 0.065 0.091]);
```

```
title(['Jet prediction for ring 1'])

% Plot the jets for ring 2
subplot(2,5,7); hold on
for m = 1:10
    posJetX2Plot = posJetX2Data(:,m,1); posJetX2Plot(posJetX2Plot == 0) = [];
    posJetY2Plot = posJetY2Data(:,m,1); posJetY2Plot(posJetY2Plot == 0) = [];
    plot(posJetX2Plot,posJetY2Plot,'Color','r');
end
plot(posRingX(:,2),posRingY(:,2),'k');
plot(posRingX(:,3),posRingY(:,3),'k');
axis([-0.026 0 0.087 0.113]);
title(['Jet prediction for ring 2'])

% Plot the jets for ring 3
subplot(2,5,8); hold on
for m = 1:10
    posJetX3Plot = posJetX3Data(:,m,1); posJetX3Plot(posJetX3Plot == 0) = [];
    posJetY3Plot = posJetY3Data(:,m,1); posJetY3Plot(posJetY3Plot == 0) = [];
    plot(posJetX3Plot,posJetY3Plot,'Color','r');
end
plot(posRingX(:,3),posRingY(:,3),'k');
plot(posRingX(:,4),posRingY(:,4),'k');
axis([-0.026 0 0.107 0.133]);
title(['Jet prediction for ring 3'])

% Calculate and plot the water layer of the rings
angPosRings = linspace(0.5*pi,0.75*pi,100);

test1 = isempty(posJetX1Plot); % Check if there is a water layer to plot in ring 2
if test1 == 0
    waterRingRad1 = sqrt(posJetX1Plot(length(posJetX1Plot))^2+posJetY1Plot(length(posJetY1Plot))^2);
    waterRingX1 = -sqrt(waterRingRad1^2./(1+tan(angPosRings).^2));
    waterRingY1 = sqrt(waterRingRad1^2 - waterRingX1.^2);
end

test2 = isempty(posJetX2Plot); % Check if there is a water layer to plot in ring 3
if test2 == 0
    waterRingRad2 = sqrt(posJetX2Plot(length(posJetX2Plot))^2+posJetY2Plot(length(posJetY2Plot))^2);
    waterRingX2 = -sqrt(waterRingRad2^2./(1+tan(angPosRings).^2));
    waterRingY2 = sqrt(waterRingRad2^2 - waterRingX2.^2);
end

% Plot the water layer from ring 2 in the jets graph for ring 1
subplot(2,5,6); hold on
if test1 == 0
    plot(waterRingX1,waterRingY1,'b');
end

% Plot the water layer from ring 3 in the jets graph for ring 2
subplot(2,5,7); hold on
if test2 == 0
    plot(waterRingX2,waterRingY2,'b');
end


clear lengthSection1 lengthSection2 lengthSection3
% Calculate the surface area per ring and save for every time step to plot
for k = 1:3 % Loop over the number of rings
    if k == 1 % For ring 1
        [xLength, yLength] = size(posJetX1Data);
        for h = 1:xLength-1 % Loop over the fractions of the jets
            for s = 1:length(hHoles) % Loop over the number of rows
                if (posJetX1Data(h,1,s) - posJetX1Data(h+1,1,s)) == 0
                    lengthSection1(h,s) = 0;
                else
                    % Calculate the length of the current section using Pythagoras
                    lengthSection1(h,s) = sqrt((posJetX1Data(h,1,s) - posJetX1Data(h+1,1,s))^2 + ...
                        (posJetY1Data(h,1,s) - posJetY1Data(h+1,1,s))^2);
                end
            end
        end
        [x,y,z] = size(posJetX1Data);
        if x == 1
            lengthSection1 = 0;
        end
        lengthSection1(lengthSection1 >= 0.001) = 0;

        if posJetX1Plot ~= 0
            % Sum the sections of the jet and the jets at the different heights to calculate the ...
            % total length
            lengthJetR1(i) = sum(sum(lengthSection1));
        else
            lengthJetR1(i) = 0;
        end
        % Use the length of the jet to calculate the total interfacial area in ring 1
        areaRing1(i) = nHoles(k) * pi * diamHoles * lengthJetR1(i);
```

```
    elseif k == 2 % For ring 2
        [xLength, yLength] = size(posJetX2Data);
        for h = 1:xLength-1 % Loop over the fractions of the jets
            for s = 1:length(hHoles) % Loop over the number of rows
                % Calculate the length of the current section using Pythagoras
                lengthSection2(h,s) = sqrt((posJetX2Data(h,1,s) - posJetX2Data(h+1,1,s))^2 + ...
                    (posJetY2Data(h,1,s) - posJetY2Data(h+1,1,s))^2);
            end
        end
        [x,y,z] = size(posJetX2Data);
        if x == 1
            lengthSection2 = 0;
        end
        lengthSection2(lengthSection2 >= 0.001) = 0;
        if sum(sum(posJetX2Data)) == 0
            lengthSection2 = 0;
        end
        if posJetX2Plot ~= 0
            % Sum the sections of the jet and the jets at the different heights to calculate the ...
            % total length
            lengthJetR2(i) = sum(sum(lengthSection2));
        else
            lengthJetR2(i) = 0;
        end
        % Use the length of the jet to calculate the total interfacial area in ring 2
        areaRing2(i) = nHoles(k) * pi * diamHoles * lengthJetR2(i);

    elseif k == 3 % For ring 3
        [xLength, yLength] = size(posJetX3Data);
        for h = 1:xLength-1 % Loop over the fractions of the jets
            for s = 1:length(hHoles) % Loop over the number of rows
                % Calculate the length of the current section using Pythagoras
                lengthSection3(h,s) = sqrt((posJetX3Data(h,1,s) - posJetX3Data(h+1,1,s))^2 + ...
                    (posJetY3Data(h,1,s) - posJetY3Data(h+1,1,s))^2);
            end
        end
        [x,y,z] = size(posJetX3Data);
        if x == 1
            lengthSection3 = 0;
        end
        lengthSection3(lengthSection3 >= 0.001) = 0;
        if sum(sum(posJetX3Data)) == 0
            lengthSection3 = 0;
        end
        if posJetX3Plot ~= 0
            % Sum the sections of the jet and the jets at the different heights to calculate the ...
            % total length
            lengthJetR3(i) = sum(sum(lengthSection3));
        else
            lengthJetR3(i) = 0;
        end
        % Use the length of the jet to calculate the total interfacial area in ring 3
        areaRing3(i) = nHoles(k) * pi * diamHoles * lengthJetR3(i);

    end
end

% Convert the interfacial area to a gl values
aglRing1(i) = areaRing1(i) ./ ((ringRadius(2)^2 - ringRadius(1)^2) * pi * hBed);
aglRing2(i) = areaRing2(i) ./ ((ringRadius(3)^2 - ringRadius(2)^2) * pi * hBed);
aglRing3(i) = areaRing3(i) ./ ((0.125^2 - ringRadius(3)^2) * pi * hBed);
aglTotal(i) = (areaRing1(i) + areaRing2(i) + areaRing3(i)) ./ ...
    ((casingRadius^2 - ringRadius(1)^2) * pi * hBed);

% Plot the a gl data
subplot(2,5,9); hold on
plot(1:i,aglRing1)
plot(1:i,aglRing2)
plot(1:i,aglRing3)
plot(1:i,aglTotal)
xlabel('Timestep'); ylabel('a g l [m^2/m^3]')
leg = legend('Ring 1', 'Ring 2', 'Ring 3', 'Total RPB');
set(leg,'location','best')

% Plot the volume present in the different rings
subplot(2,5,10); hold on
plot(1:i+1,volumeOld(:,1))
plot(1:i+1,volumeOld(:,2))
plot(1:i+1,volumeOld(:,3))
xlabel('Timestep'); ylabel('Volume in ring [m^3]')
leg = legend('Ring 1', 'Ring 2', 'Ring 3');
set(leg,'location','best')

% Plot the water layers in each ring of the RPB
subplot(2,5,1:5);
x0=20; y0=50; width=1100; height=350;
```

```
    set(gcf,'units','points','position',[x0,y0,width,height])

    % Plot all positive values
    % Plot rings
    plot([ringRadius(1) ringRadius(1)], [0 hBed],'k'); hold on; plot([ringRadius(2) ringRadius(2)],...
        [0 hBed],'k'); plot([ringRadius(3) ringRadius(3)], [0 hBed],'k');
    % Plot the locations of the holes
    for s = 1:length(hHoles)
        plot([ringRadius(1)-0.002 ringRadius(1)+0.002], [hHoles(s) hHoles(s)],'r');
        plot([ringRadius(2)-0.002 ringRadius(2)+0.002], [hHoles(s) hHoles(s)],'r');
        plot([ringRadius(3)-0.002 ringRadius(3)+0.002], [hHoles(s) hHoles(s)],'r');
    end
        % Plot the water
    plot(linspace(ringRadius(1)-ringDistance(1),ringRadius(1),ps.nRad),waterShape(:,1),'color',[0 0.4 0.8])
    plot(linspace(ringRadius(2)-ringDistance(2),ringRadius(2),ps.nRad),waterShape(:,2),'color',[0.8 0.4 0])
    plot(linspace(ringRadius(3)-ringDistance(3),ringRadius(3),ps.nRad),waterShape(:,3),'color',[0 0.8 0.3])

    % Plot all negative values
    % Plot rings
    plot([-ringRadius(1) -ringRadius(1)], [0 hBed],'k'); plot([-ringRadius(2) -ringRadius(2)],...
        [0 hBed],'k'); plot([-ringRadius(3) -ringRadius(3)], [0 hBed],'k');
    % Plot the locations of the holes
    for s = 1:length(hHoles)
        plot([-ringRadius(1)-0.002 -ringRadius(1)+0.002], [hHoles(s) hHoles(s)],'r');
        plot([-ringRadius(2)-0.002 -ringRadius(2)+0.002], [hHoles(s) hHoles(s)],'r');
        plot([-ringRadius(3)-0.002 -ringRadius(3)+0.002], [hHoles(s) hHoles(s)],'r');
    end
    % Plot the water
    plot(-fliplr(linspace(ringRadius(1)-ringDistance(1),ringRadius(1),ps.nRad)),flipud(waterShape(:,1)),...
        'color',[0 0.4 0.8])
    plot(-fliplr(linspace(ringRadius(2)-ringDistance(2),ringRadius(2),ps.nRad)),flipud(waterShape(:,2)),...
        'color',[0.8 0.4 0])
    plot(-fliplr(linspace(ringRadius(3)-ringDistance(3),ringRadius(3),ps.nRad)),flipud(waterShape(:,3)),...
        'color',[0 0.8 0.3])

    % Set the other parameters for the graph
    axis([-0.111 0.111 0 hBed]); set(findall(gca, 'Type', 'Line'),'LineWidth',2); hold off;
    xlabel('Horizontal pos. in the bed [m]','FontSize',12); ylabel('Vertical position [m]','FontSize',12);

    % Set the title depending on the current time, to make sure it "stays in place"
    modulesTime = mod(i*ps.dt, 0.1);
    modulesTime2 = mod(i*ps.dt, 1);
    if modulesTime2 == 0
        title(['Parab. approximation of water levels at ' num2str(RPM) ' rpm and ' num2str(phiIn) ...
            ' m3/h with ' num2str(length(hHoles)) 'x (' num2str(nHoles(1)) ', ' num2str(nHoles(2)) ...
            ' and ' num2str(nHoles(3)) ') holes at t = ' num2str(i*ps.dt) '.00 s'],'FontSize',12);
    elseif modulesTime == 0
        title(['Parab. approximation of water levels at ' num2str(RPM) ' rpm and ' num2str(phiIn) ...
            ' m3/h with ' num2str(length(hHoles)) 'x (' num2str(nHoles(1)) ', ' num2str(nHoles(2)) ...
            ' and ' num2str(nHoles(3)) ') holes at t = ' num2str(i*ps.dt) '0 s'],'FontSize',12);
    else
        title(['Parab. approximation of water levels at ' num2str(RPM) ' rpm and ' num2str(phiIn) ...
            ' m3/h with ' num2str(length(hHoles)) 'x (' num2str(nHoles(1)) ', ' num2str(nHoles(2)) ...
            ' and ' num2str(nHoles(3)) ') holes at t = ' num2str(i*ps.dt) ' s'],'FontSize',12);
    end
    drawnow
end
```

Code to solve the mass balance over the reactor

```
% Water accumulation calculations in RPB.
% Determination of the operating range to prevent flooding and running dry
% Author:       Tom Vercoelen
% Date created: 2017-9-10
% Last edited:  2018-4-24
function [waterShape,volume,PhiOutSep] = CalcWaterLayerParabolic(RPM,phiIn,hBed,...
    ringRadius,hHoles,nHoles,diamHoles,volumeOld,i,ps)

% Declaration of variables
PhiIn       = phiIn/3600;               % Water flow in                         [m3/s]
Dr          = ringRadius;               % Radius of the different rings         [m]
DrMax       = [0.068 0.022 0.02];       % Space between the different rings     [m]
Dholes      = diamHoles;                % Diameter of the holes                 [m]
Hbed        = hBed;                     % Height of the bed                     [m]
RPM         = RPM;                      % Rotations per minute                  [1/min]
Cv          = ps.Cv;                    % Velocity coefficient
g           = ps.g;                     % Gravitational acceleration            [m/s^2]
Gval        = ps.Gval;                  % Constant used for calculation of the additional G-force
useSyms     = 0;                        % Set 1 to use symbolic math, set 0 to use the ABC ...
                                        % formula if D1 > Hbed. Increases calculation speed
dt          = ps.dt;                    % Time step
nRadial     = ps.nRad;                  % Number of steps in the calculations of the water shape
```

```
if i == 1
    volume = volumeOld;
else
    volume      = volumeOld;
end

% Do some pre-calculations
omega       = RPM/60*2*pi;              % Radial velocity                       [rad/s]
AreaHoles   = pi/4*Dholes^2 * nHoles;   % Total area of the holes               [m^2]
Fc          = omega^2 * Dr;             % Centrifugal acceleration              [m/s^2]
Fg          = g;                        % Gravitational acceleration            [m/s^2]

% Pre-allocate some arrays for the different values used in the calculation
PhiOut = zeros(1,3);                    % Cumulative outflow through the holes in each ring ...
                                        % of the reactor      [m^3/s]
D1 = zeros(1,3);                        % Vertical height of the water in each ring        [m]
D2 = zeros(1,3);                        % Horizontal "height" of the water in each ring    [m]
CheckD1 = zeros(1,3);                   % Values to check if the water level has reached ...
                                        % it's steady state
waterShape = zeros(nRadial,3);
%% Start of the calculations
% Step 1; calculate the volume in each ring.
% Step 2; calculate the shape of this volume.
% Step 3; calculate flow through the holes.

for n = 1:length(Dr)    % Loop over number of rings

    % STEP 1; Determine the volume according to the mass balance; Acc = In - Out
    if n == 1           % Accumulation calculation for the first ring
        if volume(n) >= pi * Dr(n)^2 * Hbed
            PhiOut(n) = PhiIn;
        end
        volume(n) = volume(n) + (PhiIn ) * dt; %- PhiOut(n)) * dt;
        if volume(n) < 0
            volume(n) = 0;
        end
    elseif n > 1        % Accumulation calculation for ring 2 and 3
        if volume(1) >= pi * Dr(1)^2 * Hbed
            PhiOut(1) = PhiIn;
        end
        if volume(2) >= pi * (Dr(2)^2 - Dr(1)^2) * Hbed
            PhiOut(2) = PhiIn;
        end
        if volume(3) >= pi * (Dr(3)^2 - Dr(2)^2) * Hbed
            PhiOut(3) = PhiIn;
        end
        volume(n) = volume(n) + (PhiOut(n-1) )* dt;
        if volume(n) < 0
            volume(n) = 0;
        end
    end

    if volume(n) > 0 % If the volume in the current ring is > 0
        % STEP 2; Calculate the shape of the water using calcWaterProfile.m
        waterShape(:,n) = calcWaterProfile(Dr(n),DrMax(n),RPM,Hbed,nRadial,volume(n));
        FinalHeight(n) = waterShape(length(waterShape),n);


        % STEP 3;  Calculate the flow through the holes at the different heights
        for p = 1:length(hHoles) % Loop over the number of rows of holes
            if FinalHeight(n) > hHoles(p) % If the water if covering the current row of holes
                %Determinde the thickness of the water layer covering the holes
                DifferenceVectorTest = (waterShape(:,n) - hHoles(p));
                DifferenceVectorTest(DifferenceVectorTest < 0) = 1;
                [~,posy] = min(DifferenceVectorTest);
                layerThicknessSpecific(n) = DrMax(n)/nRadial*(nRadial-posy);
                % Calculate the flow through the current hole
                PhiOutSep(n,p) =  Cv * AreaHoles(n) * sqrt( omega^2 * (Dr(n)^2 - ...
                    (Dr(n) - layerThicknessSpecific(n))^2));
                PhiOut(n) = sum(PhiOutSep(n,:));
            elseif FinalHeight(n) <= hHoles(p)
                % If the water does not cover the current row of holes
                PhiOutSep(n,p) = 0;
            end
        end

    else % If the volume in the current ring is 0
        for p = 1:length(hHoles)
            PhiOutSep(n,p) = 0;
        end
    end
end

% Calculate the new volume in each ring
volume = volume - PhiOut*dt;
end
```

Code to calculate the shape of the water layer

```
% Function to calculate the shape of the water profile
% Author:       Tom Vercoelen
% Date created: 2018-9-10
% Last edited:  2017-4-24

function [heightWater, R] = calcWaterProfile(Dr,DrMax,RPM,h0,nRadial,volPresent)
% Define some variables
g           = 9.81;                     % Gravitational acceleration            [m/s^2]
n           = nRadial;                  % Number of sections in the water shape
R           = linspace(Dr-DrMax,Dr,n);

% Do some pre-calculations
omega       = RPM/60*2*pi;              % Radial velocity                       [rad/s]
Fc          = omega^2 * R;              % Centrifugal acceleration              [m/s^2]
Fg          = g;                        % Gravitational acceleration            [m/s^2]
angle       = atand(Fc/Fg);             % Angle at which the water will set

if volPresent < 1e-7 % If the volume inside a ring is smaller than the stated value, ...
                     % the water layer is assumed "flat"
    heightWater = zeros(nRadial,1);
else
    for i = 1:n-1 % Loop to calculate the angles of the parabolic shape
        heightFrustums(i) = (R(i+1)-R(i))*tan(angle(i+1)*0.0174532925);
    end

    for i = 1:n-1 % Loop to calculate the parabollic shape
        if i == 1
            heightWater(n-i) = h0 - heightFrustums(n-i);
        else
            heightWater(n-i) = heightWater(n-i+1) - heightFrustums(n-i);
        end
    end
    heightWater(n) = h0; % The last value equal to the bed height
    heightParab = abs(min(heightWater));

    volRight = 0; % Value that determines if the while loop can be terminated

    iterNumber = n-1;
    loop = 1;

    while volRight ~= 1
        for i = 1:n-1 % Calculate the volume of the individual water elements in the ring
            if heightWater(i) < 0 % Empty element
                testVol(i) = 0;
            elseif heightWater(i) >= h0 % Completely filled element
                testVol(i) = pi* (R(i+1)^2 - R(i)^2) * h0;
            elseif heightWater(i) >= 0 % Partially filled element
                volDeel1   = (heightWater(i)                    ) * pi * (R(i+1)^2 - R(i)^2);
                volDeel2   = (heightWater(i+1) - heightWater(i)) * pi * (R(i+1)^2         );
                volFrustum = pi * heightFrustums(i) / 12 * ( (R(i+1)*2)^2 + (R(i+1)*2) * ...
                    (R(i)*2) + (R(i)*2)^2);
                testVol(i) = volDeel1 + volDeel2 - volFrustum;
            end
        end

        totVol = sum(testVol); % Sum the volume of the individual elements

        % Check if the volume is within 0.1% of the real volume in the ring
        if totVol < 1.001 * volPresent && totVol > 0.999 * volPresent
            volRight = 1;
        elseif totVol > 1.001 * volPresent % If the volume in the ring is too LARGE, lower the water level
            heightWater = heightWater - heightParab/nRadial;
            if iterNumber < n-1
                iterNumber = iterNumber - 1;
            end
        elseif totVol < 0.999 * volPresent % If the volume in the ring is too SMALL, rais the water level
            heightWater = heightWater + heightParab/nRadial;
            if iterNumber > 1
                iterNumber = iterNumber - 1;
            end
        end
        loop = loop + 1;
        if loop >= 10*n
            volRight = 1;
        end
    end
    % Set the water out of the limits to zero or the bed height to store ...
    % the final water shape
    heightWater(heightWater > h0) = h0;
    heightWater(heightWater < 0) = 0;
end
end
```

Code to calculate the jet flight paths

```
% MATLAB programm to calculate the flight path of the jets in the RPB
% Author:       Tom Vercoelen
% Date created: 2018-2-16
% Last edited:  2018-4-24

function [posJetX1,posJetX2,posJetX3,posJetY1,posJetY2,posJetY3,posRingX,posRingY] = ...
    JetCalculator(RPM,phiOutSep,holeDiam,ringRadius,exitAngle,nHoles,compNextLayer,...
    waterShape,hHoles,DrMax,ps)

% Define the variables needed for calculation
ringDiam    = ringRadius * 2;               % [m]       -   Diameter of the rings
timeEnd     = 0.055;                        % [s]       -   End time
dt          = 0.00005;                      % [s]       -   Time step size
posJetAng   = [.3*pi .3*pi .3*pi];          % [rad]     -   Initial angular position
numJets     = nHoles;                       % [-]       -   Number of jets to draw
numJetsDraw = 10;                           % Number of jets to draw
red = 0;                                    % Enter 1 to plot the jets in red, otherwise blue

% Calculation of common variables
rads            = RPM/60*2*pi;              % [rad/s]]  -   Angular velocity
holeArea        = pi*(holeDiam/2)^2;        % [m2]      -   Surface area of each hole
openArea        = [nHoles*holeArea]';       % [m2]      -   Open area per ring
velOut          = (phiOutSep)./openArea;    % [m/s]     -   Radial velocity through holes in each ring
velOut          = [velOut]';
tangVelRings    = rads .* ringDiam ./2;     % [m/s]     -   Tangential velocity of the rings
timeArray       = 0:dt:timeEnd;             % [s]       -   Time array

% Compensate the tangential and radial velocity for exit angles
velOutReal      = velOut .* cos(exitAngle*pi/180);
tangVelJets     = tangVelRings - velOut .* sin(exitAngle*pi/180);

% Calculate the flight path starting with the HORIZONTAL and VERTICAL position without compensation
for i = 1:length(timeArray)
    FirstJetPosX(i,1:3) = timeArray(i) * tangVelJets;
    FirstJetPosY(i,1:3) = (ringDiam/2) + timeArray(i) * velOutReal;
end
posJetRad = sqrt(FirstJetPosX.^2 + FirstJetPosY.^2);
posJetAng = atan(FirstJetPosY ./ FirstJetPosX);


maxValuesPossible = [0.09 0.11 0.125];
% Set the values that are past the next ring to zero
if compNextLayer ~= 1
    maxValue = [0.09 0.11 0.125];
elseif compNextLayer == 1
    maxValue(3) = 0.125;
    for n = 1:2
        DifferenceVectorTest = (waterShape(:,n+1) - hHoles);
        DifferenceVectorTest(DifferenceVectorTest < 0) = 1;
        [valx,posy] = min(DifferenceVectorTest);
        layerThicknessSpecific(n) = DrMax(n+1)/ps.nRad*(ps.nRad-posy);
        if sum(DifferenceVectorTest) == length(DifferenceVectorTest)
            maxValue(n) = maxValuesPossible(n);
        elseif maxValuesPossible(n) - layerThicknessSpecific(n) <= ringRadius(n)
            maxValue(n) = ringRadius(n) + 0.0001;
        else
            maxValue(n) = maxValuesPossible(n) - layerThicknessSpecific(n);
        end
    end
end


for i = 1:3
    posJetRad(posJetRad(:,i) > maxValue(i),i) = 0;
end


% Compensate the flight path for the rotation of the RPB while the jets are flying
for i = 1:3
    posJetAng(:,i) = posJetAng(:,i) + [rads * timeArray]';
end

jets1X = posJetRad(:,1);
jets1X(jets1X == 0) = [];
jets2X = posJetRad(:,2);
jets2X(jets2X == 0) = [];
jets3X = posJetRad(:,3);
jets3X(jets3X == 0) = [];

% Multiply the data to create multiple jets per ring
% posJetAngMany = zeros(length(timeArray),3,numJets);
for i = 1:numJetsDraw
   posJetAngMany1(:,i) = posJetAng(1:length(jets1X),1) + 2*pi/numJets(1) * i;
```

```
end
for i = 1:numJetsDraw
   posJetAngMany2(:,i) = posJetAng(1:length(jets2X),2) + 2*pi/numJets(2) * i;
end
for i = 1:numJetsDraw
   posJetAngMany3(:,i) = posJetAng(1:length(jets3X),3) + 2*pi/numJets(3) * i;
end


% Conversion of polar coordinates to cartesian coordinates
% For the different parts of the ring, calculate the coordinates based on the quadrant
for i = 1:length(jets1X)
    for n = 1:numJetsDraw
        if posJetAngMany1(i,n) < (0.5*pi)
            posJetX1(i,n) = sqrt(jets1X(i).^2./(1+tan(posJetAngMany1(i,n)).^2));
            posJetY1(i,n) = sqrt(jets1X(i).^2 - posJetX1(i,n).^2);
        elseif (posJetAngMany1(i,n) >= (0.5*pi) && posJetAngMany1(i,n) < (1.0*pi))
            posJetX1(i,n) = -sqrt(jets1X(i).^2./(1+tan(posJetAngMany1(i,n)).^2));
            posJetY1(i,n) = sqrt(jets1X(i).^2 - posJetX1(i,n).^2);
        elseif (posJetAngMany1(i,n) >= (1.0*pi) && posJetAngMany1(i,n) < (1.5*pi))
            posJetX1(i,n) = -sqrt(jets1X(i).^2./(1+tan(posJetAngMany1(i,n)).^2));
            posJetY1(i,n) = -sqrt(jets1X(i).^2 - posJetX1(i,n).^2);
        elseif (posJetAngMany1(i,n) >= (1.5*pi) && posJetAngMany1(i,n) < (2.0*pi))
            posJetX1(i,n) = sqrt(jets1X(i).^2./(1+tan(posJetAngMany1(i,n)).^2));
            posJetY1(i,n) = -sqrt(jets1X(i).^2 - posJetX1(i,n).^2);
        elseif (posJetAngMany1(i,n) >= (2.0*pi) && posJetAngMany1(i,n) < (2.5*pi))
            posJetX1(i,n) = sqrt(jets1X(i).^2./(1+tan(posJetAngMany1(i,n)-2*pi).^2));
            posJetY1(i,n) = sqrt(jets1X(i).^2 - posJetX1(i,n).^2);
        elseif (posJetAngMany1(i,n) >= (2.5*pi) && posJetAngMany1(i,n) < (3.0*pi))
            posJetX1(i,n) = -sqrt(jets1X(i).^2./(1+tan(posJetAngMany1(i,n)-2*pi).^2));
            posJetY1(i,n) = sqrt(jets1X(i).^2 - posJetX1(i,n).^2);
        elseif (posJetAngMany1(i,n) >= (3.0*pi) && posJetAngMany1(i,n) < (3.5*pi))
            posJetX1(i,n) = -sqrt(jets1X(i).^2./(1+tan(posJetAngMany1(i,n)-2*pi).^2));
            posJetY1(i,n) = -sqrt(jets1X(i).^2 - posJetX1(i,n).^2);
        elseif (posJetAngMany1(i,n) >= (3.5*pi) && posJetAngMany1(i,n) < (4.0*pi))
            posJetX1(i,n) = sqrt(jets1X(i).^2./(1+tan(posJetAngMany1(i,n)-2*pi).^2));
            posJetY1(i,n) = -sqrt(jets1X(i).^2 - posJetX1(i,n).^2);
        end
    end
end
for i = 1:length(jets2X)
    for n = 1:numJetsDraw
        if posJetAngMany2(i,n) < (0.5*pi)
            posJetX2(i,n) = sqrt(jets2X(i).^2./(1+tan(posJetAngMany2(i,n)).^2));
            posJetY2(i,n) = sqrt(jets2X(i).^2 - posJetX2(i,n).^2);
        elseif (posJetAngMany2(i,n) >= (0.5*pi) && posJetAngMany2(i,n) < (1.0*pi))
            posJetX2(i,n) = -sqrt(jets2X(i).^2./(1+tan(posJetAngMany2(i,n)).^2));
            posJetY2(i,n) = sqrt(jets2X(i).^2 - posJetX2(i,n).^2);
        elseif (posJetAngMany2(i,n) >= (1.0*pi) && posJetAngMany2(i,n) < (1.5*pi))
            posJetX2(i,n) = -sqrt(jets2X(i).^2./(1+tan(posJetAngMany2(i,n)).^2));
            posJetY2(i,n) = -sqrt(jets2X(i).^2 - posJetX2(i,n).^2);
        elseif (posJetAngMany2(i,n) >= (1.5*pi) && posJetAngMany2(i,n) < (2.0*pi))
            posJetX2(i,n) = sqrt(jets2X(i).^2./(1+tan(posJetAngMany2(i,n)).^2));
            posJetY2(i,n) = -sqrt(jets2X(i).^2 - posJetX2(i,n).^2);
        elseif (posJetAngMany2(i,n) >= (2.0*pi) && posJetAngMany2(i,n) < (2.5*pi))
            posJetX2(i,n) = sqrt(jets2X(i).^2./(1+tan(posJetAngMany2(i,n)-2*pi).^2));
            posJetY2(i,n) = sqrt(jets2X(i).^2 - posJetX2(i,n).^2);
        elseif (posJetAngMany2(i,n) >= (2.5*pi) && posJetAngMany2(i,n) < (3.0*pi))
            posJetX2(i,n) = -sqrt(jets2X(i).^2./(1+tan(posJetAngMany2(i,n)-2*pi).^2));
            posJetY2(i,n) = sqrt(jets2X(i).^2 - posJetX2(i,n).^2);
        elseif (posJetAngMany2(i,n) >= (3.0*pi) && posJetAngMany2(i,n) < (3.5*pi))
            posJetX2(i,n) = -sqrt(jets2X(i).^2./(1+tan(posJetAngMany2(i,n)-2*pi).^2));
            posJetY2(i,n) = -sqrt(jets2X(i).^2 - posJetX2(i,n).^2);
        elseif (posJetAngMany2(i,n) >= (3.5*pi) && posJetAngMany2(i,n) < (4.0*pi))
            posJetX2(i,n) = sqrt(jets2X(i).^2./(1+tan(posJetAngMany2(i,n)-2*pi).^2));
            posJetY2(i,n) = -sqrt(jets2X(i).^2 - posJetX2(i,n).^2);
        end
    end
end
for i = 1:length(jets3X)
    for n = 1:numJetsDraw
        if posJetAngMany3(i,n) < (0.5*pi)
            posJetX3(i,n) = sqrt(jets3X(i).^2./(1+tan(posJetAngMany3(i,n)).^2));
            posJetY3(i,n) = sqrt(jets3X(i).^2 - posJetX3(i,n).^2);
        elseif (posJetAngMany3(i,n) >= (0.5*pi) && posJetAngMany3(i,n) < (1.0*pi))
            posJetX3(i,n) = -sqrt(jets3X(i).^2./(1+tan(posJetAngMany3(i,n)).^2));
            posJetY3(i,n) = sqrt(jets3X(i).^2 - posJetX3(i,n).^2);
        elseif (posJetAngMany3(i,n) >= (1.0*pi) && posJetAngMany3(i,n) < (1.5*pi))
            posJetX3(i,n) = -sqrt(jets3X(i).^2./(1+tan(posJetAngMany3(i,n)).^2));
            posJetY3(i,n) = -sqrt(jets3X(i).^2 - posJetX3(i,n).^2);
        elseif (posJetAngMany3(i,n) >= (1.5*pi) && posJetAngMany3(i,n) < (2.0*pi))
            posJetX3(i,n) = sqrt(jets3X(i).^2./(1+tan(posJetAngMany3(i,n)).^2));
            posJetY3(i,n) = -sqrt(jets3X(i).^2 - posJetX3(i,n).^2);
        elseif (posJetAngMany3(i,n) >= (2.0*pi) && posJetAngMany3(i,n) < (2.5*pi))
            posJetX3(i,n) = sqrt(jets3X(i).^2./(1+tan(posJetAngMany3(i,n)-2*pi).^2));
            posJetY3(i,n) = sqrt(jets3X(i).^2 - posJetX3(i,n).^2);
        elseif (posJetAngMany3(i,n) >= (2.5*pi) && posJetAngMany3(i,n) < (3.0*pi))
```

```
            posJetX3(i,n) = -sqrt(jets3X(i).^2./(1+tan(posJetAngMany3(i,n)-2*pi).^2));
            posJetY3(i,n) = sqrt(jets3X(i).^2 - posJetX3(i,n).^2);
        elseif (posJetAngMany3(i,n) >= (3.0*pi) && posJetAngMany3(i,n) < (3.5*pi))
            posJetX3(i,n) = -sqrt(jets3X(i).^2./(1+tan(posJetAngMany3(i,n)-2*pi).^2));
            posJetY3(i,n) = -sqrt(jets3X(i).^2 - posJetX3(i,n).^2);
        elseif (posJetAngMany3(i,n) >= (3.5*pi) && posJetAngMany3(i,n) < (4.0*pi))
            posJetX3(i,n) = sqrt(jets3X(i).^2./(1+tan(posJetAngMany3(i,n)-2*pi).^2));
            posJetY3(i,n) = -sqrt(jets3X(i).^2 - posJetX3(i,n).^2);
        end
    end
end

% Generate data for rings to plot
angPos      = linspace(0,(2*pi),400)';
ringDiam2   = [ringDiam 0.25];
for i = 1:400
    radPos(i,1:4) = (ringDiam2/2);
end
for i = 1:400
    for n = 1:4
        if angPos(i) < (0.5*pi)
            posRingX(i,n) = sqrt(radPos(i,n).^2./(1+tan(angPos(i)).^2));
            posRingY(i,n) = sqrt(radPos(i,n).^2 - posRingX(i,n).^2);
        elseif (angPos(i) >= (0.5*pi) && angPos(i) < (1.0*pi))
            posRingX(i,n) = -sqrt(radPos(i,n).^2./(1+tan(angPos(i)).^2));
            posRingY(i,n) = sqrt(radPos(i,n).^2 - posRingX(i,n).^2);
        elseif (angPos(i) >= (1.0*pi) && angPos(i) < (1.5*pi))
            posRingX(i,n) = -sqrt(radPos(i,n).^2./(1+tan(angPos(i)).^2));
            posRingY(i,n) = -sqrt(radPos(i,n).^2 - posRingX(i,n).^2);
        elseif (angPos(i) >= (1.5*pi) && angPos(i) <= (2.0*pi))
            posRingX(i,n) = sqrt(radPos(i,n).^2./(1+tan(angPos(i)).^2));
            posRingY(i,n) = -sqrt(radPos(i,n).^2 - posRingX(i,n).^2);
        end
    end
end

end
```